Development of Paper-Based Analytical Devices (μPADs) for Low-Cost, Rapid, and Ultrasensitive Enzyme-Linked Immunosorbent Assay (ELISA)

Ahmed Abdelaty Shalaby

Graduate School of Chemical Sciences and Engineering

Hokkaido University

Doctor Dissertation

2025

Title **:** Development of Paper-Based Analytical Devices (μPADs) for Low-Cost, Rapid, and Ultrasensitive Enzyme-Linked Immunosorbent Assay (ELISA)

Author **:** Ahmed Abdelaty Shalaby

Degree **:** Doctor of Philosophy

Supervisor **:** Manabu Tokeshi

Abstract

Sandwich ELISA is a common analytical technique used for the detection of antibodies and proteins or antigens in biological samples. Typically, sandwich ELISA is performed using a 96-microwell plate, where a capture antibody (cAb) specific for the required antigen is immobilized on the surface of the wells. When the sample is added to the wells, the antigen attached to the immobilized cAb. Then, after a suitable washing process, another enzyme-labeled detection antibody (dAb) is added to attach to the antigen. This is followed by a second washing, and a substrate is added, which reacts with the enzyme and produces a signal that is related to the antigen concentration. Conventional sandwich ELISA is a specific and sensitive technique; however, it is time-consuming because overnight incubation is needed to immobilize cAb, and it has other disadvantages that large sample and reagent volumes are required, the microwell plate reader used for signal readout is expensive, and a highly trained analyst must carry out the work. Microfluidic paper-based analytical devices (μPADs) are a very attractive approach for overcoming all these disadvantages. Since the introduction of μPADs by Whitesides' group in 2007, μPADs have attracted huge interest from researchers as ways to simplify complex analytical techniques in different applications. by the integration between ELISA and μPADs, we can have the high sensitivity and specificity of the ELISA assays with the simplicity and portability of μPADs. In Chapter 1 "General Introduction", I discussed the current perspectives of μPADs, their fabrication, applications, and challenges. Also, the current perspective of ELISA-based μPADs was discussed.

In Chapter 2, a rapid, simple, and low-cost sandwich ELISA-based μPAD is presented for the determination of β'-component protein, a major allergenic protein in salmon roe. This μPAD employed a simple and rapid method to immobilize the capture antibody which reduced the immobilization time to 5 minutes instead of overnight for conventional ELISA. The immobilization was done by drying the capture antibody at 50 ºC for just 5 minutes. The assay

parameters were optimized to achieve the optimal sensitivity with a minimal assay time. Under the optimal conditions, the μPAD-ELISA assay took 15 minutes, and it provided consistent performance over a wide range of β'-component concentrations: there was a good linear relationship over a range of 0.10–60.0 ng mL^{-1} and a limit of detection of 1.59 ng mL^{-1}. Compared to the conventional ELISA assay for the same target, the developed μPAD-ELISA requires minimal reagent volumes and shorter assay times. These advantages are expected to contribute to the rapid and sensitive detection of food allergens in processed food as well as the establishment of a good food allergy labeling system.

In Chapter 3, I introduced a simple, rapid, and ultra-sensitive paper-based biosensing platform integrated into a custom-designed 3D-printed microplate for the bioluminescence detection of the breast cancer biomarker HER2. This hybrid system combines the advantages of microporous cellulose paper, which enables efficient antibody immobilization via passive adsorption within minutes and without requiring surface modification, and a reusable microplate architecture that supports high-throughput analysis. The assay is completed in just 20 minutes—significantly shorter than the typical 5-hour duration of conventional ELISA methods. The 3D-printed microplate was engineered with two critical features: embedded microvalves and modifiable surface wettability via surfactant treatment. These functionalities allow precise fluid control—enabling retention of sample and reagent solutions during incubation while facilitating selective drainage of washing buffer through an adsorption pad during rinsing. The microvalves are integrated at the base of each well and play a dual role in retaining fluids during reaction steps and allowing buffer flow during washing. The device dimensions are compatible with standard commercial plate readers, allowing easy integration into existing laboratory workflows. To ensure optimal valve performance and device reusability, a polyethylene glycol diacrylate (PEGDA)-based resin was selected for 3D printing. This material provides an ideal combination of mechanical strength, chemical resistance, and

biocompatibility, supporting both fluid handling and repeated use. After each assay, only the paper discs are replaced, making the platform cost-effective and sustainable. Bioluminescence detection is carried out using a sandwich immunoassay with NanoLuc luciferase as the signal reporter, delivering approximately 100-fold greater signal intensity compared to traditional luciferases. A strong linear correlation was observed between the bioluminescence output and the logarithmic concentration of HER2 over a wide dynamic range (0.1–1000 pg/mL). The assay achieved a remarkably low limit of detection (LOD) of 1.3 fg/mL—representing more than 10,000-fold improvement over commercial colorimetric ELISA kits and traditional platforms. Validation using HER2-spiked human serum (5–800 pg/mL) showed excellent reproducibility (CV 9.5%) and recovery rates between 86% and 108%. While the small reagent volume used (5 μL) contributes to the assay's sensitivity, it also makes the system highly susceptible to pipetting errors, suggesting that precision dispensing could further improve the assay's reproducibility. This modular paper-in-3D-printed microplate platform—combining passive capillary driven microfluidics, paper-based simplicity, precise fluidic control, and high-sensitivity bioluminescent readout—offers a powerful and low-cost solution for rapid, quantitative biomarker detection. The system demonstrates strong potential for applications in the early diagnosis of cancers, infectious diseases, and other clinically relevant conditions.

In the last chapter, a summary of the results and findings from the research was discussed. Moreover, the challenges and the future prospects were introduced.

Table of Contents

Abstract i

Abbreviations viii

CHAPTER 1 General Introduction 1

1.1 Microfluidic technology and PON applications 2

1.2 Cancer impact and importance of early diagnosis 3

1.3 Paper-based analytical devices (PADs) and their fabrication methods 7

1.3.1 Printing-based fabrication methods for PADs 8

1.3.2 Nonprinting-based fabrication methods for PADs 9

1.4 Paper-based devices for cancer diagnosis 10

1.4.1 Colorimetric methods 10

1.4.2 Fluorescence methods 29

1.4.3 Chemiluminescence methods 32

1.4.4 Electrochemical methods 36

1.4.5 Electrochemiluminescence methods 42

1.4.6 Conclusion and future perspectives 46

1.4.7 Thesis focus and objectives 48

1.5 References 50

CHAPTER 2 Straightforward high-temperature antibody immobilization for rapid and simple microfluidic paper-based ELISA for detection of β'-component (Onc k 5) protein, a major IgE-binding protein in salmon roe 72

2.1 Introduction 73

2.2 Experimental 76

2.2.1 Materials 76

2.2.2 β'-c protein and antibodies 77

2.2.3 Design and fabrication of ELISA μPAD 77

2.2.4 Sandwich ELISA for β'-c protein detection 79

2.2.5 Image capturing and data analyses 79

2.3 Results and discussion 81

2.3.1 Optimization of sandwich ELISA parameters 81

2.3.2 μPAD ELISA vs. conventional ELISA for β'-c detection 91

2.4 Conclusion 93

2.5 References 95

CHAPTER 3 Paper in 3D printed microplate hybrid microfluidic device for low-cost, rapid, and ultrasensitive paper-based bioluminescence detection of human epidermal growth factor receptor2 (HER2) breast cancer biomarker 98

3.1 Introduction 99

3.2 Experimental 102

3.2.1 Materials and instruments 102

3.2.2 Labeling the detection antibody with Nluc 103

3.2.3 Removing unreacted NanoLuc-HaloTag protein 104

3.2.4 3D printing ink formulation 105

3.2.5 Design and fabrication of the paper-3D printed microplate hybrid device .. 105

3.2.6 Optimization of capture antibody and detection antibody concentrations .. 107

3.2.7 Optimization of blocking buffer concentration 107

3.2.8 Optimization of antigen reaction time 108

3.2.9 Optimization of detection antibody reaction time 108

3.2.10 Sandwich ELISA for HER2 detection 108

3.2.11 Detection of HER2 in human serum 110

3.2.12 Storage condition of reagents and plate 110

3.3 Results and discussion 110

3.3.1 Paper disc use in the 3D printed microplate hybrid device 110

3.3.2 Immobilization of capture antibody 115

3.3.3 Optimization of capture antibody and detection antibody concentrations .. 115

3.3.4 Optimization of blocking buffer concentration 116

3.3.5 Optimization of antigen reaction time 118

3.3.6 Optimization of detection antibody reaction time 119

3.3.7 Bioluminescence sandwich ELISA for detection of HER2 120

3.3.8 Detection of HER2 in human serum 124

3.4 Conclusion 125

CHAPTER 4 Conclusion and Future Prospectives 131

4.1 Conclusion 132

4.2 Future Prospectives 134

Acknowledgement..... 135

Abbreviations

The following abbreviations are used in the manuscript

Abbreviation	Full name
β'-c	β' component protein
µPADs	Microfluidic Paper-based Analytical Devices
3DGS	3-dimensional graphene sheet
ABTS	2,2’-azinobis-(3-ethylbenzothiazoline-6-sulfonate)
AFP	Alpha-fetoprotein
AGET ATRP	Activators generated electron transfer for atom transfer radical polymerization
AgNPs	Silver Nanoparticles
AQP1	Aquaporin-1
AuNFs	Gold nanoflowers
AuNPs	Gold Nanoparticles
AuNRs	Gold nanorods
BRCA-1	Breast cancer gene 1
BTA	Bladder tumor antigen
CCs	Capillaric circuits
CA125	Cancer antigen 125
CA153	Cancer antigen 153
CA19-9	Carbohydrate antigen 19-9
CE	Counter electrode
CEA	Carcinoembryonic antigen
CL	Chemiluminescence

CMs	Carbon microspheres
CNDs	Carbon nanodots
CNSs	Carbon nanospheres
CNTs	Carbon nanotubes
Con A	Concanavalin A
CS-PWE	Cuboid silver modified paper working electrode
CT	Computed Tomography
CV	Cyclic voltammetry
Cys	Cysteamine
CysA	Cysteamine
Cyt c	Cytochrome c
DPV	Differential pulse voltammetry
DSN	Duplex-specific nuclease
EC MSPs	Elastic copolymer multistructured pseudo-papers
ECL	Electrochemiluminescence
ELISA	Enzyme-Linked Immunosorbent Assay
ePADs	Electrochemical paper-based analytical devices
EpCAM	Epithelial cell adhesion molecule
FITC	Fluorescein isothiocyanate
FRET	Fluorescence resonance energy transfer
GDH	Glutamate dehydrogenase
GN	Graphene
GOx	Glucose oxidase
GQDs	Graphene quantum dots

HCG	Human chorionic gonadotropin
HER2	Human epidermal growth factor receptor 2
HPV	Human papilloma virus
HRP	Horseradish peroxidase
ITX	2-Isopropylthioxanthone
IPA	Isopropanol
IL	Ionic liquid
IL-6	Interleukin 6
LFIA	Lateral flow immunoassay
LPA	Lysophosphatidic Acid
MCR	Microfluidic chain reaction
MIPs	Molecularly imprinted polymers
MMP9	Matrix metalloproteinase 9
MMP9	Matrix metalloproteinase 9
MOF	Metal organic framework
MRI	Magnetic Resonance Imaging
MSNs	Mesoporous silica nanoparticles
MUC16	Mucin-16
MWCNTs	Multiwalled carbon nanotubes
MWCNTs	Multiwalled carbon nanotubes
NC	Nitrocellulose membrane
NC MSPs	Nitrocellulose multistructured pseudo-papers
NGC	Nanoporous gold-chitosan
NGQDs	Nitrogen dopped graphene quantum dots
NH_2-G	Amino functional graphene

NMP22	Nuclear matrix protein 22
NPG	Nanoporous gold
NPS	Nanoporous silver
NSC	Nanoporous silver-chitosan
NSE	Neuron specific enolase
OPD	o-phenylenediamine
PEGDA	Polyethylene glycol diacrylate
PETTA	Pentaerythritol tetraacrylate
P-acid	4,4'-(2,5-dimethoxy-1,4-phenylene)bis(ethyne-2,1-diyl) dibenzoic acid
PADs	Paper-based Analytical Devices
PAH	charged poly(allylamine hydrochloride)
PAMAM	Polyamidoamine
PANI/Au-PWE	Polyaniline- Au nanoparticles modified paper working electrode
PB-PEDOT	Prussian blue (PB)- poly (3,4- ethylenedioxythiophene) (PEDOT)
PCA3	Prostate cancer antigen 3
PCR	Polymerase Chain Reaction
PEAK1	Pseudopodium-enriched atypical kinase one, SGK269.
PET scan	Positron Emission Tomography scan
PON	Point-OF-Need
PP	Polypropylene
p-PLLA	Porous Poly(L-lactic) acid
PSA	Prostate specific antigen
Pt–AgANP	Pt-Ag alloy nanoparticles
PVA	Poly vinyl alcohol

QDs	Quantum dots
RE	Reference electrode
rGO	Reduced graphene oxide
RT-LAMP	Reverse transcription loop-mediated isothermal amplification
SERS	Surface Enhanced Raman Spectroscopy
SOx	Sarcosine oxidase
SPR	Surface Plasmon Resonance
SVAu	Surface villous gold
SWV	Square wave voltammetry
TPO	Diphenyl(2,4,6-trimethylbenzoyl)phosphine oxide
Thi	Thionine
TMB	3,3',5,5'-tetrammethylbenzidine
TPA	Tri-n-propylamine
UCNPs	Up conversion nanoparticles
VCP	Valosin-containing protein
WE	Working electrode
ZNRs	ZnO nanorods

CHAPTER 1 General Introduction

1.1 Microfluidic technology and PON applications

There has been a persistent interest in developing analytical tools for point-of-need (PON) applications in areas such as medical diagnostics, environmental monitoring, food safety, and therapeutic drug management [1]. When microfluidic technology emerged, it was anticipated to revolutionize PON measurement systems. However, as the field progressed, it became evident that despite their compact size, most microfluidic devices relied on bulky external components, including pumps, valves, and instrumentation, which limited their portability. Consequently, the majority of microfluidic devices remain confined to laboratory environments, where they are widely used for tasks such as cell sorting, DNA amplification and analysis, and chemical assays. In parallel, efforts have been made to adapt microfluidics for use beyond the laboratory by employing capillary flow-driven mechanisms, thereby eliminating the dependence on external pumps and valves [2, 3].

A pivotal study published by the Whitesides group in 2007 [4] introduced the use of photoresist-patterned paper to create channels and zones for colorimetric detection, sparking a surge of research in this area. This innovation gained widespread attention due to the universal availability of paper, the simplicity of the patterning methods, and the ability to control fluid flow and conduct chemical and biochemical reactions without requiring powered equipment. This approach became known as microfluidic paper-based analytical devices (μPADs), a term later generalized to paper-based analytical devices (PADs) to encompass a broader range of geometries and designs, including those that are not strictly microfluidic in nature.

PADs offer simple, rapid, ultra-sensitive, and low-cost platforms for detection of proteins in biological samples for early diagnosis of diseases such as cancers, and for health protection such as allergenic proteins in food. Here, I will discuss the current perspectives of PADs and its applications for detection of proteins for early diagnosis of cancers.

1.2 Cancer impact and importance of early diagnosis

Cancer is a leading cause of mortality worldwide and ranks as the first or second cause of death in more than 60% of the world's countries. Globally in 2020, newly diagnosed cancer cases exceeded 19 million with a more than 51% mortality rate (that is, more than 9.9 million deaths) [5]. In the United States alone in 2022, the estimated number of new cancer cases was 1.9 million with a more than 31% mortality rate [6]. There are about 36 major cancer types according to the type of organ, and breast cancer is the most common and death-leading type in women, while lung cancer is the most death-leading type in men (**Fig. 1-1**) [5]. Cancer occurs for several reasons including gene mutations, infections, environmental factors, and even wrong lifestyle habits [7]. Cancer refers to a large group of diseases that can affect almost any tissue or organ. It starts when abnormal cells uncontrollably grow and go beyond the normal organ boundaries, develop a malignancy, and invade the neighboring organs and body parts [7].

The disease burden and number of deaths from cancer can be severely reduced through early detection and proper treatment. Successful cancer treatment depends mainly on the stage when the cancer is diagnosed, so early diagnosis is crucial for decreasing the mortality rate [8, 9]. Currently, cancer is diagnosed with various imaging techniques like X-ray, ultrasound, computed tomography (CT), magnetic resonance imaging (MRI), positron emission tomography (PET), and mammography techniques [7, 10]. These methods are unsuitable for early diagnosis, they cannot differentiate between malignant and benign tumors, they suffer from low sensitivity and specificity, they use bulky and complicated instruments that require highly trained operators, and they are expensive [10]. Histopathology can be used to detect the malignancy of the tissues by taking a biopsy of the tumor that has already been identified using imaging techniques, but it cannot be used alone for the early detection of cancer [10]. Finding

rapid, sensitive, and specific methods for the detection of cancer in the early stages and even before the symptoms appear is a challenge for researchers worldwide.

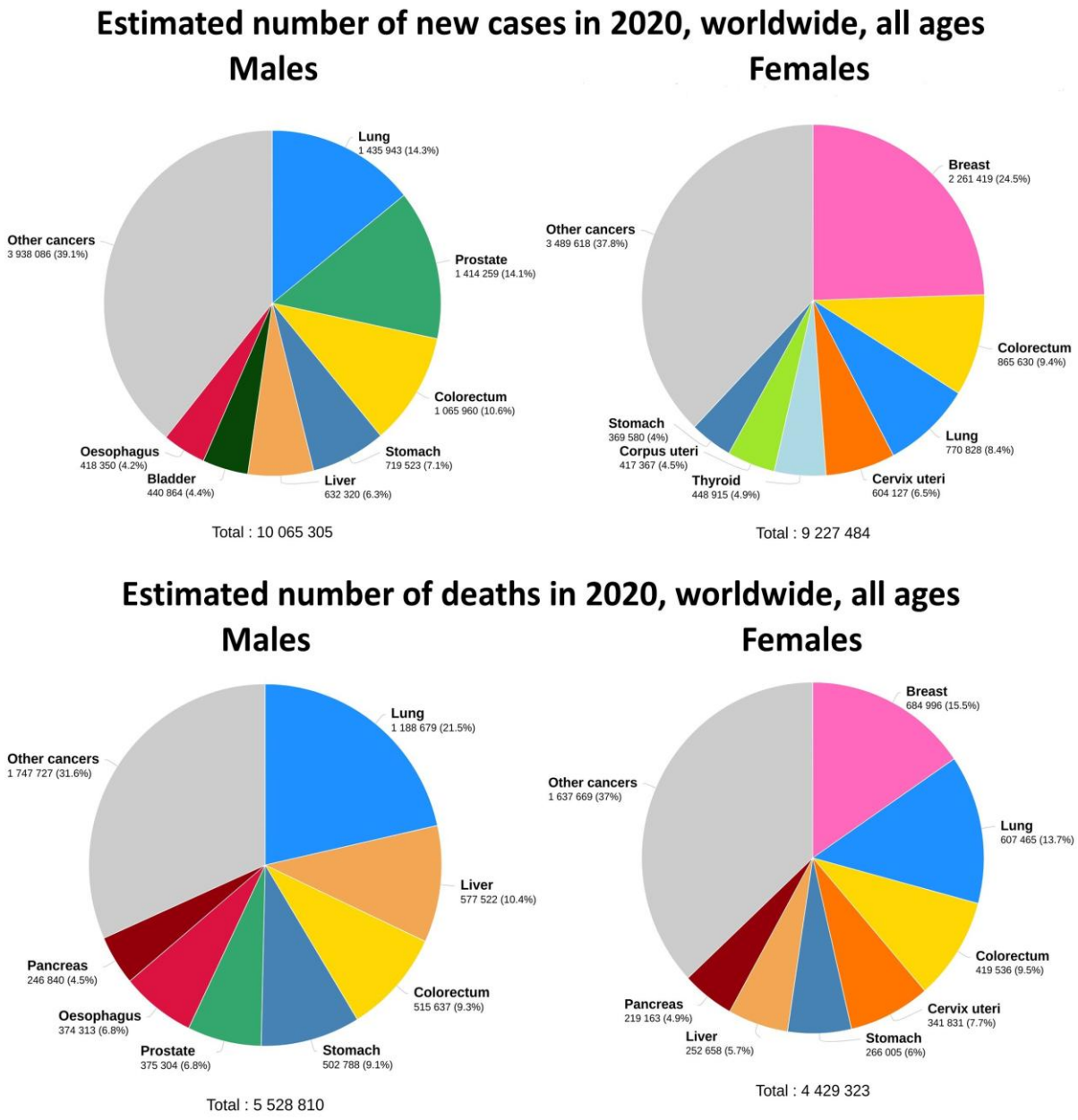

Fig. 1- 1 The total number of cases of the comon cancers in males and females and the total number of deaths. Figures are reproduced from the website, CANCER TODAY (https://gco.iarc.fr/today)

Detection of biomarkers is an extremely attractive way to diagnose cancer of various types because it is specific, highly sensitive, and can be measured quickly. Biomarkers are biological molecules produced by the body in normal states or as a response to abnormal conditions like cancer or any disease, and these molecules are present in the body fluids or tissues [7]. Cancer biomarkers can be divided into invasive biomarkers which can be detected in tissue biopsies and non-invasive biomarkers which can be detected in liquid biopsies [11]. Liquid biopsies involve the sampling and analyzing of non-solid biological samples (like blood, sputum, saliva, sweat, and urine) potentially containing cancer related material, and they help in discovering a wide range of information about any tumors in a simple and non-invasive way. Non-invasive biomarkers, as the cancer related material, are usually preferred because the samples in which they are found are easy to collect and suitable not only for diagnosis but also for monitoring follow-up treatment progression [7]. **Fig. 1-2** provides examples of non-invasive biomarkers: biomolecular structures (proteins, enzymes, antibodies, metabolites,

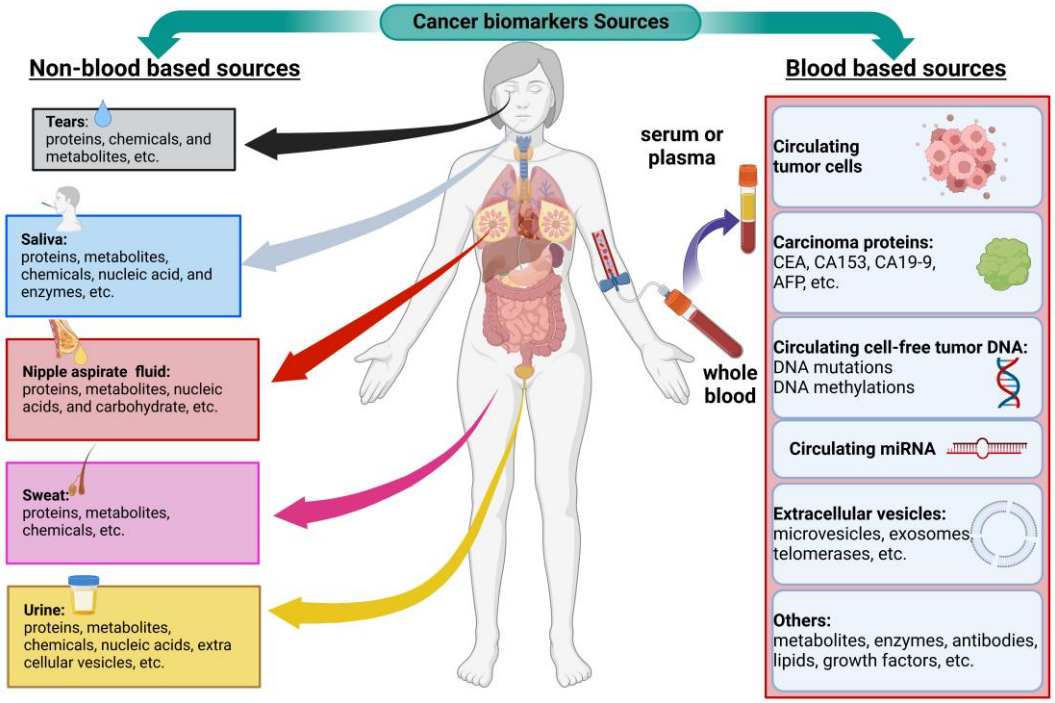

Fig. 1- 2 Overview of main sources of different types of non-invasive biomarkers.

lipids, growth factors, nucleic acids like RNA, miRNA, and DNA) and cellular structures (extracellular vessels, circulating tumor cells, and circulating cancer stem cells) [12] that can be found in different body fluids. Cancer biomarkers have been determined by different instrumental methods: colorimetric [13-16], fluorescence [17-19], electrochemical methods [20-24], enzyme-linked immunosorbent assay (ELISA) [25-27], chemiluminescence (CL) [28, 29], electrochemiluminescence (ECL) [30-34], surface plasmon resonance (SPR) [35-37], surface enhanced Raman spectroscopy (SERS) [37-42], polymerase chain reaction (PCR) [43-45] methods. However, these methods require complex protocols that are time-consuming and that require expensive, bulky, and sophisticated equipment, and they consume high amounts of reagents; all these disadvantages make them generally unsuitable for use, especially in developing countries. Overcoming these disadvantages and developing accurate, portable, simple, and low-cost devices that can be used for the detection of cancer biomarkers currently is a global challenge, and paper-based analytical devices (PADs) are one of the most attractive approaches to meeting this challenge. PADs or microfluidic paper-based analytical devices (μPADs) opened a new era to introduce new point-of-need (PON) devices in different fields such as environmental monitoring [46-49], food safety [50-53], and clinical diagnostics for cancer and other diseases [16, 46, 54-60]. This chapter summarizes the current status of PADs for cancer diagnosis. It adds to the literature that includes reviews taking a general perspective [61-63]; or reviews focusing on: functionalization of the paper substrate [64]; different PAD configurations and design (LFAs, 2D and 3D μPADs) [65]; sensing techniques such as colorimetry [16] or electrochemical [66] detection; and specific applications such as detection of bacteria and viruses [55], detection of food contaminants [67], food safety and quality analysis [68], personalized health care [69], and crime scene investigation [70]. This chapter discusses the different PADs used for cancer biomarker detection in detail through discussing the different paper substrates used and their surface modifications, the different configurations

of PADs and their fabrication methods, assay principles, recognition elements and modifications, sensing techniques, and improvement methods for the produced signal.

1.3 Paper-based analytical devices (PADs) and their fabrication methods

Since the pioneering report from Whitesides' group in 2007 introducing paper-based bioassays by using a photoresist to pattern microfluidic channels and detection zones on chromatography paper [4], PADs have attracted huge interest because of the worldwide availability of paper, the existence of different and easy methods for paper patterning, and most importantly, the ability of paper to manipulate flow of samples and reagents and to carry out chemical and biochemical reactions without the need for external pumps [62].

The PADs are mainly fabricated by bonding a hydrophobic barrier on a hydrophilic substrate as well-defined microchannels to manipulate samples and reagents. Broadly speaking, the 'paper' in PADs is defined as a porous membrane that drives fluids by capillary force [71] and there are different types of paper substrates including filter paper, chromatographic paper, nitrocellulose membranes, and poly (L-lactic) acid membranes that are used in PADs. Several review articles have provided overviews of the current fabrication status of PADs [71-73] and their potential for commercialization [74]. PAD fabrications have been undertaken using numerous methods. The choose of a suitable substrate and fabrication process depends mainly on the device application, the required sensitivity, the assay steps, and the detection method [62]. Here, first the fabrication techniques that are commonly used to produce PADs for cancer diagnosis are introduced; then the different types of PADs used for cancer diagnosis by the detection of different cancer biomarkers are discussed.

1.3.1 Printing-based fabrication methods for PADs

Various PADs fabrication techniques have been proposed and they can be generally classified into printing and nonprinting methods to pattern hydrophobic microfluidic channels on the paper substrate. One of the promising features found in most printing-based techniques is that the hydrophobic barrier pattern can be simply generated by computer-aided design software such as AutoCAD, CorelDRAW, Illustrator, or AutoPAD [75] and it can be directly printed out using a commercial printer. This allows researchers to generate or revise their design quickly and to fabricate the PADs in a short time at a low cost. In 2009, two different groups [76] became the first to demonstrate the use of a solid wax printer (Xerox ColorQube series) and a hot plate to fabricate PADs. The process consists of printing wax patterns on a paper surface followed by melting the wax into the paper to form the hydrophobic barriers. Due to the simplicity and low-cost advantages of wax printing, it is the most widely used printing method in PAD fabrication even today. Unfortunately, since 2016 the Xerox solid wax printer is no longer commercially available, and researchers have had to seek alternative solutions that follow a similar simple fabrication procedure to wax printing. Methods like laser printing [77, 78], injection printing [79], and thermal transfer printing [80] are practicable approaches to fabricate PADs by low-cost printers in the market.

Screen printing is another commonly used printing method for fabricating PADs. A wax screen printing method was introduced by Dungchai et al. that uses a custom-made nylon screen as a mask to transfer the wax pattern onto a filter paper [81]. Then the filter paper with printed wax is heated on a hot plate to form the hydrophobic barrier. In addition to wax, polydimethylsiloxane [82] and polystyrene [83] can also be used as the hydrophobic barrier polymer for PAD fabrication by screen printing. Screen printing is an inexpensive fabrication method, and it is also applicable to mass production. Printing screens are broadly available

worldwide and cost less than US$ 5 per 100 cm^2 [81]. The no printer requirement makes screen printing method more accessible for researchers to produce PADs with few facility constraints.

1.3.2 Nonprinting-based fabrication methods for PADs

Compared to printer-based methods that commonly use a printer to transfer hydrophobic barrier layouts onto a paper substrate, nonprinting-based fabrication methods normally use master molds, stamps, or masks to create a fluid constraint barrier on the substrate. One highly-recognized work in 2007 that spurred PADs development was based on a photolithography process [4]. This process starts with UV exposure of the photoresist (e.g., SU-8) impregnated paper followed by baking and developing procedures to form the hydrophobic barrier patterns on the paper substrate. Photolithography is advantageous for its high resolution and dimensional stability while wax-based hydrophobic barrier printing methods usually suffer from resolution loss due to lateral spreading after the hot plate heating step.

A major drawback of photolithography is that it is expensive and requires photoresists, organic solvents, and photolithography facilities. Intensive training to operate the photolithography apparatus in a cleanroom environment is also required, another big drawback. On the other hand, a cutting method is a relatively simpler and cheaper nonprinting fabrication approach for PADs compared to photolithography. The paper is simply cut into the desired shape that geometrically constrains and guides the fluid flow inside the paper. Craft cutters [84, 85] and lasers [86, 87] are commonly cutting tools in this PAD fabrication method. Compared to all of the aforementioned printing and non-printing methods that require tools to transfer the pattern onto paper. direct drawing by hand is the most straightforward approach that allows rapid production at a low cost. Graphite pencils were used to hand-draw an electrode on a paper

for biosensing applications [88]. For PADs, a wax pen [89] or a brush soaked with polystyrene solution [90] has been used to form hydrophobic barriers on paper by hand drawing.

1.4 Paper-based devices for cancer diagnosis

Cancer biomarkers have been determined using various types of 2D, 3D, and hybrid PADs based on different assays principles such as sandwich immunoassays, aptamer-antigen interactions, and RNA and DNA hybridizations. As detection techniques colorimetric, luminescence, and electrochemical approaches have been used. To improve the sensitivity, specificity, and detection limits, different modifications have been done for the paper substrates, recognition elements, and PAD designs. In this section, the different PADs and detection techniques used, and the advantages and disadvantages of each type are discussed.

1.4.1 Colorimetric methods

Colorimetric detection methods form the most widely used technique group in μPADs [16, 62, 91-93]; they are based on the appearance of color in the presence of the analyte of interest. The sharp contrast between the white background of the paper substrate and the produced color provides a good signal-to-noise ratio. The colorimetric signals can be detected visually by the naked eye for qualitative and semi-quantitative measurements, or they can be detected with simple equipment for quantitative measurements. There are different types of colorimetric PADs used like spot tests, dipsticks, lateral flow assays (LFAs), and 2D and 3D μPADs. Dipsticks are generally not used for cancer diagnosis, maybe because they need a relatively large sample volume to allow dipping of the device and such a volume is not commonly available in liquid biopsies therefore, dipsticks are explained only briefly, and other types of colorimetric paper-based devices are discussed in detail.

1.4.1.1 Dipstick assays

Dipsticks are simple PADs: a paper strip is impregnated with a probe which can change its color in the presence of the target species. The end of the strip impregnated with the detection probe is dipped into the sample to react with it and produce color or change the probe color [94]. The most common dipsticks are the urine test strips that are used nowadays for simultaneous multiple species screening in urine and for monitoring of different organ disorders like diabetes, hydration state, and kidney diseases [95]. While dipsticks are easy to fabricate, use, and analyze the results by the naked eye, making them suitable for emergency use, they give only qualitative or semi-quantitative information, and they have low accuracy and precision, making them unsuitable for follow-up use [95, 96].

1.4.1.2 Spot tests

A spot test for copper was introduced by West [97] in 1945. The test determined metal ions by drying reagents on a paper without any boundaries to control the liquid flow. After introducing the concept of patterning the paper with hydrophobic materials, spot tests came to be used in many different fields and applications [16, 62, 93]. Most cancer biomarker determination techniques depend on typical antibody-antigen interactions. Spot tests are implemented on simple μPAD devices which consist of a hydrophilic circular zone containing dried reactants, and a sample containing the target analyte is added to the circular zone. To control the reagents and sample flow, the circular reaction zone can be surrounded by a hydrophobic barrier or just separated by cutting. In 2014, Song's group used screen printing to fabricate a microzone plate immunosensor for determination of carcinoembryonic antigen (CEA) [98]. Primary antibody was immobilized on the paper zone using chitosan and porous gold to capture the CEA antigen, and $ZnFe_2O_4$-multiwalled carbon nanotubes ($ZnFe_2O_4$@MWCNTs) labeled antibody was used as a recognition element by which the $ZnFe_2O_4$@MWCNTs catalyzed the 3,3',5,5'-tetramethylbenzidine (TMB) oxidation by H_2O_2

to produce a blue color (**Fig. 1-3A**)[98]. As a simple fabrication method, hand drawing on filter paper using polystyrene dissolved in toluene was used to fabricate a microzone plate for CEA immunoassay (**Fig. 1-3B**) [90]. Wax printing was used by Mazzu-Nascimento et al. [99] to develop a paper-based microwell plate for the determination of CEA in serum based on the biotin-avidin peroxidase catalyzed oxidation of TMB. To assess and improve the test accuracy, sensitivity, and prevent false results and misleading outcomes, Mazzu-Nascimento et al. used Youden's J index statistical analysis to evaluate the assay cut-off value. Using the same wax printing fabrication method, in a different report, Mazzu-Nascimento et al. [100] determined sarcosine in urine as a prostate cancer biomarker based on a double enzymatic reaction using sarcosine oxidase (Sox) and horseradish peroxidase (HRP). By modifying the paper surface with positively charged poly(allylamine hydrochloride) (PAH), the enzyme was concentrated on the surface with the result of color enhancement and improved sensitivity (**Fig. 1-3C**) [101].

Also in the colorimetric detection of biomarkers, nanostructures were used for color enhancement and improved assay sensitivity; gold nanoparticles (AuNPs) were used as the antibody label for enhancing the color intensity change in different assays based on: their SPR change [102], their peroxidase-like activity [103], their ability to induce the deposition of Au-Ag nanoparticles[104], and their catalytic activity toward azo-dye degradation [105]. Nanocomposites attached to detection Ab were used to mimic the peroxidase catalytic activity by which the sensitivity of CEA immune assay was improved (**Fig. 1-3B**) [90]. Dual surfactant capped silver nanoparticles (AgNPs) have been employed for determination of citrate in urine as a prostate cancer biomarker with high selectivity, using just naked-eye readout [106]. Surface functionalized cellulose paper has been used to determine telomerase in a cell extract based on its catalytic activity for telomere elongation, and methylene blue was used as the colorimetric probe [107].

Another way to enhance the colorimetric signal is by changing the paper substrate. While nitrocellulose (NC) membranes have been commonly used for colorimetric determination of different biomarkers [102-104], a porous poly(L-lactic) acid nanofiber (p-PLLA) membrane was introduced as a paper substrate for AFP determination; compared to NC, p-PLLA has a lower background leading to better sensitivity [108]. Finally, spot test devices are easy to fabricate and easy to use, and there is no need to combine different paper substrates or membranes. But the devices are inappropriate when sequential delivery of reagents is needed, and when the assay needs multiple steps in strict sequence to be implemented on the device.

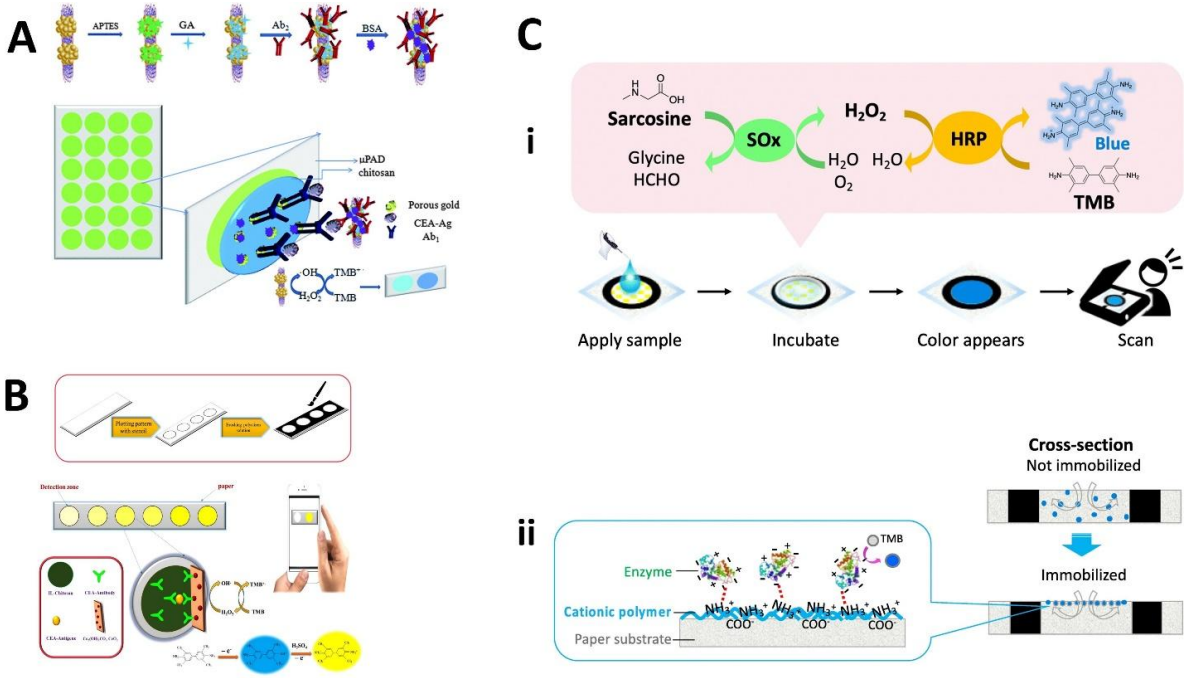

Fig. 1- 3 Schematic representation for fabricated paper-based colorimetric immunosensor for CEA. Reprinted from ref [98] with permission from the Royal Society of Chemistry, Copyright 2014. (B) Schematic representation of hand drawing to fabricate a polystyrene patterned paper device for CEA determination and illustration for the assay procedure. Reprinted from ref [90] with permission from Elsevier, Copyright 2018. (C) (i) Illustration for sarcosine determination principle using double enzymatic technique and steps of the assay. (ii) Mechanism of color enhancement using cationic polymer. Reprinted from ref [101] with permission from Springer Nature, Copyright 2021.

1.4.1.3 Lateral flow assays

Lateral flow assays (LFA) are one of the most popular techniques for PON devices. LFA devices are inexpensive, portable, and easy to use for in situ applications. The most common commercial LFA devices are pregnancy test devices and Covid-19 antigen test kits; the latter have been invaluable tools for rapid diagnosis of positive cases at home (rather than having to go to a medical facility) which has helped in decreasing the virus spread and mitigating the Covid-19 pandemic. Mainly LFA devices consist of a sample pad, conjugation pad, NC membrane, and absorption pad. These four parts are cut in strip shapes and connected to each other to provide one-dimensional flow (**Fig. 1-4A**) [62, 109]. The sample containing the target is introduced to the sample pad, then flows through the conjugation pad and reacts with the recognition probe. Then the target-conjugated probe complex flows through the NC membrane which contains two lines, the first one is the test line which contains immobilized antibody specific for the target, and the second line is the control line which contains immobilized antibody specific for the probe. The sample continues flowing to the absorption pad to remove the excess sample and the unreacted probe. In the case of a positive sample, both test and control lines produce a visible signal, while in a negative sample case, only the control line produces a visible signal.

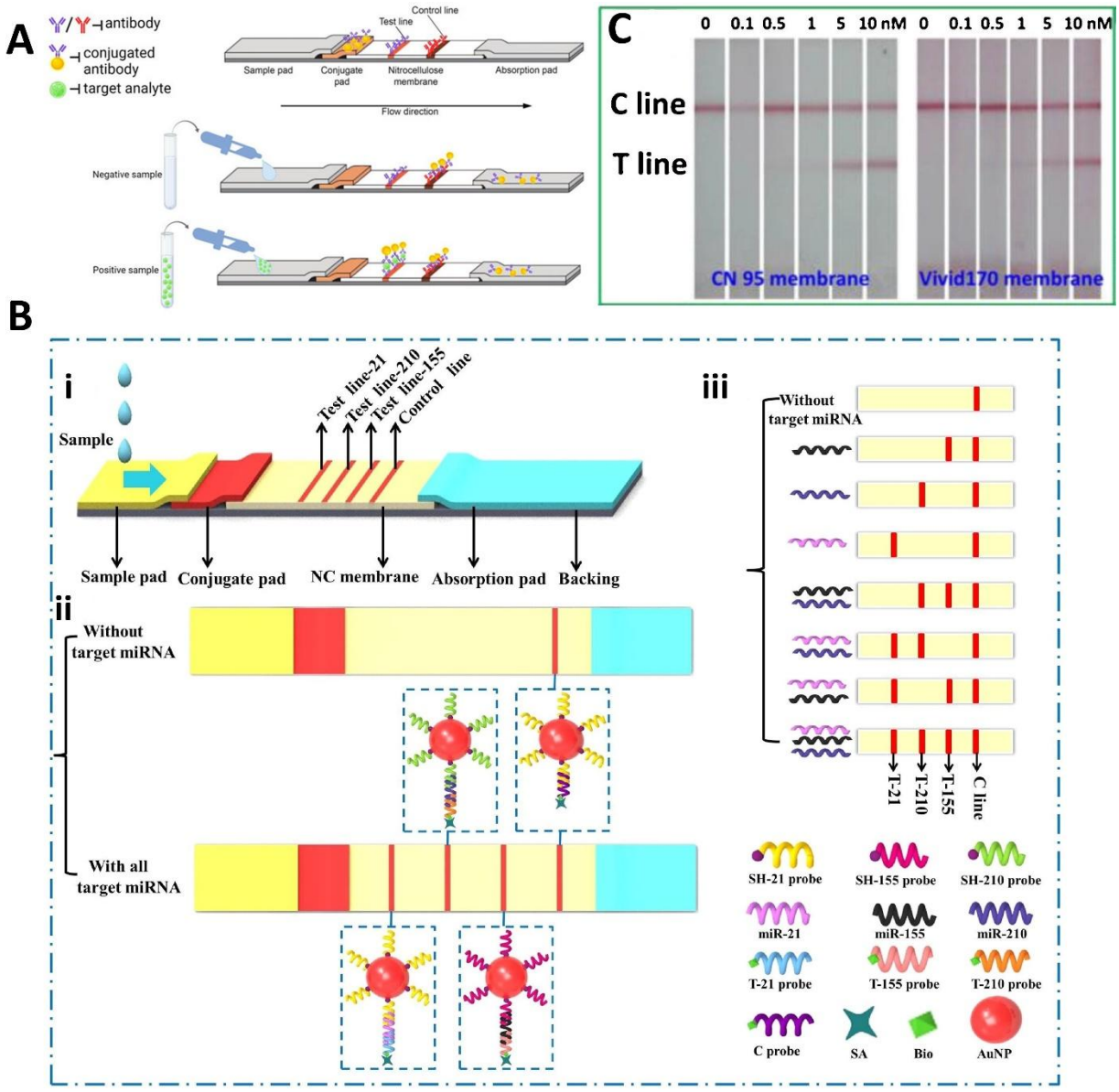

Fig. 1- 4 (A) Schematic representation of a typical LFA and illustration for the sample flow and assay procedure. Reprinted from ref [109]. Published by Frontiers with Open access CC-BY 4.0, Copyright 2022. (B) i: schematic illustration of LFA device for simultaneous determination of multiple miRNAs, ii: with and without miRNA, iii: the principle for detection of multiple miRNAs on the LFA device. Reprinted from ref [110] with permission from Elsevier, Copyright 2018. (C) NC membranes with different pore sizes affect the AuNPs-DNA migration. Reprinted from ref [110] with permission from Elsevier, Copyright 2018.

Primarily, LFA is used in qualitative analysis by visually observing whether or not the test line produces a signal like the control line. During the last few decades, researchers have developed LFA devices to be used for quantitative analysis by correlating the produced test line signal to the concentration of the target in the sample. Presently, LFA serves as the base for various PAD devices [62], and it is used in different applications including food safety [111, 112], virus diagnosis [113], hormone [114], and cancer biomarker [16, 115, 116] detections. Improving the LFA performance for quantitative and qualitative analyses depends mainly on improving the test line colorimetric signal produced on the membrane. Several approaches have been reported like modifying the membrane surface in the test and control lines, modifying the recognition element in the assay by using different nanoparticles, and improving the target capturing efficiency. Liu's group developed an LFA device for determination of miRNA-215 based on a sandwich type nucleic acid hybridization reaction using an AuNP labeled DNA probe (abbreviated as DNA-miRNA-DNA/AuNPs) [117]. The accumulation of AuNPs on the test line produces a visible colorimetric signal which is visually compared with the control line for qualitative analysis or measured using a portable strip reader for quantitative analysis. Using the same approach, Zheng et al. [110] developed an LFA device for simultaneous determination of three miRNAs, the NC membrane contained three test lines for miRNA-21, miRNA-210, and miRNA-155 (**Fig 1-4B**); moreover, they found that the pore size of the NC membrane affects the migration rate of the AuNP-DNA conjugates and this affects the assay sensitivity and detection limit (**Fig 1-4C**) [110]. By separating the NC membrane with a wax line along its length to form two detection zones, two bladder cancer biomarkers, nuclear matrix protein 22 (NMP22) and bladder tumor antigen (BTA), in urine were detected simultaneously [118]. Another LFA device for qualitative detection of lysophosphatidic acid (LPA) as an ovarian cancer biomarker was developed based on a lock and key strategy (**Fig. 1-5**). Inserting LPA into polydiacetylenes (PDAs) blocks changes the gap between the lowest

unoccupied molecular orbital and the highest occupied molecular orbital (LUMO-HOMO gap) leading to a color change of the test zone from blue to red (**Fig. 1-5A**) [119].

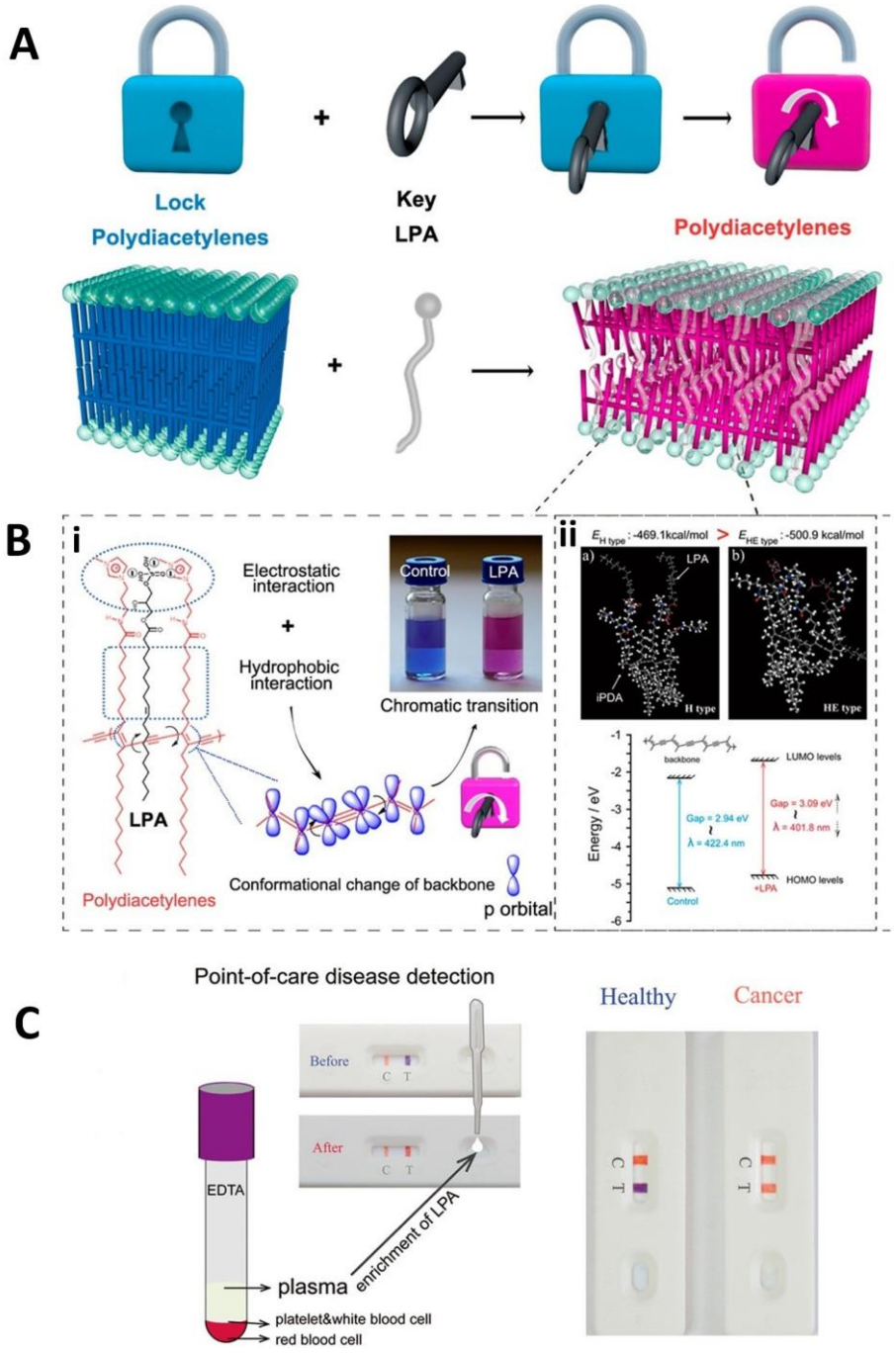

Fig. 1- 5 (A) Illustration of the lock and key concept of LPA and PDA, (B) i: Interaction between LPA and PDA, ii: simulation for binding modes between LPA and PDA, (C) schematic illustration of LFA device for LPA detection. Reprinted from ref [119] with permission from the American Chemical Society, Copyright 2017.

Sene et al. [120] developed an LFA device for determination of Interleukin 6 (IL-6) biomarker in plasma based on sandwich immunoassay; they used AuNPs labeled antibody as recognition element, the colorimetric signal produced due to the accumulation of AuNPs on the test line recorded by digital camera and the color intensity was correlated to IL-6 concentration. Human epidermal growth factor receptor 2 (HER2) has been determined in human serum using AuNPs/aptamer modified with a biotin complex on an LFA device; the test line was treated with streptavidin to catch the biotin modified aptamer, while the control zone was treated with polycation polymer to catch the AuNPs [121].

A synthetic cancer biomarker has been used for indirect determination of matrix metalloproteinase 9 (MMP9) as a colorectal cancer biomarker through the injection of a patient with MMP-sensitive iron oxide NPs conjugated with substrate-reporter tandem protein; the MMPs cleave the reporter, releasing it into the urine (**Fig. 1-6A i**) [122]. The reporter is determined in the collected urine using a colorimetric LFA based on the sandwich complex technique, whereby a captured antibody is immobilized on the NC membrane to capture the reporter from the sample, then streptavidin-AuNPs detection reagent becomes attached to the captured reporter producing a colored line on the membrane for which the integrated intensity is related to the reporter concentration (**Figs. 1-6A ii, iii**) [122].

The capturing efficiency of the target is one of the important factors for improving the LFA performance which is affected by the flow speed of the target on the membrane. A magnetic focus lateral flow sensor (mLFS) was developed for the determination of Valosin-containing protein (VCP) as a cervical cancer biomarker. The device uses Fe_3O_4 core/Au shell magnetic nanoparticles labeled antibodies as a colorimetric probe. The flow speed of the target can be slowed down by using a simple magnet which provides a longer residence time for the target-probe on the detection zone; this results in more biomarkers being captured and, therefore, a more intense colorimetric signal (**Fig. 1-6B**) [123]. A549 exosome as a human lung

cancer biomarker was quantitatively determined by competitive LFA using the AuNP labeled CD63 aptamer probe, in which the color of the test zone is inversely proportional to the exosome presence; the AuNP probe is first captured on the test zone producing a colorimetric signal which will disappear in the presence of exosome resulting in a decrease of the test zone color intensity [124]. Huang et al. [125] used self-assembled AuNPs networks to enhance the colorimetric signal in the test line and they significantly improved the sensitivity by providing multiple reaction cycles with the assembled AuNPs.

Even though LFA devices are popular and easy to use, generally they work best for qualitative analysis, and they suffer from such drawbacks as cross-reactivity which leads to false negatives and positive results [126]. In addition, LFA devices require connection of different membranes in the correct form and the construction process needs consideration of many different parameters [102]. Also, LFA devices have only one-dimensional reagent flow and they cannot manipulate complex fluidic properties in multiple dimensions. Moreover, the inability to provide sequential addition of reagents and washing steps affects the reproducibility and sensitivity of paper-based immunoassays [127].

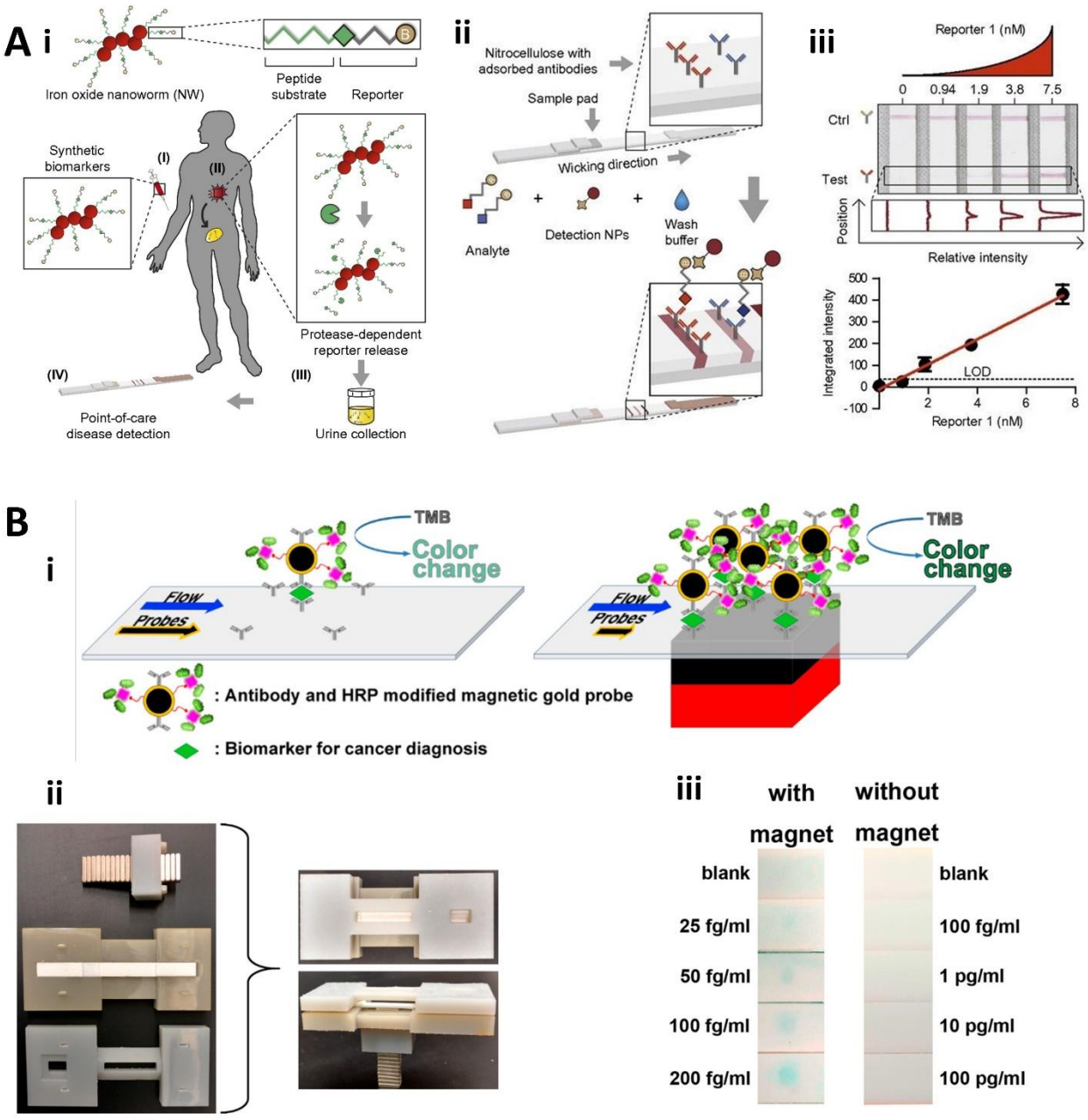

Fig. 1- 6 (A) i: MMP-sensitive iron oxide NPs conjugated to substrate-reporter tandem protein and the cycle of how it is used as a cancer biomarker in urine, ii: the colorimetric LFA for the determination of the reporter protein, and iii: an image of the LFA membrane showing a linear increase in the test zone intensity with the reporter concentration. Reprinted from ref [122]. Published under the exclusive PNAS License to Publish, Copyright 2014. (B) i: Illustration of mLFS concept, how the magnet slows the magnetic probe speed to improve the capturing efficiency, ii: digital image of 3D printed kit for the mLFS device, and iii: digital images of

mLFS membrane that demonstrate how the magnet improves the colorimetric signal produced. Reprinted from ref [123] with permission from the American Chemical Society, Copyright 2019.

1.4.1.4 Multidirectional flow 2D, 3D, and hybrid µPADs

Multidirectional flow µPADs have several advantages over spot test and LFA devices, where µPADs can manipulate fluidic flow in multiple directions making them suitable for simultaneous determination of multiple species. Also, µPADs can provide sequential addition of reagents and washing steps which leads to decreased cross reactivity and improved assay sensitivity [16, 62]. These advantages come from the ability to easily fabricate devices with multiple channels and reaction zones; for example, fabrication of 2D and 3D µPADs by combining several paper layers with different patterns.

The first 2D µPAD was introduced by Whiteside's group for determination of glucose and it had chromatographic paper patterned using a photoresist [4]. While 2D µPADs are formed from only one layer and offer fluidic flow only horizontally in different directions, 3D µPADs offer vertical fluidic flow between different layers making them more suitable for multistep assays. 3D µPADs can be fabricated by bending, twisting, folding, and stacking of 2D layers [62, 128]. The main problem that can affect the accuracy of the 3D µPADs is the misalignment of their paper layers which can be overcome by origami techniques [62, 129]. Both 2D and 3D µPADs are applied in applications for quantitative analysis based on their manipulability in washing and multistep assays.

There are several colorimetric devices used for cancer biomarker detection. A semi quantitative distance-based device for determination of CEA in serum was introduced by Chen et al. [130]. Their device consists of one circular reaction zone and one channel and it is fabricated by cutting chromatographic paper. The assay is based on washing out unreacted HRP

labeled antibody from the reaction zone into the channel containing TMB substrate to produce a blue color, so increasing the CEA concentration leads to a smaller amount of unreacted antibody and a shorter colored distance in the channel.

Mesgari et al. [131] used laser cutting to fabricate 2D μPAD consisting of two circular zones connected with one channel for cytochrome c (Cyt c) determination; the two separated zones facilitate the sequential multi-step reaction. Using the same fabrication technique, another device containing two detection zones, one for target and the other one for a reference was fabricated for determination of citrate as prostate cancer biomarker [132]. By adding a second zone, in the middle before the detection zone (**Fig. 1-7A**), the detection probe is kept separately from the sample and other reagents until start of the assay for miRNA-21 determination [133]. PSA was determined in serum with the 2D μPAD fabricated by using hydrophobic ink to plot a pattern on chromatographic paper and AuNP labeled antibody as recognition element to produce a colorimetric signal [134]. in a case where washing steps were important for improving the sensitivity, Liu et al. [135] introduced a ring-oven washing technique (**Fig. 1-7B**) which improved the detection limit for sandwich immunoassay determination of CEA to 0.03 ng mL^{-1} from the detection limit of the conventional washing technique of 0.5 ng mL^{-1}.

Another simple 3D μPAD for simultaneous determination of CEA and AFP was fabricated using wax printing [136]. This device had two stacked layers (**Fig. 1-7C**): the first layer included the central zone for introducing the recognition probe (Pd/Fe_3O_4@C NPs) connected to the reaction zones which contained capturing antibodies, and the second layer had detection zones which contained the colorimetric substrate. When the two layers were stacked, reaction zones were formed. Another 3D μPAD was developed for CEA quantification. The device contained a rotatable detection layer allowing switching between flow and storing states and also switching between reaction and washing states (**Fig. 1-7D**) [137].

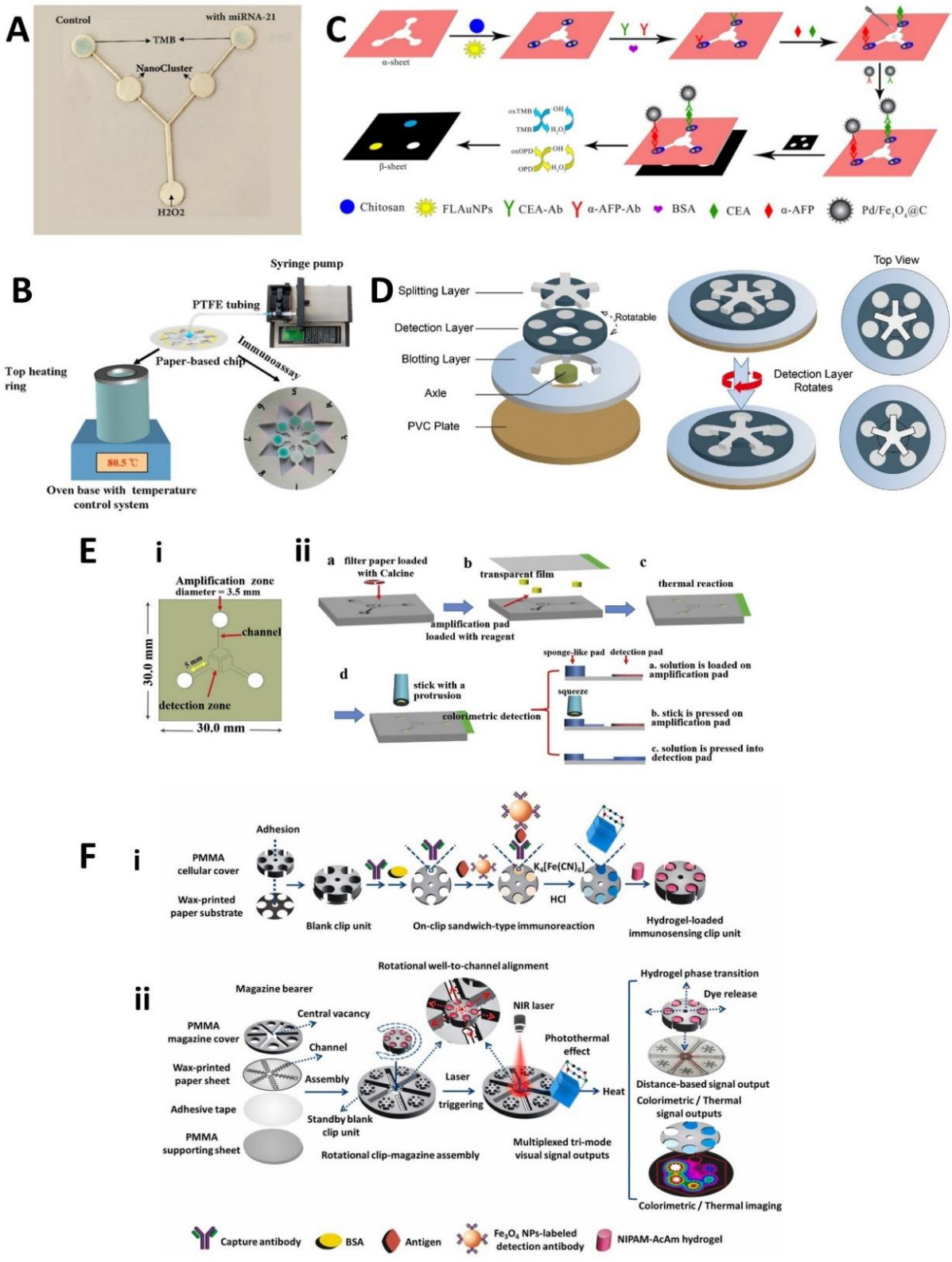

Fig. 1- 7 (A) 2D μPAD consisting of several zones for reaction and storing of the probe and reagents until starting the assay. Reprinted from ref [133] with permission from Elsevier,

Copyright 2020. (B) Illustration for the ring-oven washing technique for 2D μPAD to improve the immunoassay sensitivity. Reprinted from ref [135] with permission from the American Chemical Society, Copyright 2015. (C) 3D μPAD consisting of two wax-printed paper layers for simultaneous determination of CEA and AFP. Reprinted from ref [136] with permission from Elsevier, Copyright 2015. (D) Illustration of the 3D μPAD containing a rotatable detection layer that can switch between flow and storing states. Reprinted from ref [137] with permission from Springer Nature, Copyright 2020. (E) i: Chip design, ii: illustration for hybrid PVA/paper μPAD for detection of PCA3 using RT-LAMP. Reprinted from ref [138] with permission from Elsevier, Copyright 2020. (F) Schematic illustration of the hybrid PMMA/paper device for PSA detection. i: Sandwich immunoassay steps, ii: device assembly and tri-mode quantitative measurement using colorimetric, distance, and thermal imaging. Reprinted from ref [139] with permission from Elsevier, Copyright 2020.

Hybrid μPADs systems are composed of paper with other materials like plastic, glass, poly methyl methacrylate (PMMA), and poly dimethyl siloxane (PDMS), which makes them versatile and superior platforms that can take the advantages of each material and avoid its limitations [140, 141]. A 3D printed module combined with chromatographic paper and a sponge-like polyvinyl alcohol (PVA) pad was developed for determination of prostate cancer antigen 3 (PCA3) using reverse transcription loop-mediated isothermal amplification (RT-LAMP) (**Fig. 1-7E**). Sponge pad was used in the thermal mode for amplification and then pressed to diffuse the product to the detection paper pad which contained chromogenic reagents [138]. Moreover, another of the big advantages of hybrid devices is the ability to measure multiple signals using the same device. Fu et al. [139] developed a PMMA/paper hybrid device (**Fig. 1-7F**) for detection of PSA in serum using immunoassay reaction. The device uses tri-mode visual outputs and it can determine the concentration of PSA based on colorimetric,

distance, or thermal imaging. A pumpless hybrid μPAD for thioredoxin-1 detection as a breast cancer biomarker was developed by Lee et al. [142]. Their device can automatically manipulate sequential addition of reagents and washing steps.

As described above, colorimetric based PADs are very popular for detection of cancer biomarkers and many devices have been reported; a summary of devices and performance values is given in **Table 1-1**. signals of colorimetric PADs are easily detected by the naked eye, or by simple equipment like a smartphone, digital camera, or scanner for quantitative analysis, but the devices have some drawbacks: they have high background noise leading to low sensitivity, they have a narrow dynamic range, and they are easily affected by external factors like surrounding light, reagent colors, and sample colors [16, 62].

Table 1- 1 Colorimetric paper-based microfluidic sensors for detection of cancer biomarkers.

Biomarker	Type	Organ	Sample	Type of PAD	Substrate	Fabrication[a]	Assay type	Recognition element	Detection system	Linear Range	LOD	Ref.
A549 NSCLC exosomes	**Extracellular vesicles**	**Lung**	Cell culture	LFA	NC membrane	Cutting	Competitive aptamer assay	AuNP labeled CD63's aptamer	Deaccumulation of AuNPs	_	Qualitative	[124]
AFP	**Protein**	**Liver**	Synthetic serum	Spot test	NC membrane	Pretreat the membrane with BSA then spot the reagents	Antigen-Antibody interaction	AuNP-Cys labeled Ab	Change in NPs SPR because of antigen interaction	0.1- 100 ng/mL	1.054 ng/mL	[102]
			Serum	Spot test	p-PLLA membrane	Cutting	Sandwich Immunoassay	AuNP labeled Ab	Increasing colored AuNP amount by increasing AFP concentration	10-400 ng/mL	_	[108]
			Serum	Spot test	p-PLLA membrane	Cutting	Sandwich Immunoassay	AuNP labeled Ab	Fluorescence quenching	0.01-400 ng/mL	0.17 pg/mL	[108]
			Serum	3D-μPADs	Chromatography paper	Wax printing	Sandwich immunoassay	Peroxidase-like activity Pd/Fe_3O_4@C NPs labeled Ab	OPD- H_2O_2	0.005-30 ng/mL	1.7 pg/mL	[136]
BTA	**Protein**	**Bladder**	Urine	LFA	NC membrane	Cutting + wax printing	Sandwich immunoassay	Colloidal Au labeled Ab	Accumulation of Au particles	_	Qualitative	[118]
CA125	**Protein**	**Ovarian**	Serum	Spot test	Glass-supported NC membrane	_	Sandwich Immunoassay	AuNP labeled Ab	Inducing silver deposition	Up to 1000 U/mL	30 U/mL	[104]
CEA	**Protein**	**Several organs**	Serum	Spot test	Chromatography paper	Screen printing	Sandwich Immunoassay	$ZnFe_2O_4$@MWNTs labeled Ab	TMB- H_2O_2	0.005–30 ng/mL	2.6 pg/mL	[98]
			Serum	Spot test	Chromatography paper	Wax printing	Sandwich Immunoassay	Biotin-peroxidase-avidin conjugate labeled Ab	TMB- H_2O_2	_	_	[99]
			Serum	Spot test	Filter paper	Stencil and hand drawing	Sandwich Immunoassay	$Co_2(OH)_2CO_3$-CeO_2 nanocomposite labeled Ab	TMB- H_2O_2	0.002 – 75 ng/mL	0.51 pg/mL	[90]
			Serum	2D-μPADs	Filter paper	Cutting	Sandwich immunoassay	HRP labeled Ab	TMB- H_2O_2	0.1 – 20 ng/mL	0.03 ng/mL	[135]
			Serum	2D-μPADs	Chromatography paper	Cutting	Sandwich immunoassay	HRP labeled Ab	TMB- H_2O_2	_	2 ng/mL	[130]
			Serum	3D-μPADs	Chromatography paper	Wax printing	Sandwich immunoassay	Peroxidase like activity Pd/Fe_3O_4@C NPs labeled Ab	TMB- H_2O_2	0.005-30 ng/mL	1.7 pg/mL	[136]
			Serum	3D-μPADs	Chromatography paper	Wax printing	Sandwich immunoassay	HRP labeled Ab	TMB- H_2O_2	0.5 – 70 ng/mL	0.015 ng/mL	[137]
			Serum	LFA	NC membrane	Cutting	Sandwich immunoassay	AuNP labeled Ab	Self-assembly of network AuNPs	0.1 fg/mL – 10 ng/mL	10 pg/mL	[125]
Citrate	**Small molecule**	**Prostate**	Urine	Spot test	Filter paper	Laser printing of waxy ink	NPs aggregation	Dual surfactant capped AgNPs	Aggregation of AgNPs	_	25 μM	[106]
			Urine	2D-μPADs	Filter paper	Cutting	Peroxidase-like activity of Cys-AuNCs	Cys-AuNCs	Inhibiting the peroxidase activity of Cys-AuNCs	1.0 μM -10 mM	0.4 μM	[132]
Cyt c	**Protein**	**Several organs**	Serum	2D-μPADs	Filter paper	Cutting	Peroxidase-like activity of β-$Co(OH)_2$ CMK	β-$Co(OH)_2$ CMK labeled DNA aptamer against Cyt c	Catalyzing TMB- H_2O_2 oxidation	50 nM – 1.0 mM	1.0 nM	[131]
HER2	**Protein**	**Breast**	Serum	LFA	NC membrane	Cutting	Aptamer based assay	Aptamer/AuNPs complex	Accumulation of AuNPs	0 -50 nM	24 nM	[121]
IL-6	**Cytokine (protein)**	**Several organs**	Plasma	LFA	NC membrane	Cutting	Sandwich immunoassay	AuNP labeled Ab	Accumulation of AuNPs	1.25 – 9000 ng/mL	0.38 ng/mL	[120]
LPA	**Phospholipid**	**Ovarian**	plasma	LFA	NC membrane	Cutting	Lock-key strategy,	Polydiacetylenes (PDAs)-based probe	Color change due to LUMO–HOMO gap change	_	Qualitative	[119]

	derivative						inserting LPA "key" into the PDAs "lock"					
miRNA-155	**Nucleic acid**	**Several organs**	Spiked Serum	LFA	NC membrane	Cutting	Sandwich nucleic acid hybridization reaction "ssDNA-microRNA-ssDNA/AuNPs"	AuNP labeled DNA	Accumulation of AuNPs	0.01 – 5 nM	0.007 nM	[110]
miRNA-21	**Nucleic acid**	**Several organs**	Spiked Serum	LFA	NC membrane	Cutting	Sandwich nucleic acid hybridization reaction "ssDNA-microRNA-ssDNA/AuNPs"	AuNP labeled DNA	Accumulation of AuNPs	0.1 -10 nM	0.068 nM	[110]
			Serum	2D-µPADs	Filter paper	Cutting	Peroxidase-like activity of Ag/Pt NCs	DNA-Ag/Pt NCs	Inhibiting the Catalytic TMB-H_2O_2 oxidation	1 – 700 pM	0.6 pM	[133]
miRNA-210	**Nucleic acid**	**Several organs**	Serum	LFA	NC membrane	Cutting	Sandwich nucleic acid hybridization reaction "ssDNA-microRNA-ssDNA/AuNPs"	AuNP labeled DNA	Accumulation of AuNPs	0.05 – 10 nM	0.017 nM	[110]
miRNA-215	**Nucleic acid**	**Several organs**	Cell lysate	LFA	NC membrane	Cutting	Sandwich nucleic acid hybridization reaction "DNA-miRNA-DNA/AuNPs"	AuNP labeled DNA	Accumulation of AuNPs	0 – 0.075 nM	60 pM	[117]
MMP9	**Matrix metallo-proteinase**	**Colo-rectal**	Urine	LFA	NC membrane	Cutting	Sandwich complex assay	Streptavidin-AuNPs	Accumulation of AuNPs	1-7 nM	1 nM	[122]
MUC16	**Protein**	**Ovarian**	Synthetic serum	Spot test	NC membrane	Pretreat the membrane with BSA then spotting the reagents	Antigen-antibody interaction	AuNP-Cys labeled Ab	Change in NPs SPR because of antigen interaction	0.1-10 ng/mL	0.413 ng/mL	[102]
NMP22	**Protein**	**Bladder**	Urine	LFA	NC membrane	Cutting + wax printing	Sandwich immunoassay	AuNP labeled Ab	Accumulation of Au particles	_	Qualitative	[118]
$p16^{INK4a}$	**Protein**	**Cervix**	Cervical scrape specimen	Spot test	NC membrane	Cutting	Antigen-antibody interaction	HRP labeled Ab attached to AuNPs	TMB- H_2O_2	_ (Positive or Negative results)	300 cell Hela 300 cell CasKi 3000 cell SiHa	[103]
PCA3	**Nucleic acid**	**Prostate**	_	Hybrid	Chromato-graphy paper	Cutting	RT-LAMP	Calcein	Calcein – pyrophosphate reaction	0.001 – 10 pg/ µL	0.34 fg/µL	[138]
PEAK1	**Enzyme**	**Pancreas**	_	Spot test	Chromato-graphy paper	Photolithography	Sandwich Immunoassay	AuNP labeled Ab	Catalytic degradation of azo dye in presence of $NaBH_4$	1.0 – 10^4 ng/mL	1.0 ng/mL	[105]
PSA	**Protein**	**Prostate**	Serum	2D-µPADs	Chromato-graphy paper	Plotting	Sandwich immunoassay	AuNP labeled Ab	Enlargement of AuNPs	0.5 – 50 µg/L	360.2 ng/L	[134]
			Serum	Hybrid	Filter paper	Wax printing	Sandwich immunoassay	Fe_3O_4 NP labeled Ab	Conversion of iron oxide to Prussian blue	Colorimetry: 3.0–80 ng/mL Distance based: 3.0-60 ng/mL	2.7 & 2.8 ng/mL	[139]
sarcosine	**Amino acid**	**Prostate**	Urine	Spot test	Chromato-graphy paper	Wax printing	Double enzymatic reaction	Sarcosine- SOX-HRP-ABTS	ABTS- H_2O_2	Up to mM	0.21 mM	[100]
			Urine	Spot test	Filter paper	Wax printing	Double enzymatic reaction	Sarcosine-SOX HRP-TMB	TMB- H_2O_2	Up to 10 µM	0.6 µM	[101]
Telomerase	**Enzyme**	**Several Organs**	Hela Cells extract	Spot test	Cellulose paper	Cutting	Enzymatic activity toward	(Oligonucleotides attached to UCNPs for photoluminescence) or	Telomeric elongation then capturing amplification using	_	5 HeLa cells/µL	[107]

							telomeric elongation	Methylene Blue for colorimetry	UCNPs and methylene blue as probes			
Thio-redoxin-1	**Protein**	**Breast**	Serum	Hybrid	NC membrane	Cutting	Sandwich immunoassay	HRP labeled Ab	TMB- H_2O_2	0-200 ng/mL	4.1 ng/mL	[142]
VCP	**Protein**	**Cervix**	Tissue lysate	LFA	NC membrane	Cutting	Sandwich immunoassay	HRP-modified magnetic AuNP labeled Ab	TMB- H_2O_2	_	21.82 fg/mL	[123]

a: Fabrication method mentioned is mainly for patterning the main substrate in the device.

Biomarker abbreviations: NSCLC, non-small cell lung cancer; AFP, alpha-fetoprotein; BTA, bladder tumor antigen; CA125, cancer antigen 125; CEA, carcinoembryonic antigen; Cyt c, cytochrome c; HER2, human epidermal growth factor receptor 2; IL-6, interleukin 6; LPA, lysophosphatidic Acid; miRNA-155, microRNA 155; miRNA-21, microRNA 221; miRNA-210, microRNA 210; miRNA-215, microRNA 215; MMP9, matrix metalloproteinase 9; MUC16, mucin-16; NMP22, nuclear matrix protein 22; PCA3, prostate cancer antigen 3; PEAK1, pseudopodium-enriched atypical kinase one; PSA, prostate specific antigen; VCP, Valosin-containing protein. **Types of PAD and substrate abbreviations:** LFA, lateral flow assays; 2D-μPADs, 2-dimensional microfluidic paper-based analytical devices; 3D-μPADs, 3-dimensional microfluidic paper-based analytical devices; NC, nitrocellulose; p-PLLA, porous poly(L-lactic) acid. **Assay type and recognition element abbreviations:** RT-LAMP, reverse transcription loop-mediated isothermal amplification; AuNP, gold nanoparticles; AgNP, silver nanoparticles; Cys, cysteine; Ab, antibody; HRP, horse radish peroxidase; UCNPs, up-conversion nanoparticles; PDAs, polydiacetylenes; NCs, nanoclusters; SOx, sarcosine oxidase; TMB, 3,3',5,5'-tetrammethylbenzidine; ABTS, 2,2'-azinobis-(3-ethylbenzothiazoline-6-sulfonate); SPR, surface plasmon resonance; ODP, o-phenylenediamine.

1.4.2 Fluorescence methods

Fluorescence became a powerful tool for cancer biomarker detection using PADs due to its high sensitivity and low detection limit compared to the colorimetric methods. These two advantageous features are made possible by decreasing interference through a fluorescence probe "turn on" and "turn off" feature. Fluorescence detection techniques depend on the presence of a fluorescence probe which can be photoexcited and measurement of the emitted fluorescence which can be correlated to the target concentration. Several fluorescent probes have been used for biomarker detection such as metal nanoparticles, nanoclusters, quantum dots, fluorescent organic dyes, and other small fluorescent molecules [143-145]. Improving the fluorescence signal produced from PADs is the main objective for researchers who want to improve the sensitivity of the assays. Several PADs have used fluorescent dye labeled Abs or labeled DNAs as their recognition element for determination of biomarkers [146-150]. Photonic NC substrate fabricated by casting and etching using self-assembled monodispersed SiO_2 nanoparticles (**Fig. 1-8A**) was used for the determination of AFP and CEA, and the fluorescence emitted from the PAD was enhanced by the photonic NC substrate [146]. Also, by changing the diameter of the SiO_2 nanoparticles, the pore size of the photonic NC substrate could be controlled which led to control of the wicking rate of the aqueous solutions. For telomerase detection, modification of a cellulose paper surface using polyamidoamine (PAMAM) dendrimer increased the immobilized TS primer leading to capture of more probes and enhancing the fluorescence signal and sensitivity [148]. Also for determination of miRNA, the fluorescence signal could be enhanced using the duplex-specific nuclease (DSN) amplification technique and fluorophore labeled DNA as a probe (**Fig. 1-8B**) [149].

Another method for amplification of the fluorescence signal is using a secondary Ab labeled with initiator DNA which triggers fluorophore labeled DNA strand hybridization [151]. Nanoparticles, especially quantum dots (QDs), have received more and more interest due to

their unique characteristics such as high fluorescence efficiency, high stock shift, resistance to photobleaching, narrow emission spectra, and simultaneous excitation of multiple fluorescence colors [152-155]. To form highly specific probes, QDs can be attached to Abs [156], DNAs, or aptamers [157-160] specific to the target biomarker. Liang et al. [157, 159] modified a paper surface with graphene oxide that can be used to turn off the QD fluorescence which will be turned on after the target is added which leads to minimized interference (**Fig. 1-8C**) [157]. The fluorescence quenching of the QDs due to ion exchange between dissolved Ag from AgNP labeled detection Ab and CdTe QD was used to detect MMP7 as a renal cancer biomarker (**Fig. 1-8D**) [161]. For CEA detection, Lv et al. [162] used a glutamate dehydrogenase (GDH) functionalized AuNP labeled Ab to generate NH_3 which changed the structure of the NH_2-MIL-125 (Ti) metal organic framework (MOF) impregnated into the paper leading to fluorescence turn on (**Fig. 1-8E**). Fluorescent polystyrene latex particles have been used as a label for detecting Abs for CEA and CA199 biomarkers based on fluorescence scattering [163]. When fluorescence signals are measured in a dark background, fluorescence-based PADs have good sensitivity and a good detection limit, but they have some drawbacks. These include: needing a source for the excitation wavelength such as a UV lamp, UV LED, or a laser source; adding other instrumentation for the sensor; and needing lengthy methods to prepare the fluorescent probes which increase the cost and time for fabrication. Moreover, most papers used have autofluorescent properties that can interfere with the measured fluorescence signal when detecting the analyte. These fluorescence-based PADs and their performance values are summarized in **Table 1-2**.

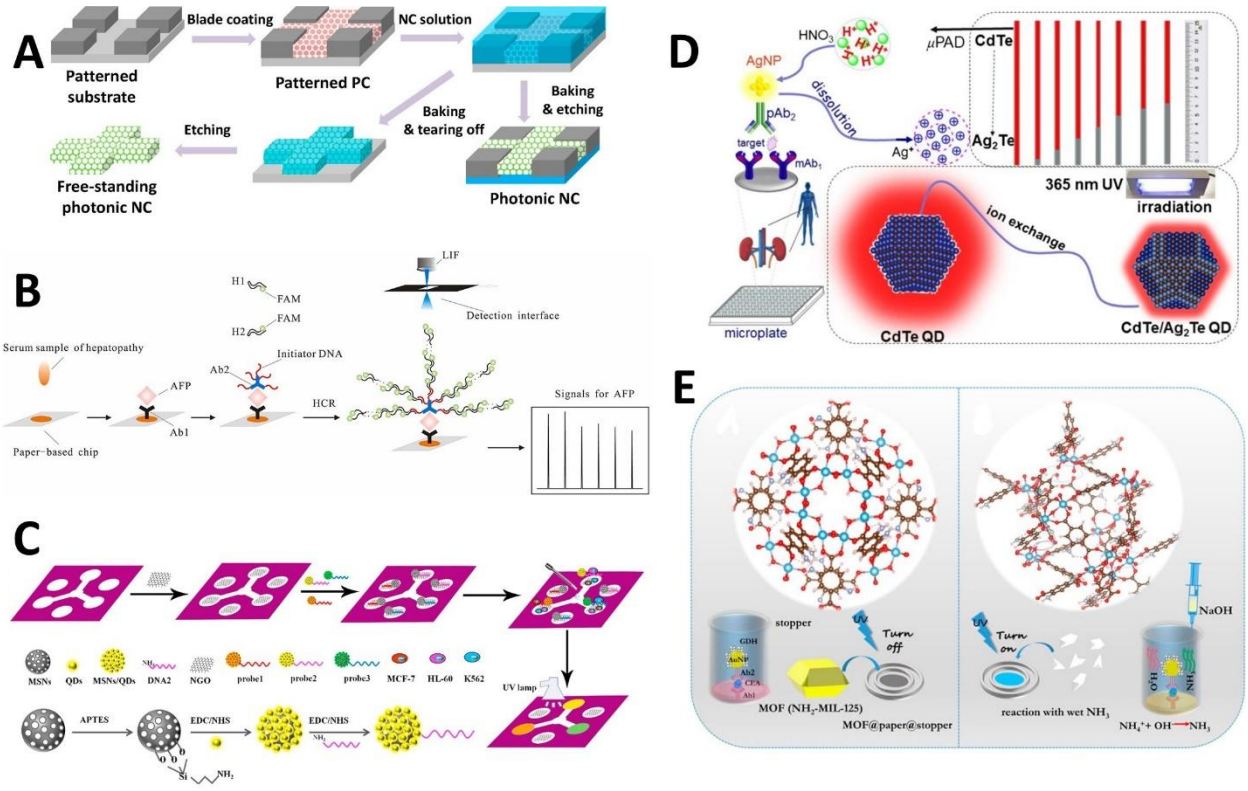

Fig. 1- 8 (A) Illustration describing preparation of photonic NC substrate. Reprinted from ref [146] with permission from the American Chemical Society, Copyright 2016. (B) Illustration of the spot test device for determination of AFP using initiator DNA labeled Ab performing a hybridization chain reaction. Reprinted from ref [151] with permission from Elsevier, Copyright 2021. (C) 2D μPAD for multiplexed detection of cancer cells using QD labeled DNA as fluorescence probe. Reprinted from ref [157] with permission from Elsevier, Copyright 2016. (D) Distance based 2D μPAD for MMP7 detection based on quenching of the QD fluorescence due to ion exchange. Reprinted from ref [161] with permission from Springer Nature, Copyright 2020. (E) Detection of CEA based on fluorescence turn on of MOF impregnated paper due to structural change. Reprinted from ref [162] with permission from the American Chemical Society, Copyright 2018.

1.4.3 Chemiluminescence methods

Chemiluminescence (CL) is a technique based on luminescence produced from a chemical reaction. High sensitivity and low noise level due to the absence of any external excitation light source are characteristics of CL methods [164, 165]. Since no excitation light source is required, the resultant simple instrumentation for CL detection makes it an attractive detection method in PADs [62, 165]. Oxidation of luminol is the best known CL reaction and the most efficient because of the high quantum yield of luminol [166, 167]. Sandwich immunoassays are commonly used for the CL detection of biomarkers in which HRP enzyme labeled detection Abs are widely used for CL signal enhancement due to the ability of HPR to catalyze the luminol oxidation by H_2O_2 [168]. Enhancement of the CL signal in PADs can be achieved by using catalysts such as enzymes and metal NPs. HRP labeled Ab has been used to detect Ab in the CL determination of CEA, AFP, and PSA with a 2D μPAD fabricated by dipping in dissolved plastic [169]. Another device fabricated by the wax screen printing method was used for CL detection of AFP, CA125, and CEA with the HRP labeled Ab and luminol-p-iodophenol – H_2O_2 system [170]. Metal nanoparticles such as AgNPs and AuNPs are commonly used for CL signal enhancement. Ge et al. [171] developed an origami 3D μPAD using the AgNP catalyzed luminol-H_2O_2 CL reaction for simultaneous determination of AFP, CA153, CA199, and CEA biomarkers in whole blood samples. AuNP conjugated HRP labeled Ab was used for CEA detection by Wang et al. [172] to produce stable and reproducible CL signals in the sandwich immunoassay, and the captured Abs were chemically attached to the paper through surface modification by periodate oxidation for the aldehyde groups. Mesgari et al. [131] determined Cyt c by using cobalt hydroxide decorated mesoporous carbon nanostructures "β-$Co(OH)_2$ CMK" attached to an aptamer specific to Cyt c. In the presence of the target, the aptamer attaches to Cyt c and β-$Co(OH)_2$ CMK nanostructure becomes free and available to catalyze the luminol oxidation. Li et al. [173] used TiO_2 nanoparticles coated on

multiwalled carbon nanotubes (TiO_2/MWCNTs) with labeled Ab as the detection Ab to enhance the CL for PSA determination, and they found that the TiO_2/MWCNTs gave a better CL signal than TiO_2 nanoparticles alone. Gao et al. [174] introduced multi-structured pseudo-papers (MSPs) prepared using self-assembly of dispersed SiO_2 crystal in PDMS mold to enhance the CL signal of luminol. A 3D ring-oven washing technique was used to improve the washing efficiency and decrease the non-specific binding to enhance the CL immunoassay [175]. Even though normally CL offers higher sensitivity and lower detection limits than fluorescence and colorimetry, due to the absence of background fluorescence and absence of an excitation light source, CL generally suffers from low specificity. **Table 1-2** summarizes the CL PDAs and their performance values.

Table 1- 2 Fluorescence and chemiluminescence paper-based microfluidic sensors for detection of cancer biomarkers.

Biomarker	Type	Sample	Paper substrate	Fabrication [a]	Detection method	Assay type	Recognition element	Linear range	LOD	Type of PAD	Ref.
AFP	Protein	_	Photonic NC substrate	Casting and etching using self-assembled monodisperse nanoparticles	FL	Sandwich immune-assay	FITC labeled Ab	0.05 -0.50 µg/mL	0.032 µg/mL	Hybrid	[146]
		Serum	Plasma treated chromatography paper	Wax printing	FL	Sandwich immune-assay	CdTe QDs embedded SiO_2NPs labeled Ab	0.001-20.0 ng/mL	0.4 pg/mL	Spot test	[156]
		Serum	Chromato-graphy paper	Wax printing	FL	Sandwich immune-assay	FITC labeled Ab	0.1 – 1000 ng/mL	0.05 ng/mL	3D-µPADs	[150]
		Serum	Filter paper	Wax printing	FL	Sandwich immune-assay	Initiator DNA Labeled Ab	2.5 -1 000 pg/mL	1.0 pg/mL	Spot test	[151]
		Whole blood	Chromato-graphy paper	Wax printing	CL	Sandwich immune-assay	AgNP labeled Ab	2.5 – 110 ng/mL	1.0 ng /mL	3D-µPAD	[171]
		Serum	Chromato-graphy paper	Screen printing	CL	Sandwich immune-assay	HRP labeled Ab	0.1 -35 ng/mL	0.06 ng/mL	Spot test	[170]
		Serum	EC MSPs	Casting and etching using self-assembled monodisperse nanoparticles	CL	Sandwich immune-assay	HRP labeled Ab	1-50 ng/mL	_	2D-µPAD	[174]
		Serum	Chromato-graphy paper	Dipping in foamed plastic solution	CL	Sandwich immune-assay	HRP labeled Ab	5 – 80 ng/mL	2 ng/mL	2D-µPAD	[169]
BRCA-1	Gene expression		Filter paper	Wax printing	FL	DNA hybrid-ization	Cy3-DNA	Qualitative (Yes/No)	400 fmol	Spot test	[147]
CA125	Protein	Serum	Chromato-graphy paper	Screen printing	CL	Sandwich immune-assay	HRP labeled Ab	0.5 – 80 U/mL	0.33 U/mL	Spot test	[170]
CA125	Protein	Serum	EC MSPs	Casting and etching using self-assembled monodisperse nanoparticles	CL	Sandwich immune-assay	HRP labeled Ab	1 – 100 U/mL	_	2D-µPAD	[174]
CA153	Protein	Whole blood	Chromato-graphy paper	Wax printing	CL	Sandwich immune-assay	AgNP labeled Ab	1.0 – 100 U/mL	0.4 U/mL	3D-µPAD	[171]
CA199	Protein	Serum	Chromato-graphy paper	Wax printing	FL	Sandwich immune-assay	FITC labeled Ab	0.1 – 1000 U/mL	0.09 U/mL	3D-µPADs	[150]
		Serum	Chromato-graphy paper	Photo-lithography	FL	Sandwich immune-assay	Polystyrene latex particle labeled Ab	0.01 – 25 U/mL	0.1 U/mL	2D-µPADs	[163]
		Whole blood	Chromato-graphy paper	Wax printing	CL	Sandwich immune-assay	AgNP labeled Ab	0.5 – 150 U/mL	0.06 U/mL	3D-µPAD	[171]
CEA	Protein	_	Photonic NC substrate	Casting and etching using self-assembled monodisperse nanoparticles	FL	Sandwich immune-assay	FITC labeled Ab	0.05 -0.50 µg/mL	0.021 µg/mL	Hybrid	[146]
		Serum	Chromato-graphy paper	Photolitho-graphy	FL	Sandwich immune-assay	Polystyrene latex particle labeled Ab	1 pg/mL – 0.1 ng/mL	1 pg/mL	2D-µPADs	[163]
		Serum	Chromato-graphy paper	Cutting	FL	Sandwich immune-assay	GDH-AuNP labeled Ab	0.1 – 200 ng/mL	0.041 ng/mL	Spot test	[162]
		Serum	Chromato-graphy paper	Wax printing	FL	Sandwich immune-assay	FITC labeled Ab	0.1 – 1000 ng/mL	0.03 ng/mL	3D-µPADs	[150]
		Whole blood	Chromato-graphy paper	Wax printing	CL	Sandwich immune-assay	AgNP labeled Ab	0.1 – 130 ng/mL	0.02 ng/mL	3D-µPAD	[171]
		Serum	Chromato-graphy paper	Wax printing	CL	Sandwich immune-assay	AgNPs-HRP labeled Ab	0.01 – 30 ng/mL	6.5 pg/mL	Spot test	[172]
		Serum	Chromato-graphy paper	Screen printing	CL	Sandwich immune-assay	HRP labeled Ab	0.1 – 70 ng/mL	0.05 ng/mL	Spot test	[170]
		Serum	Chromato-graphy paper	Photolithography	CL	Sandwich immune-assay	HRP labeled Ab	0.1 – 80 ng/mL	_	Hybrid	[168]
		Serum	EC MSPs	Casting and etching using self-assembled monodisperse nanoparticles	CL	Sandwich immune-assay	HRP labeled Ab	1 – 100 ng/mL	_	2D-µPAD	[174]
		Serum	Chromato-graphy paper	Dipping in foamed plastic solution	CL	Sandwich immune-assay	HRP labeled Ab	0.05 – 80 ng/mL	0.02 ng/mL	2D-µPAD	[169]
		Serum	Chromato-graphy paper	Cutting	CL	Sandwich immune-assay	HRP labeled Ab	5 – 80 pg/mL &	2 pg/mL	3D-µPAD	[175]

								0.1 -10.0 ng/mL			
Cyt c	**Protein**	Serum	Filter paper	Cutting	CL	Cyt c – aptamer interaction	β-$Co(OH)_2$ CMK attached with DNA aptamer against Cyt c	10^{-13} – 5 x 10^{-9} M	2 x 10^{-14} M	2D-μPAD	[131]
EpCAM	**Protein**	10% bovine serum	Modified cellulose paper	Wax printing	FL	Quenching of FRET due to aptamer-protein reaction	QDs-Apt and Cy3 labeled DNA	1-100 nM	600 pM	Spot test	[158]
H_2O_2	**Small molecule**	MCF-7 cancer cells	Chromato-graphy paper	Wax printing	FL	Induced DNA cleavage	SiO_2/NGQDs-DNA	0.3 nM – 1.0 mM	0.1 nM	3D-μPADs	[159]
HL-60	**Cells**	Cell culture	Chromato-graphy paper	Wax printing	FL	Aptamer-cell binding	MSNs/QDs–DNA	210 – 7x10^7 cells/mL	70 cells/mL	2D-μPADs	[157]
K562	**Cells**	Cell culture	Chromato-graphy paper	Wax printing	FL	Aptamer-cell binding	MSNs/QDs–DNA	200 – 7x10^7 cells/mL	65 cells/mL	2D-μPADs	[157]
MCF-7	**Cells**	Cell culture	Chromato-graphy paper	Wax printing	FL	Aptamer-cell binding	MSNs/QDs–DNA	180 – 8x10^7 cells/mL	62 cells/mL	2D-μPADs	[157]
miRNA-21	**Nucleic acid**	A549 and HeLa	Filter paper	Wax printing	FL	DNA cut off by DNS	Fluorophore labeled DNA	0.5 – 200 fM	0.2 fM	3D-μPADs	[149]
miRNA-31	**Nucleic acid**	A549 and HeLa	Filter paper	Wax printing	FL	DNA cut off by DNS	Fluorophore labeled DNA	1.0 -200 fM	0.5 fM	3D-μPADs	[149]
MMP7	**Matrix metallo-proteinase**	Serum	Chromato-graphy paper	Cutting	FL-Distance	Exchange Ag ion with Cd in CdTe QD	AgNP labeled Ab	0.01 – 30 ng/mL	7.3 pg/mL	2D-μPADs	[161]
PSA	**Protein**	Serum	Chromato-graphy paper	Wax printing	CL	Sandwich immunoassay	TiO_2/MWCNTs labeled Ab	0.001 – 20 ng/mL	0.8 pg/mL	Spot test	[173]
		Serum	Chromato-graphy paper	Dipping in foamed plastic solution	CL	Sandwich immunoassay	HRP labeled Ab	1 – 50 ng/mL	0.2 ng/mL	2D-μPAD	[169]
Telomerase	**Enzyme**	7 cell lines	PAMAM dendrimer)-activated Chromato-graphy paper	Hand drawing using permanent marker	FL	Enzymatic activity toward telomeric elongation	Cy5-DNA	10-1000 HeLa cells	10 HeLa cells	Spot test	[148]

a: Fabrication method mentioned is mainly for patterning the main substrate in the device.

Biomarker abbreviations: AFP, alpha fetoprotein; BRCA-1, breast cancer gene 1; CA125, cancer Antigen 125; CA153, cancer Antigen 153; CA199, cancer Antigen 199; CEA, carcinoembryonic antigen; Cyt c, cytochrome c; EpCAM, epithelial cell adhesion molecule; miRNA, micro-RNA; MMP7, matrix metalloproteinase 7; PSA, prostate specific antigen. **Paper substrate abbreviations:** NC, nitrocellulose; EC MSPs, elastic copolymer multi-structured pseudo-papers; PAMAM, polyamidoamine. **Detection method and assay type abbreviations:** FL, fluorescence; CL, chemiluminescence; FRET, fluorescence resonance energy transfer; DNS, duplex-specific nuclease. **Recognition element abbreviations:** QD, quantum dot; FITC, fluorescein isothiocyanate; Ab, antibody; AgNP, silver nanoparticles; AuNP, gold nanoparticles; HRP, horse radish peroxidase; GDH, glutamate dehydrogenase; NGQDs, nitrogen doped graphene quantum dots; MSNs, mesoporous silica nanoparticles; MWCNTs, multiwalled carbon nanotubes.

1.4.4 Electrochemical methods

Electrochemical paper-based analytical devices (ePADs) have gained interest since 2009 when they were introduced by Henry's group for determination of glucose, lactate, and uric acid in human serum [176]. ePADs offer inexpensive, highly sensitive, and selective platforms for quantitative analysis. Moreover, the availability of portable low cost potentiostats and the ability of ePADs to be integrated with smartphone platforms make them very promising as different PON immunosensors for cancer diagnosis and clinical applications [59, 129, 177]. In principle, immunosensor ePADs are based on performing a specific antibody-antigen reaction on the surface of an electrode and measuring an electrochemical signal such as current, resistance, or impedance. The ePAD designs mainly consider three aspects: the electrode material and fabrication, the electrochemical detection strategy, and the electrochemical signal readout [178, 179].

1.4.4.1 Electrode material and fabrication

Like ordinary electrochemical systems, ePADs consist of three electrodes: a working electrode (WE) which is the main critical one for detection and device performance; a reference electrode (RE) which should be near the WE to decrease the voltage drop; and a counter electrode (CE) which should be larger than the WE to allow for unlimited current transfer [62]. Several materials are suitable for fabricating electrodes of ePADs; the RE and CE are commonly fabricated using Ag/AgCl and carbon ink respectively, while the WE is commonly fabricated using carbon or a noble metal. Metallic electrode materials such as Pt, Au, and Ag have high electrochemical activity but at the same time, they are expensive and have narrow potential windows. Carbon electrodes are cheaper and have wider potential windows, making them suitable for a wider range of targets [178]. Various types of carbon materials have been used for biomarker detection by ePADs [129], including graphene [180-182], reduced graphene

oxide (rGO) [183], and carbon nanotubes (CNTs) [184]. Carbon-metal hybrids have also been used to amplify the electrochemical signal. This is done by fabricating the electrode directly using prepared graphene modified metal nanoparticles [183, 185], or by modification of the fabricated carbon electrode surface [177]. In cancer biomarker detection, there are several techniques for electrode fabrication using conductive ink [178] such as syringe filtering and cutting [184], hand drawing [183], manual brushing [186], and stencil printing [182], but screen printing is the most common one [180, 181, 187-192]. For biosensing, especially cancer biomarker detection, commonly the surface of the carbon or modified carbon WE is modified with biofunctional target specific elements, like antibodies, enzymes, aptamers, and DNAs. These biofunctional elements can be attached directly by adsorption to the paper substrate or WE surface, or they can be attached to the WE after modifying it first with other materials like glutaraldehyde, thiol-Au, and chitosan [183-185, 187, 192-194]. Cao et al. [192] used a screen printed carbon WE and attached Ab directly to the paper on the other side of the WE for determination of HCG antigen. On the other hand, Draz et al. [185] used graphene modified Ag nanocomposite as the WE and immobilized Abs for multiplexed determination of AFP and CEA. Ji et al. [184] also attached anti-PSA Abs directly to the surface of the MWCNT WE. Moreover, modifying the paper surface of a carbon WE with chitosan and MWCNTs before immobilizing the Ab has been done to enhance the electronic conductivity and increase the sensitivity [187, 193]. While the role of the biofunctional elements is to increase the specificity and selectivity of the ePADs, other modifications for enhancing and amplifying the electrochemical signal to increase the sensitivity of the ePADs have been done using metal NPs such as nanoporous silver (NPS) [188], AuNPs [195], MnO_2-AuNPs [196], cuboid silver nanoparticles (CS) [197], and MoS_2-AuNPs [182].

1.4.4.2 Electrochemical detection strategy and electrochemical signal readout

Several strategies are used for electrochemical detection with PADs and strategy selection depends on the target analyte. The strategies include direct measurement for electrochemically active metals and drugs through their oxidation on the WE surface [198, 199], while for electrochemically inactive targets such as biomarkers, affinity based recognition elements like antibodies, aptamers, enzymes, and molecularly imprinted polymer (MIP) have been used [180, 182, 186, 187, 194]. Due to the high specificity of Abs, aptamers, and enzymes, multiplexed detection of several biomarkers can be done by splitting the sample into multiple detection zones. , Zang et al. [193] developed an ePAD for detection of four biomarkers simultaneously using a two-layer PAD. The first layer contained the RE and CE, while the second layer contained eight detection zones of MWCNT modified WEs (four pairs of WEs), and each WEs pair was modified with Ab specific for one target biomarker (**Fig. 1-9A**).

The detection of biomarkers is often based on sandwich immunoassay techniques (**Fig. 1-9B**), whereby a primary antibody is immobilized on a modified electrode surface to capture the analyte, and a secondary antibody is labeled with a peroxidase enzyme like HRP [187, 193] or nanostructures having a peroxidase-like activity [200-202]. In addition, a label free detection technique can be used such as measuring the change in the response of thionine and a metallic nanostructure modified WE after formation of an antibody-antigen immune complex [183-185, 191, 203], an aptamer-antigen conjugate [180, 194], a miRNA-DNA hybrid [182], and an MIP-antigen conjugate [186]. MIPs are an inexpensive replacement for antibodies, DNA, and aptamers-based probes. Qi et al. [186] introduced a MIP modified carbon electrode for CEA detection using differential pulse voltammetry (DVP) (**Fig. 1-9C**). Many cancer biomarker detection ePADs use DPV [180-182, 186, 187, 191-196, 201-206]. However, other techniques are also used like cyclic voltammetry (CV) [190], square wave voltammetry (SWV) [188, 197],

chronoamperometry [183], impedimetric [185], and electrical conductivity [184]. **Table 1-3** summarizes the ePADs used for cancer biomarker detection and their performance values.

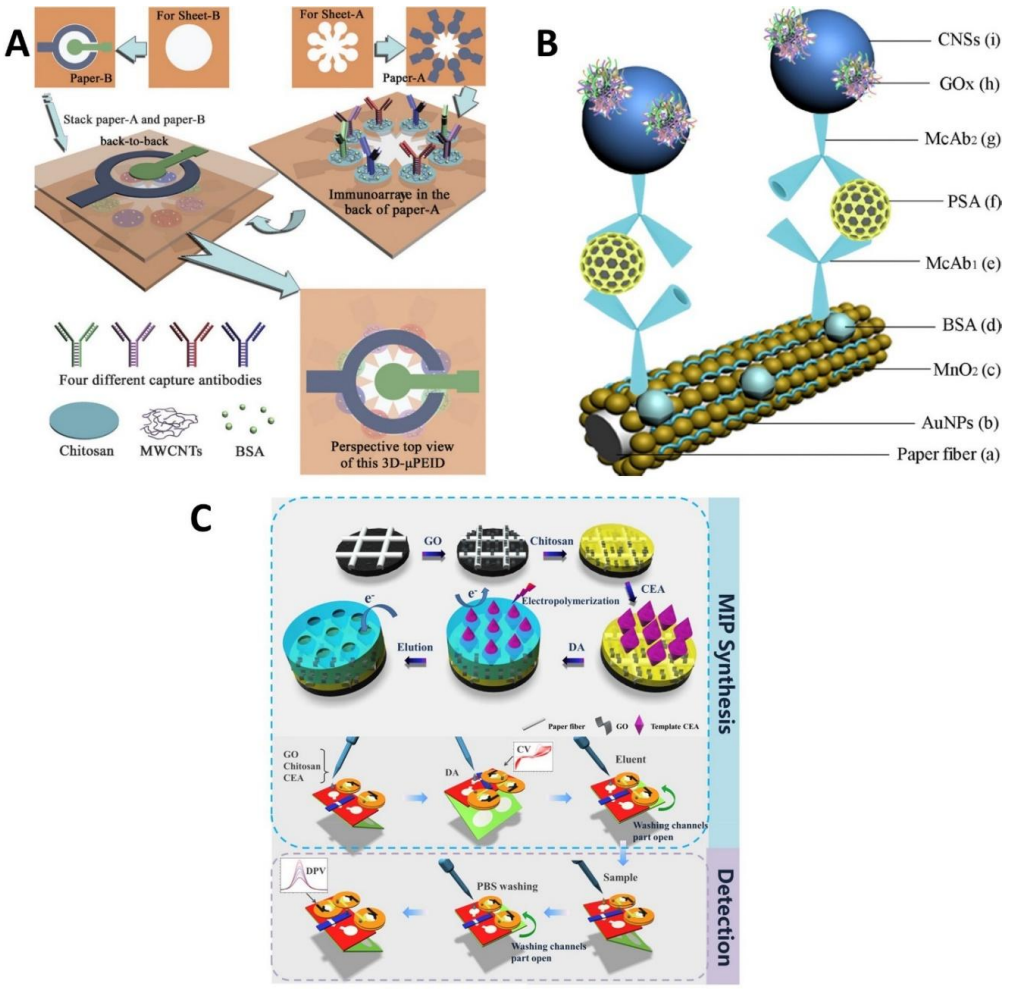

Fig. 1- 9 (A) Illustration of ePADs for multiplexed detection of four different biomarkers. The detection layer consists of 8 different detection zones. The WE is modified using MWCNTs and antibodies specific for each target. Reprinted from ref [193] with permission from the Royal Society of Chemistry, Copyright 2012. (B) Illustration for sandwich immunoassay on ePADs, in which the primary antibody is attached to the surface of the modified paper WE to capture the antigen, and the secondary detection antibody is labeled with an enzyme or enzymatic-like activity nanoparticles attached to the antigen. Reprinted from ref [196] with permission from Elsevier, Copyright 2014. (C) Illustration of ePADs for CEA detection using MIP modified WE. Reprinted from ref [186] with permission from Elsevier, Copyright 2019.

Table 1- 3 Electrochemical paper-based analytical devices (ePADs) for detection of cancer biomarkers.

Biomarker	WE	WE fabrication	WE modification	Detection concept	Recognition element	EC technique	Linear range	LOD	Ref.
AFP	Carbon	Screen printing	MWCNTs/Chitosan/Ab	Sandwich immunoassay	HRP labeled Ab	DPV	0.05 – 95 ng/mL	0.01 ng/mL	[193]
	Carbon	Screen printing	NPS/Ab	Sandwich immunoassay	NGC-metal ion labeled Ab	SWV	0.1 pg/mL – 100 ng/mL	0.08 pg/mL	[188]
	Carbon	Screen printing	PANI/Au/Ab	Sandwich immunoassay	3DGS@redox probe labeled Ab	DPV	0.001 – 100 ng/mL	0.80 pg/mL	[195]
	Carbon	Screen printing	GO-Chitosan/Ab	Sandwich immunoassay	Ab labeled with initiator for AGET ATRP	DPV	0.01 – 100 ng/mL	0.01 ng/mL	[205]
	Graphene modified Ag nanocomposite	Screen printing	Ab	Formation of Ab-antigen immunocomplex	_	Impedimetric	_	1.0 ng/mL [a]	[185]
CA125	Carbon	Screen printing	MWCNTs/Chitosan/Ab	Sandwich immunoassay	HRP labeled Ab	DPV	0.001 – 75 U/mL	0.20 mU/mL	[187]
	Carbon	Screen printing	MWCNTs/Chitosan/Ab	Sandwich immunoassay	HRP labeled Ab	DPV	0.02 – 85 U/mL	6.0 U/mL	[193]
	Carbon	Screen printing	CS/Ab	Sandwich immunoassay	NSC-metal ion labeled Ab	SWV	0.03 – 100 U/mL	0.02 mU/mL	[197]
	Carbon	Screen printing	GO-Chitosan/Ab	Sandwich immunoassay	Ab labeled with initiator for AGET ATRP	DPV	0.05 – 100 ng/mL	0.05 ng/mL	[205]
	Carbon	Screen printing	AuNRs/Ab	Sandwich immunoassay	Metal ion coated Au/BSA nanospheres	DPV	0.1 mU/mL – 50 U/mL	0.06 mU/mL	[206]
	AgNPs/rGO	Hand drawing	Cys/Au NPs/AgNPs-rGO/Ab	Formation of antigen-Ab conjugate	_	Chronoampero metry	0.78 – 400 U/mL	0.78 U/mL	[183]
	Carbon	Screen printing	rGO/Thi/AuNPs/Ab	Formation of antigen-Ab conjugate	_	DPV	0.1 – 200 U/mL	0.01 U/mL	[203]
CA153	Carbon	Screen printing	GO-Chitosan/Ab	Sandwich immunoassay	Ab labeled with initiator for AGET ATRP	DPV	0.05 – 100 ng/mL	0.05 ng/mL	[205]
CA199	Carbon	Screen printing	MWCNTs/Chitosan/Ab	Sandwich immunoassay	HRP labeled Ab	DPV	0.05 – 120 U/mL	8.0 U/mL	[193]
	Carbon	Screen printing	CS/Ab	Sandwich immunoassay	NSC metal ion labeled Ab	SWV	0.03 – 100 U/mL	0.04 mU/mL	[197]
CEA	Carbon	Screen printing	MWCNTs/Chitosan/Ab	Sandwich immunoassay	HRP labeled Ab	DPV	0.05 – 50 ng/mL	0.01 ng/mL	[187]
	Carbon	Screen printing	MWCNTs/Chitosan/Ab	Sandwich immunoassay	HRP labeled Ab	DPV	0.05 – 105 ng/mL	5.0 pg/mL	[193]
	Carbon	Screen printing	NPS/Ab	Sandwich immunoassay	NGC metal ion labeled Ab	SWV	0.1 pg/mL – 100 ng/mL	0.06 pg/mL	[188]
	Carbon	Screen printing	PANI/Au/Ab	Sandwich immunoassay	3DGS@redox probe labeled Ab	DPV	0.001 – 100 ng/mL	0.50 pg/mL	[195]
	Carbon	Screen printing	Flower-like AuNPs/Ab	Sandwich immunoassay	Ag-Au bimetallic NPs labeled Ab	Amperometry	0.001 – 50 ng/mL	0.30 pg/mL	[200]
	Carbon	Screen printing	GO-Chitosan/Ab	Sandwich immunoassay	Ab labeled with initiator for AGET ATRP	DPV	0.01 – 100 ng/mL	0.01 ng/mL	[205]
	Carbon	Screen printing	AuNRs/Ab	Sandwich immunoassay	Metal ion coated Au/BSA nanospheres	DPV	0.1 pg/mL – 50 ng/mL	0.08 pg/mL	[206]
	Carbon	Screen printing	ZNRs/rGO/Ab	Sandwich immunoassay	rGO/Ag@BSA labeled Ab	CV	0.001 – 100 ng/mL	0.33 pg/mL	[190]
	Carbon	Screen printing	NH_2-G/ Thi/ AuNPs/Ab	Formation of Ab-antigen immunocomplex	Response current from thionine	DPV	0.05 – 500 ng/mL	10.0 pg/mL	[191]
	Graphene modified Ag nanocomposite	Screen printing	Ab	Formation of Ab-antigen immunocomplex	_	Impedimetric	_	10.0 ng/mL [a]	[185]
	Carbon	Manual brushing	MIP	MIP-Antigen conjugation	_	DPV	1 – 500 ng/mL	0.32 ng/mL	[186]
	Carbon	Screen printing	NH_2-G/ Thi/ AuNPs/Aptamer	Formation of Aptamer-Antigen conjugate	_	DPV	0.01 – 500 ng/mL	2.0 pg/mL	[180]
HCG	Carbon	Screen printing	ZNRs/rGO/Ab	Sandwich immunoassay	rGO/Ag@BSA labeled Ab	CV	0.002 – 120 mU/mL	0.0007mU/mL	[190]
	Carbon	Screen printing	Ab	Sandwich immunoassay	AuNPs labeled Ab / ALP labeled Ab	DPV	0.001 – 100 U/mL	0.36 mU/mL	[192]
HL-60	Carbon	Screen printing	AuNPs/aptamer	Cell-aptamer interaction	HRP labeled folic acid	DPV	$5.0x10^2$ – $7.5x10^7$ cells/mL	350 cells/mL	[204]

Huh7 Cancer cell	Carbon	Screen printing	Chitosan/Ab	Sandwich immunoassay	QD coated silica NP labeled Ab	SWV	5 – 1x10^6 cells/mL	5 cells/mL	[189]
K-562 Cancer cell	Carbon	Screen printing	Con A/IL/3D AuNPs@GN	sandwich-type assay	Con A labeled dendritic PdAg NPs	DPV	1x10^3 – 5x10^6 cells/mL	200 cells/mL	[201]
	Carbon	Screen printing	Folic acid functionalized AuNPs	sandwich-type assay	Folic acid-Au@PtPd NPs	DPV	1x10^2 – 2x10^7 cells/mL	31 cells/mL	[202]
miRNA-155	Carbon	Stencil printing	rGO/AuNPs Or MoS_2/AuNPs	Formation of DNA–miRNA hybrid	_	DPV	0 – 1 µg/mL	25.7 nM Or 59.6 nM	[182]
miRNA-21	Carbon	Stencil printing	rGO/AuNPs Or MoS_2/AuNPs	Formation of DNA–miRNA hybrid	_	DPV	0 – 1 µg/mL	12 nM Or 51.6 nM	[182]
NSE	Carbon	Screen printing	PB-PEDOT/ AuNPs/Aptamer	Formation of aptamer-antigen conjugate	_	DPV	0.05 – 500 ng/mL	10.0 pg/mL	[180]
PEAK1	Carbon	Screen printing	GO/Ab	Sandwich immunoassay	AuNP labeled Ab	DPV	0.01 – 1000 ng/mL	10.0 pg/mL	[181]
PSA	Carbon	Screen printing	MnO_2-AuNPs/Ab	Sandwich immunoassay	Gox/CNSs labeled Ab	DPV	0.005 – 100 ng/mL	0.0012 ng/mL	[196]
	Carbon	Screen printing	ZNRs/rGO/Ab	Sandwich immunoassay	rGO/Ag@BSA labeled Ab	CV	0.001 – 110 ng/mL	0.35 pg/mL	[190]
	MWCNTs	Syringe filtering and cutting	Ab	Formation of Ab-antigen immunocomplex	_	Electrical conductivity	0 – 500 ng/mL	1.18 ng/mL	[184]
	Carbon	Screen printing	rGO/Thi/AuNPs-Aptamer	Formation of aptamer-antigen conjugate	_	DPV	0.05 – 200 ng/mL	10.0 pg/mL	[194]

a: This is LOD in the determination of a single biomarker at the time while in a multiplexed assay, LODs for both AFP and CEA are 100 ng/mL.

Biomarker abbreviations: CA125, cancer antigen 125; CEA, carcinoembryonic antigen; AFP, alpha fetoprotein; CA199, carbohydrate antigen 199; PSA, prostate specific antigen; HCG, human chorionic gonadotropin; NSE, neuron specific enolase; PEAK1, pseudopodium-enriched atypical kinase one; miRNA, micro-RNA. **WE modification abbreviations:** MWCNTs, multi-walled carbon nanotubes; AgNP, silver nanoparticles; GN, graphene; NH_2-G, amino functional graphene; GO, graphene oxide; rGO, reduced graphene oxide; NPS, nanoporous silver; PANI, polyaniline; CS, cuboid silver; AuNP, gold nanoparticles; AuNR, gold nanorods; ZNRs, zinc oxide nanorods; Con A, concanavalin A; IL, ionic liquid; Thi, thionine; Cys, cysteamine; PB-PEDOT, prussian blue-poly (3,4- ethylenedioxythiophene); MIP, molecularly imprinted polymer. **Recognition element abbreviations:** HRP, horse radish peroxidase; NGC, nanoporous gold-chitosan; 3DGS, 3-dimensional graphene sheets; GOx, glucose oxidase; NSC, nanoporous silver-chitosan; AGET ATRP, activators generated by electron transfer for atom transfer radical polymerization; QD, quantum dots; BSA, bovine serum albumin. **EC technique abbreviations:** CV, cyclic voltammetry; DPV, differential pulse voltammetry; SWV, square wave voltammetry.

1.4.5 Electrochemiluminescence methods

Luminescence induced by an electrochemical reaction is the basis of the electrochemiluminescence (ECL) technique. Two strategies can be used to generate ECL, annihilation and co-reactants [207]. In an annihilation approach, oxidized and reduced species form on the electrode surface during pulsing or cycling of the electrode potential, and the ECL generated when the oxidized and reduced species react produces an excited species. A co-reactant approach is more common in ECL sensor fabrication, a co-reactant interacts with a luminophore to generate an excited state. Both luminophore and co-reactant are oxidized or reduced on the electrode surface when a potential is applied and that produces radical ions and intermediate species which together generate the excited species that will emit ECL [207-209], as described in **Fig. 1-10**. Several luminophores are used in both conventional ECL and ECL-based PADs [210, 211]. $Ru(bpy)_3^{2+}$ is commonly used due to its strong luminescence, good solubility in different organic and aqueous solvents, and its reversible electron transfer reaction occurring at low potential [212]. Ge et al. [213] introduced an ECL PAD for multiplexed detection of four cancer biomarkers based on sandwich immunoassay using $Ru(bpy)_3^{2+}$ labeled antibodies as the recognition element (**Fig. 1-11A**). Another device was developed by Sun et

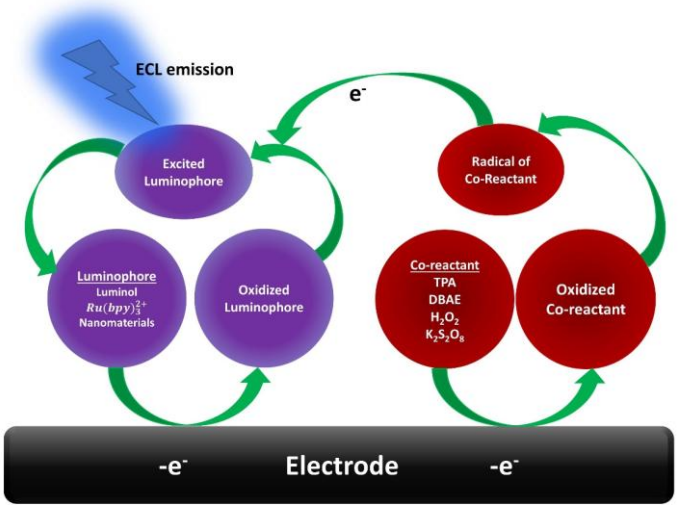

Fig. 1- 10 Typical ECL process using a co-reactant approach

al. [214] based on the same concept for CEA and PSA detection using a rotational ECL PAD to improve efficiency of the multistep assays and washing steps, thereby increasing the ECL signal (**Fig. 1-11B**). Nanoparticles have also been used commonly as luminophores in ECL PADs including metal nanoparticles, QDs, graphene QDs [207, 215]. , Wang et al. [216] introduced an ECL PAD for determination of four biomarkers on only two detection zones based on a potential resolution strategy in which sandwich immunoassay was used for detecting two antigens on the same electrode. Specifically, they used $Ru(bpy)_3^{2+}$ labeled antibodies and carbon nanodot (CND) labeled antibodies recognition elements, and by changing the operational constant potential (-1.2 V for CNDs and +1.2 V for $Ru(bpy)_3^{2+}$) they controlled which luminophore interacted (**Fig. 1-11C**). Combinations between nanoparticles and inorganic luminophores have been used to enhance ECL signals [217-219]. By using $Ru(bpy)_3^{2+}$-Au nanocage labeled detection antibody in the detection of CEA, Gao et al. [220] achieved the sub-pg/mL detection limit. Other luminophores also have been used such as 4,4'-(2,5-dimethoxy-1,4-phenylene)bis(ethyne-2,1-diyl) dibenzoic acid (P-acid) [221], luminol [217], and $Ru(phen)_3^{2+}$ [222]. By optimizing electrode designs and detection strategies, ECL can provide better sensitivity, and spatial and temporal resolution compared to CL. **Table 1-4** summarizes ECL PADs used for cancer biomarker detection and their performance values.

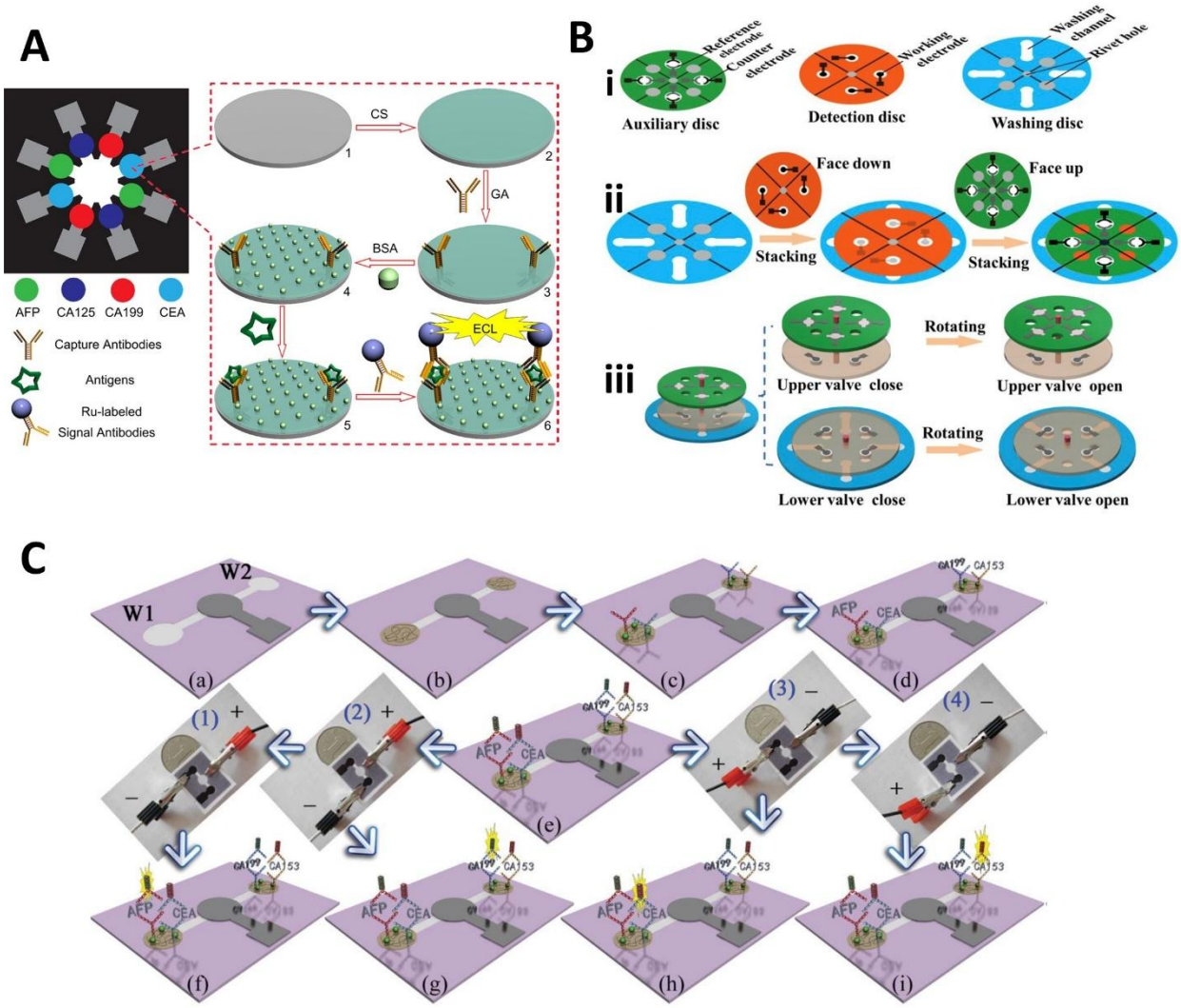

Fig. 1- 11 (A) ECL PAD for multiplexed detection of four biomarkers, a chitosan/glutaraldehyde modified electrode was used to immobilize the captured Ab, and Ru(bpy)32+ labeled Ab was used as a recognition element. Reprinted from ref [213] with permission from Elsevier, Copyright 2012. (B) Illustration of components and operation of a rotational ECL PAD for CEA and PSA detection. Reprinted from ref [214] with permission from Elsevier, Copyright 2018. (C) ECL PAD for detection of four biomarkers using two detection zones by controlling the operational constant potential. Reprinted from ref [216] with permission from the Royal Society of Chemistry, Copyright 2012.

Table 1- 4 Electrochemiluminescence paper-based analytical devices (ECL PADs) for detection of cancer biomarkers.

Biomarker	Electrode modification	Recognition element (Luminophore)	ECL co-reactant	Linear range	LOD	Ref.
AFP	Chitosan/glutaraldehyde/Ab	$Ru(bpy)_3^{2+}$ labeled Ab	TPA	0.5 – 100 ng/mL	0.15 ng/mL	[213]
	MWCNTs/chitosan/glutaraldehyde/Ab	CND labeled Ab	$K_2S_2O_8$	_	0.02 ng/mL	[216]
	Porous AgNP/Ab	CdTe QDs-NPG CNS labeled Ab	H_2O_2	3.0 pg/mL – 50 ng/mL	1.0 pg/mL	[223]
CA125	Chitosan/glutaraldehyde/Ab	$Ru(bpy)_3^{2+}$labeled Ab	TPA	1.0 – 100 U/mL	0.6 U/mL	[213]
	AuNP/Ab	Luminol-AuNP labeled Ab	-	0.01 – 100 U/mL	0.0074 U/mL	[217]
	Porous AgNP/Ab	Luminol-NPG CNS Labeled Ab	H_2O_2	5.0 mU/mL – 50 U/mL	1.2 mU/mL	[223]
	GN-Ag-Au NP/Ab	CMs/CdTe QD labeled Ab	$K_2S_2O_8$	0.008 – 50 U/mL	2.5 mU/mL	[224]
CA153	MWCNTs/chitosan/glutaraldehyde/Ab	$Ru(bpy)_3^{2+}$labeled Ab	TPA	_	5.0 mU/mL	[216]
	AuNF/Ab	GQDs/SVAu nanocage labeled Ab	$K_2S_2O_8$	0.005 – 500 U/mL	0.0014 U/mL	[219]
CA199	Chitosan/glutaraldehyde/Ab	$Ru(bpy)_3^{2+}$labeled Ab	TPA	0.5 – 100 U/mL	0.17 U/mL	[213]
	MWCNTs/chitosan/glutaraldehyde/Ab	CND labeled Ab	$K_2S_2O_8$	_	6.0 mU/mL	[216]
	Chitosan/ glutaraldehyde/Ab	$Ru(bpy)_3^{2+}$@AuNP labeled Ab	-	0.01 – 200 U/mL	0.0055 U/mL	[218]
CCRF-CEM Cells	3D microporous Au/aptamer	Con A-AuPd NP	$K_2S_2O_8$	500 – 3.5 x 10^7 cells/mL	265 cells/mL	[225]
CEA	Chitosan/glutaraldehyde/Ab	$Ru(bpy)_3^{2+}$labeled Ab	TPA	1.0 – 100 ng/mL	0.5 ng/mL	[213]
	MWCNTs/chitosan/glutaraldehyde/Ab	$Ru(bpy)_3^{2+}$labeled Ab	TPA	_	4.0 pg/mL	[216]
	Chitosan/glutaraldehyde/Ab	$Ru(bpy)_3^{2+}$labeled Ab	TPA	0.005 – 50 ng/mL	0.001 ng/mL	[226]
	GO/chitosan/AuNP/Ab	P-acid/NPS labeled Ab	TPA	0.001 – 10 ng/mL	0.8 pg/mL	[221]
	AuNP/AgNP	$Ru(bpy)_3^{2+}$@Au nanocages labeled Ab	TPA	0.001 – 50 ng/mL	0.7 pg/mL	[220]
	MWCNTs/chitosan/glutaraldehyde/Ab	$Ru(bpy)_3^{2+}$labeled Ab	TPA	0.1 – 100 ng/mL	0.07 ng/mL	[214]
	Porous AgNP/Ab	$Ru(bpy)_3^{2+}$ -NPG CNSs labeled Ab	H_2O_2	1.0 pg/mL – 50 ng/mL	0.8 pg/mL	[223]
	NPS/Ab	CdTe QDs/NPS labeled Ab	$K_2S_2O_8$	0.5 pg/mL – 20 ng/mL	0.12 pg/mL	[227]
	GN/AuNP/Ab	(P-acid/Pt–AgANP) labeled Ab	TPA	0.001 – 100 ng/mL	0.3 pg/mL	[228]
HCG	NPG/Ab	$Ru(bpy)_3^{2+}$labeled Ab	TPA	0.005 – 4000 mU/mL	0.0019 mU/mL	[229]
HL-60 Cells	3D microporous Au/aptamer	Con A-AuPd NP	$K_2S_2O_8$	400 – 2.0 x 10^7 cells/mL	236 cells/mL	[225]
K562 Cells	3D microporous Au/aptamer	Con A-AuPd NP	$K_2S_2O_8$	420 – 5.0 x 10^7 cells/mL	241 cells/mL	[225]
MCF-7 Cells	3D microporous Au/aptamer	Con A-AuPd NP	$K_2S_2O_8$	450 – 1.0 x 10^7 cells/mL	250 cells/mL	[225]
MUC 1	AuNR/thiolated capture probe	$Ru(phen)_3^{2+}$	TPA	0.025 – 50 nM	0.0083 nM	[222]
PSA	GO/chitosan/AuNP/Ab	P-acid/NPS labeled Ab	TPA	0.003 – 20 ng/mL	1.0 pg/mL	[221]
	MWCNTs/chitosan/glutaraldehyde/Ab	$Ru(bpy)_3^{2+}$labeled Ab	TPA	0.1 – 50 ng/mL	0.03 ng/mL	[214]

Biomarker abbreviations: AFP, alpha fetoprotein; CA125, cancer antigen 125; CA153, cancer antigen 153; CA199, carbohydrate 199; CEA, carcinoembryonic antigen; HCG, human chorionic gonadotropin; MUC 1, mucin 1; PSA, prostate specific antigen. **Electrode modification abbreviations:** Ab, antibody; MWCNTs, multi-walled carbon nanotubes; AgNP, silver nanoparticles; AuNP, gold nanoparticles; GN, graphene; AuNF, gold nanoflowers; GO, graphene oxide; NPS, nanoporous silver; NPG, nanoporous gold; AuNR, gold nanorods. **Luminophore and ECL co-reactant abbreviations:** CND, carbon nanodots; QD, quantum dots; CNS, carbon nanospheres; GQD, graphene quantum dots; SVAu, surface villous gold; Con A, concanavalin A; P-acid, 4,4'-(2,5-dimethoxy-1,4-phenylene)bis(ethyne-2,1-diyl) dibenzoic acid; TPA, tri-n-propylamine.

1.4.6 Conclusion and future perspectives

Early diagnosis of cancer is facing a huge challenge with the methods currently used especially in developing countries since they are expensive, they have low specificity and sensitivity, and they are not suitable for routine follow-up and diagnosis. Detection of cancer biomarkers is an attractive concept for solving this challenge. Paper provides an inexpensive substrate and is available all over the world which has led to huge interest in it for developing PADs for cancer biomarker detection. PADs have been developed using different detection methods and assays, and colorimetric methods are most commonly used because their visual signal is easy to read by the naked eye or by integration with a simple device. But colorimetric methods have low sensitivity and a narrow dynamic range, and they are easily affected by external factors like surrounding light, reagent colors, and sample colors. Several approaches have been taken to improve the performance of colorimetric devices by using different paper substrate materials such as chromatographic paper, NC membranes, and p-PLLA. Also, modifications for the paper substrate or recognition element using enzymes and nanomaterials can help in improving the sensitivity and detection limit. Moreover, the fabrication of different 3D PAD designs can facilitate sequential addition of reagents and washing steps, improving the detection limits.

Fluorescence methods have been used in cases where they offer better sensitivity compared to colorimetry. The “turn on” and “turn off” feature of a fluorescence probe helps in decreasing the interference effect. Improving the fluorescence signal has been done using modifications for the paper substrates and detection elements using nanomaterials. Fluorescence needs a light excitation source which adds instrumentation to the devices and can increase the noise level in the measured signals. Also, lengthy methods for fluorescent probe preparation are necessary. Moreover, the autofluorescence of most paper materials can interfere with the measured fluorescence. Chemiluminescence offers better luminescence measurements

than fluorescence. Since there is no external excitation light source, the device is simple, and the noise level is very low leading to better detection limit and sensitivity. Luminol oxidation is the most common chemiluminescence reaction used due to the high quantum yield of luminol. Enhancement of the chemiluminescence signal can be achieved using catalysts such as enzymes and peroxidase-like activity metal nanostructures. Low specificity is the main drawback of chemiluminescence methods.

Electrochemical methods provide highly sensitive and selective platforms for quantitative cancer biomarker analysis; they are based on an antibody-antigen reaction occurring on an electrode surface followed by measurement of the electrochemical signal. Screen-printed carbon electrodes are commonly used as the working electrode because they are inexpensive to fabricate and have wide potential windows. To improve electrochemical signals, several electrode modifications have been done using molecularly imprinted polymers, organic compounds, nanoparticles, or combinations of them before immobilization to capture the antibody. Also, labeling the detection antibody with enzyme and metallic nanostructures facilitates the improvement of the sensitivity and detection limits. Several electrochemical techniques are used with PADs such as cyclic voltammetry, differential pulse voltammetry, square wave voltammetry, impedimetric, and chronoamperometry. Electrochemiluminescence is a chemiluminescence technique whereby an excited species is formed on an electrode surface. It can provide better sensitivity, and spatial and temporal resolution than chemiluminescence through optimizing electrode designs and detection strategies. $Ru(bpy)_3^{2+}$ is the most common luminophore used due to its strong luminescence and good solubility in both aqueous and non-aqueous solvents, but other luminophores such as luminol, and P-acid have been reported to be applicable. Like electrochemiluminescence, several modifications of the electrode surface and the detection antibody using enzymes and nanoparticles have been used to realize better sensitivity and detection limits.

The PADs present promising approaches to early diagnosis of diseases as seen from the discussed reports which show high commercial potential. However, commercialized products are not yet available in the market due to several challenges. These challenges include the complicated workflow of the regulatory process for commercialization of point-of-care diagnostic devices and providing it to the users. Where before taking marketing approval for a new device, the device should pass through a specific route to ensure the impact on the patient health, especially in relevance to the accuracy and the false positive and false negative results. Also, it should fulfill essential requirements for design, production, and information provided to the user. Moreover, the variations in the requirements and the workflow between the regulatory authorities in the different countries increase the time for distributing the new devices globally. The performance of the device itself, such as measurement accuracy and storage stability, is also an issue for practical application. However, these issues, such as regulation and device performance, will eventually be resolved as R&D progresses. The future development of hybrid PADs using different materials and substrates and the integration of PADs with portable signal readers and smartphones will provide PADs of exceptional value which will foster faster commercialization of PADs for diseases diagnosis.

1.4.7 Thesis focus and objectives

The main objective of this thesis is to contribute to the development of advanced analytical tools that address the critical needs of point-of-need (PON) applications, with a particular focus on paper-based ELISA for medical diagnostics and food safety.

The research begins with the development of a novel protocol for rapid immobilization of antibodies on cellulose paper, that allows immobilization in 5 minutes. Followed by the development of a μPAD-based ELISA for detecting the allergenic protein β'-c, with optimizations enabling detection within 15 minutes using minimal reagent volumes, achieving a detection limit of 1.59 ng/mL. The study

highlights the advantages of μPADs in improving the simplicity, cost-effectiveness, and practicality of allergen detection.

The thesis further advances the field by introducing a hybrid platform that integrates paper-based assays with a 3D-printed microplate for ultra-sensitive bioluminescence detection of the HER2 breast cancer biomarker. This system employs cellulose paper for rapid antibody immobilization and a microplate designed with flow control features, allowing completion of highly sensitive assays in just 20 minutes with reagent volumes as low as 5 μL. With a detection limit of 1.69 pg/mL, the platform is significantly more sensitive than conventional ELISA kits. The reusability and compatibility of the microplate with commercial readers enhance its practicality.

Overall, the advancements presented in this thesis underscore the transformative potential of μPADs and hybrid diagnostic platforms in achieving faster, more sensitive, and cost-effective analytical solutions. These innovations pave the way for impactful applications in medical diagnostics and food safety, addressing global challenges in healthcare and public health.

1.5 References

[1] N. Convery, N. Gadegaard, 30 years of microfluidics, Micro Nano Eng., 2(2019) 76-91.

[2] M. Zimmermann, H. Schmid, P. Hunziker, E. Delamarche, Capillary pumps for autonomous capillary systems, Lab. Chip, 7(2007) 119-25.

[3] D. Juncker, H. Schmid, U. Drechsler, H. Wolf, M. Wolf, B. Michel, et al., Autonomous microfluidic capillary system, Anal. Chem., 74(2002) 6139-44.

[4] A.W. Martinez, S.T. Phillips, M.J. Butte, G.M. Whitesides, Patterned paper as a platform for inexpensive, low-volume, portable bioassays, Angew. Chem. Int. Ed., 46(2007) 1318-20.

[5] H. Sung, J. Ferlay, R.L. Siegel, M. Laversanne, I. Soerjomataram, A. Jemal, et al., Global cancer statistics 2020: GLOBOCAN estimates of incidence and mortality worldwide for 36 cancers in 185 countries, CA Cancer J. Clin., 71(2021) 209-49.

[6] R.L. Siegel, K.D. Miller, H.E. Fuchs, A. Jemal, Cancer statistics, 2022, CA Cancer J. Clin., 72(2022) 7-33.

[7] P.R. Karmakar, Epidemiology of Cancer: Asian Perspective Revised, in: S.K. Basu, C.K. Panda, S. Goswami (Eds.), Cancer Diagnostics and Therapeutics, 1 ed., Springer, Singapore, 2022, pp. 489-508.

[8] T. Kavetskyy, M. Alipour, O. Smutok, O. Mushynska, A. Kiv, D. Fink, et al., Magneto-immunoassay of cancer biomarkers: Recent progress and challenges in biomedical analysis, Microchem J., 167(2021) 106320.

[9] L. Wu, X. Qu, Cancer biomarker detection: recent achievements and challenges, Chem. Soc. Rev., 44(2015) 2963-97.

[10] A.B. Chinen, C.M. Guan, J.R. Ferrer, S.N. Barnaby, T.J. Merkel, C.A. Mirkin, Nanoparticle probes for the detection of cancer biomarkers, cells, and tissues by fluorescence, Chem. Rev., 115(2015) 10530-74.

[11] A. Alba-Bernal, R. Lavado-Valenzuela, M.E. Dominguez-Recio, B. Jimenez-Rodriguez, M.I. Queipo-Ortuno, E. Alba, et al., Challenges and achievements of liquid biopsy technologies employed in early breast cancer, EBioMedicine, 62(2020) 103100.

[12] G.D. Dakubo, Cancer Biomarkers in Body Fluids: Springer International Publishing Switzerland; 2016.

[13] S. Suan Ng, H. Ling Lee, P. Bothi Raja, R.A. Doong, Recent advances in nanomaterial-based optical biosensors as potential point-of-care testing (PoCT) probes in carcinoembryonic antigen detection, Chem. Asian. J., 17(2022) e202200287.

[14] H. Wang, T. Wu, M. Li, Y. Tao, Recent advances in nanomaterials for colorimetric cancer detection, J. Mater. Chem. B, 9(2021) 921-38.

[15] H. Mollasalehi, E. Shajari, A colorimetric nano-biosensor for simultaneous detection of prevalent cancers using unamplified cell-free ribonucleic acid biomarkers, Bioorg. Chem., 107(2021) 104605.

[16] M. Carneiro, L.R. Rodrigues, F.T.C. Moreira, M.G.F. Sales, Colorimetric paper-based sensors against cancer biomarkers, Sensors, 22(2022) 3321.

[17] X. Wu, Y. Li, M.Y. Yang, C.B. Mao, Simultaneous ultrasensitive detection of two breast cancer microRNA biomarkers by using a dual nanoparticle/nanosheet fluorescence resonance energy transfer sensor, Mater. Today Adv., 12(2021) 100163.

[18] X. Zhao, X. Dai, S. Zhao, X. Cui, T. Gong, Z. Song, et al., Aptamer-based fluorescent sensors for the detection of cancer biomarkers, Spectrochim. Acta A Mol. Biomol. Spectrosc., 247(2021) 119038.

[19] K. Djebbi, J. Xing, T. Weng, M. Bahri, M.A. Elaguech, C. Du, et al., Highly sensitive fluorescence multiplexed miRNAs biosensors for accurate clinically diagnosis lung cancer disease using LNA-modified DNA probe and DSN enzyme, Anal. Chim. Acta., 1208(2022) 339778.

[20] F. Arshad, F. Nabi, S. Iqbal, R.H. Khan, Applications of graphene-based electrochemical and optical biosensors in early detection of cancer biomarkers, Colloids Surf. B Biointerfaces, 212(2022) 112356.

[21] J.I. Omage, E. Easterday, J.T. Rumph, I. Brula, B. Hill, J. Kristensen, et al., Cancer diagnostics and early detection using electrochemical aptasensors, Micromachines, 13(2022) 522.

[22] I.M. Mostafa, Y. Tian, S. Anjum, S. Hanif, M. Hosseini, B.H. Lou, et al., Comprehensive review on the electrochemical biosensors of different breast cancer biomarkers, Sens. Actuators B Chem., 365(2022) 131944.

[23] I.K. Oktaviyanti, D.S. Ali, S.A. Awadh, M.J.C. Opulencia, S. Yusupov, R. Dias, et al., Recent advances on applications of immunosensing systems based on nanomaterials for CA15-3 breast cancer biomarker detection, Anal. Bioanal. Chem., 415(2022) 367.

[24] L. Jing, C. Xie, Q. Li, M. Yang, S. Li, H. Li, et al., Electrochemical biosensors for the analysis of breast cancer biomarkers: from design to application, Anal. Chem., 94(2022) 269-96.

[25] R. Goldoni, A. Scolaro, E. Boccalari, C. Dolci, A. Scarano, F. Inchingolo, et al., Malignancies and biosensors: a focus on oral cancer detection through salivary biomarkers, Biosensors, 11(2021) 396.

[26] J. Shen, B. Situ, X. Du, Z. Wang, R. Hu, B. Li, et al., Aggregation-Induced emission luminogen-based dual-mode enzyme-linked immunosorbent assay for ultrasensitive detection of cancer biomarkers in a broad concentration range, ACS Sens., 7(2022) 766-74.

[27] N. Alijaj, B. Pavlovic, P. Martel, A. Rakauskas, V. Cesson, K. Saba, et al., Identification of urine biomarkers to improve eligibility for prostate biopsy and detect high-grade prostate cancer, Cancers, 14(2022) 1135.

[28] O.L. Bodulev, I.Y. Sakharov, A Microtiter-Plate chemiluminescence method for the determination of microrna-141 based on the application of catalytic hairpin assembly and a streptavidin-polyperoxidase conjugate, J. Anal. Chem., 77(2022) 450-7.

[29] Q.L. Shu, Y.F. Zhu, Y.P. Xiao, K.S. Chen, X. Mai, X.J. Zheng, et al., A novel chemiluminescence biosensor based on dual aptamers bound nanoparticles with multi-site signal amplification for sensitive detection of carcinoembryonic antigen, Microchem. J., 179(2022) 107482.

[30] Y. Liu, N. Zhang, J.B. Pan, J. Song, W. Zhao, H.Y. Chen, et al., Bipolar electrode array for multiplexed detection of prostate cancer biomarkers, Anal. Chem., 94(2022) 3005-12.

[31] X. Fan, S. Wang, H. Liu, Z. Li, Q. Sun, Y. Wang, et al., A sensitive electrochemiluminescence biosensor for assay of cancer biomarker (MMP-2) based on NGQDs-Ru@SiO2 luminophore, Talanta, 236(2022) 122830.

[32] H.M. Gao, Z. Zhang, Y.C. Zhang, H.W. Yu, S.Z. Rong, L.Q. Meng, et al., Electrochemiluminescence immunosensor for cancer antigen 125 detection based on novel resonance energy transfer between graphitic carbon nitride and NIR CdTe/CdS QDs, J. Electroanal. Chem., 886(2021) 115104.

[33] Y.G. Feng, J.H. Zhu, X.Y. Wang, A.J. Wang, L.P. Mei, P.X. Yuan, et al., New advances in accurate monitoring of breast cancer biomarkers by electrochemistry, electrochemiluminescence, and photoelectrochemistry, J. Electroanal. Chem., 882(2021) 115010.

[34] X. Chen, H. Song, Z. Li, R. Liu, Y. Lv, Lanthanide nanoprobes for the multiplex evaluation of breast cancer biomarkers, Anal. Chem., 93(2021) 13719-26.

[35] A. Kumar, A. Kumar, S.K. Srivastava, A study on surface plasmon resonance biosensor for the detection of CEA biomarker using 2D materials graphene, Mxene and MoS_2, Optik, 258(2022) 168885.

[36] A. Gade, A. Sharma, N. Srivastava, S.J.S. Flora, Surface plasmon resonance: A promising approach for label-free early cancer diagnosis, Clin. Chim. Acta., 527(2022) 79-88.

[37] F. Usman, J.O. Dennis, A.I. Aljameel, M.K.M. Ali, O. Aldaghri, K.H. Ibnaouf, et al., Plasmonic biosensors for the detection of lung cancer biomarkers: A review, Chemosensors, 9(2021) 326.

[38] A. Pollap, P. Swit, Recent advances in sandwich sers immunosensors for cancer detection, Int. J. Mol. Sci., 23(2022) 4740.

[39] L. Huang, Y. Zhu, C. Xu, Y. Cai, Y. Yi, K. Li, et al., Noninvasive diagnosis of gastric cancer based on breath analysis with a tubular surface-enhanced raman scattering sensor, ACS Sens., 7(2022) 1439-50.

[40] M. Haroon, M. Tahir, H. Nawaz, M.I. Majeed, A.A. Al-Saadi, Surface-enhanced Raman scattering (SERS) spectroscopy for prostate cancer diagnosis: A review, Photodiagn. Photodyn. Ther., 37(2022) 102690.

[41] S. Dey, E. Ahmed, P.S. Somvanshi, A. Ibn Sina, A. Wuethrich, M. Trau, An electrochemical and Raman scattering dual detection biosensor for rapid screening and biomolecular profiling of cancer biomarkers, Chemosensors, 10(2022) 93.

[42] X. Lu, C. Yao, L. Sun, Z. Li, Plasmon-enhanced biosensors for microRNA analysis and cancer diagnosis, Biosens. Bioelectron., 203(2022) 114041.

[43] S. Zhang, C. Liu, X. Zou, X. Geng, X. Zhou, X. Fan, et al., MicroRNA panel in serum reveals novel diagnostic biomarkers for prostate cancer, PeerJ, 9(2021) e11441.

[44] X. Chen, H. Ruan, Z. Ma, J. Hu, W. Xu, L. Yin, et al., Polymerase chain reaction in the detection of mir-455-5p and sphingosine-1 phosphate proteins in cervical carcinoma with the help of gold nanoparticles-based, J. Biomed. Nanotechnol., 17(2021) 1535-44.

[45] A. Stahlberg, N. Zoric, P. Aman, M. Kubista, Quantitative real-time PCR for cancer detection: the lymphoma case, Expert. Rev. Mol. Diagn., 5(2005) 221-30.

[46] Y. Hou, C.C. Lv, Y.L. Guo, X.H. Ma, W. Liu, Y. Jin, et al., Recent advances and applications in paper-based devices for point-of-care testing, J. Anal. Test., (2022) 1-27.

[47] A. Manbohi, S.H. Ahmadi, Portable smartphone-based colorimetric system for simultaneous on-site microfluidic paper-based determination and mapping of phosphate, nitrite and silicate in coastal waters, Environ. Monit. Assess., 194(2022) 190.

[48] X.Y. Liu, Z. Chen, R.S. Gao, C.Y. Kan, J.H. Xu, A paper-based fluorescent and colorimetric portable device with smartphone application for Fe^{3+} sensing, J. Environ. Chem. Eng., 10(2022) 107650.

[49] R.F. Menger, J.J. Beck, T. Borch, C.S. Henry, Colorimetric paper-based analytical device for perfluorooctanesulfonate detection, ACS EST. Water, 2(2022) 565-72.

[50] Y. Yan, D. Zhao, W. Li, X. Li, Y. Chang, Q. Zhang, et al., An origami paper-based analytical device for rapid and sensitive analysis of acrylamide in foods, Micromachines, 13(2021) 13.

[51] H. Zhang, X.T. Li, Q.Y. Zhu, Z.X. Wang, The recent development of nanomaterials enhanced paper-based electrochemical analytical devices, J. Electroanal. Chem., 909(2022) 116140.

[52] J. Zhuang, Z. Zhao, K. Lian, L. Yin, J. Wang, S. Man, et al., SERS-based CRISPR/Cas assay on microfluidic paper analytical devices for supersensitive detection of pathogenic bacteria in foods, Biosens. Bioelectron., 207(2022) 114167.

[53] L.S.A. Busa, S. Mohammadi, M. Maeki, A. Ishida, H. Tani, M. Tokeshi, Advances in microfluidic paper-based analytical devices for food and water analysis, Micromachines, 7(2016) 86.

[54] S. Soni, B.J. Toley, Paper-based nucleic acid sample preparation for point-of-care diagnostics, Sens. Actuators B Chem., 355(2022) 131272.

[55] K.T.L. Trinh, W.R. Chae, N.Y. Lee, Recent advances in the fabrication strategies of paper-based microfluidic devices for rapid detection of bacteria and viruses, Microchem J, 180(2022) 107548.

[56] A. Yamaguchi, H. Miyaguchi, A. Ishida, M. Tokeshi, Paper-based analytical device for the on-site detection of nerve agents, ACS. Appl. Bio. Mater., 4(2021) 6512-8.

[57] T. Komatsu, Y. Sato, M. Maeki, A. Ishida, H. Tani, M. Tokeshi, Rapid, sensitive universal paper-based device enhances competitive immunoassays of small molecules, Anal. Chim. Acta., 1144(2021) 85-95.

[58] T. Komatsu, M. Maeki, A. Ishida, H. Tani, M. Tokeshi, Paper-based device for the facile colorimetric determination of lithium ions in human whole blood, ACS Sens., 5(2020) 1287-94.

[59] V. Primpray, O. Chailapakul, M. Tokeshi, T. Rojanarata, W. Laiwattanapaisal, A paper-based analytical device coupled with electrochemical detection for the determination of dexamethasone and prednisolone in adulterated traditional medicines, Anal. Chim. Acta., 1078(2019) 16-23.

[60] W. Li, X. Zhang, S. Chen, Y. Ji, R. Li, Paper-based fluorescent devices for multifunctional assays: Biomarkers detection, inhibitors screening and chiral recognition, Chin. Chem. Lett., 33(2022) 4405-10.

[61] S. Das, Gagandeep, R. Bhatia, Paper-based microfluidic devices: Fabrication, detection, and significant applications in various fields, Rev. Anal. Chem., 41(2022) 112-36.

[62] E. Noviana, T. Ozer, C.S. Carrell, J.S. Link, C. McMahon, I. Jang, et al., Microfluidic paper-based analytical devices: from design to applications, Chem. Rev., 121(2021) 11835-85.

[63] A. Dukle, A.J. Nathanael, B. Panchapakesan, T.H. Oh, Role of Paper-based sensors in fight against cancer for the developing world, Biosensors, 12(2022) 737.

[64] K. Ratajczak, M. Stobiecka, High-performance modified cellulose paper-based biosensors for medical diagnostics and early cancer screening: A concise review, Carbohyd. Polym., 229(2020) 115463.

[65] N. Yonet-Tanyeri, B.Z. Ahlmark, S.R. Little, Advances in multiplexed paper-based analytical devices for cancer diagnosis: a review of technological developments, Adv. Mater. Technol., 6(2021) 2001138.

[66] J. Mettakoonpitak, K. Boehle, S. Nantaphol, P. Teengam, J.A. Adkins, M. Srisa-Art, et al., Electrochemistry on paper-based analytical devices: A review, Electroanal., 28(2016) 1420-36.

[67] M.L. Wang, J.R. Cui, Y. Wang, L. Yang, Z.Z. Jia, C.J. Gao, et al., Microfluidic paper-based analytical devices for the determination of food contaminants: developments and applications, J. Agric. Food Chem., 70(2022) 8188-206.

[68] A. Nilghaz, S.M. Mousavi, M.S. Li, J.F. Tian, R. Cao, X.G. Wang, Paper-based microfluidics for food safety and quality analysis, Trends Food Sci. Tech., 118(2021) 273-84.

[69] K. Mahato, A. Srivastava, P. Chandra, Paper based diagnostics for personalized health care: Emerging technologies and commercial aspects, Biosens. Bioelectron., 96(2017) 246-59.

[70] G. Musile, Y. Agard, L. Wang, E.F. De Palo, B. McCord, F. Tagliaro, Paper-based microfluidic devices: On-site tools for crime scene investigation, Trends Analyt. Chem., 143(2021) 116406.

[71] S. Nishat, A.T. Jafry, A.W. Martinez, F.R. Awan, Paper-based microfluidics: Simplified fabrication and assay methods, Sens. Actuators B Chem., 336(2021) 129681.

[72] W.K. Coltro, D.P. de Jesus, J.A. da Silva, C.L. do Lago, E. Carrilho, Toner and paper-based fabrication techniques for microfluidic applications, Electrophoresis, 31(2010) 2487-98.

[73] Y. He, Y. Wu, J.-Z. Fu, W.-B. Wu, Fabrication of paper-based microfluidic analysis devices: A review, RSC Adv., 5(2015) 78109-27.

[74] T. Akyazi, L. Basabe-Desmonts, F. Benito-Lopez, Review on microfluidic paper-based analytical devices towards commercialisation, Anal. Chim. Acta., 1001(2018) 1-17.

[75] N.S. DeChiara, D.J. Wilson, C.R. Mace, An open software platform for the automated design of paper-based microfluidic devices, Sci. Rep., 7(2017) 16224.

[76] E. Carrilho, A.W. Martinez, G.M. Whitesides, Understanding wax printing: a simple micropatterning process for paper-based microfluidics, Anal. Chem., 81(2009) 7091-5.

[77] J.S. Ng, M. Hashimoto, Fabrication of paper microfluidic devices using a toner laser printer, RSC Adv., 10(2020) 29797-807.

[78] R. Ghosh, S. Gopalakrishnan, R. Savitha, T. Renganathan, S. Pushpavanam, Fabrication of laser printed microfluidic paper-based analytical devices (LP-microPADs) for point-of-care applications, Sci. Rep., 9(2019) 7896.

[79] A. Prabhu, M.S. Giri Nandagopal, P. Peralam Yegneswaran, H.R. Singhal, N.K. Mani, Inkjet printing of paraffin on paper allows low-cost point-of-care diagnostics for pathogenic fungi, Cellulose, 27(2020) 7691-701.

[80] R.A. Ruiz, J.L. Gonzalez, M. Vazquez-Alvarado, N.W. Martinez, A.W. Martinez, Beyond wax printing: Fabrication of paper-based microfluidic devices using a thermal transfer printer, Anal. Chem., 94(2022) 8833-7.

[81] W. Dungchai, O. Chailapakul, C.S. Henry, A low-cost, simple, and rapid fabrication method for paper-based microfluidics using wax screen-printing, Analyst, 136(2011) 77-82.

[82] S. Mohammadi, M. Maeki, R.M. Mohamadi, A. Ishida, H. Tani, M. Tokeshi, An instrument-free, screen-printed paper microfluidic device that enables bio and chemical sensing, Analyst, 140(2015) 6493-9.

[83] Y. Sameenoi, P.N. Nongkai, S. Nouanthavong, C.S. Henry, D. Nacapricha, One-step polymer screen-printing for microfluidic paper-based analytical device (muPAD) fabrication, Analyst, 139(2014) 6580-8.

[84] C.L. Cassano, Z.H. Fan, Laminated paper-based analytical devices (LPAD): fabrication, characterization, and assays, Microfluid. Nanofluid., 15(2013) 173-81.

[85] T.R. de Oliveira, W.T. Fonseca, G. de Oliveira Setti, R.C. Faria, Fast and flexible strategy to produce electrochemical paper-based analytical devices using a craft cutter printer to create wax barrier and screen-printed electrodes, Talanta, 195(2019) 480-9.

[86] G. Chitnis, Z. Ding, C.L. Chang, C.A. Savran, B. Ziaie, Laser-treated hydrophobic paper: an inexpensive microfluidic platform, Lab Chip, 11(2011) 1161-5.

[87] P. Spicar-Mihalic, B. Toley, J. Houghtaling, T. Liang, P. Yager, E. Fu, CO2 laser cutting and ablative etching for the fabrication of paper-based devices, J. Micromech. Microeng., 23(2013) 067003.

[88] C.L. Chagas, L. Costa Duarte, E.O. Lobo-Junior, E. Piccin, N. Dossi, W.K. Coltro, Hand drawing of pencil electrodes on paper platforms for contactless conductivity detection of inorganic cations in human tear samples using electrophoresis chips, Electrophoresis, 36(2015) 1837-44.

[89] Y. Lu, W. Shi, L. Jiang, J. Qin, B. Lin, Rapid prototyping of paper-based microfluidics with wax for low-cost, portable bioassay, Electrophoresis, 30(2009) 1497-500.

[90] N. Alizadeh, A. Salimi, R. Hallaj, Mimicking peroxidase activity of Co2(OH)2CO3-CeO2 nanocomposite for smartphone based detection of tumor marker using paper-based microfluidic immunodevice, Talanta, 189(2018) 100-10.

[91] T. Komatsu, R. Maeda, M. Maeki, A. Ishida, H. Tani, M. Tokeshi, Dip-type paper-based analytical device for straightforward quantitative detection without precise sample introduction, ACS Sens., 6(2021) 1094-102.

[92] T. Komatsu, S. Mohammadi, L.S. Busa, M. Maeki, A. Ishida, H. Tani, et al., Image analysis for a microfluidic paper-based analytical device using the CIE L*a*b* color system, Analyst, 141(2016) 6507-9.

[93] L.S.A. Busa, M. Maeki, A. Ishida, H. Tani, M. Tokeshi, Simple and sensitive colorimetric assay system for horseradish peroxidase using microfluidic paper-based devices, Sens. Actuators B Chem., 236(2016) 433-41.

[94] J. Hu, S. Wang, L. Wang, F. Li, B. Pingguan-Murphy, T.J. Lu, et al., Advances in paper-based point-of-care diagnostics, Biosens. Bioelectron., 54(2014) 585-97.

[95] L. Liu, D. Yang, G. Liu, Signal amplification strategies for paper-based analytical devices, Biosens. Bioelectron., 136(2019) 60-75.

[96] C.B. Nielsen, H. Birn, F. Brandt, J.D. Kampmann, Urinary dipstick is not reliable as a screening tool for albuminuria in the emergency department-a prospective cohort study, Diagnostics, 12(2022) 457.

[97] P.W. West, Selective spot test for copper, Ind. Eng. Chem. Anal. Ed., 17(1945) 740-1.

[98] W. Liu, H. Yang, Y. Ding, S. Ge, J. Yu, M. Yan, et al., Paper-based colorimetric immunosensor for visual detection of carcinoembryonic antigen based on the high peroxidase-like catalytic performance of ZnFe2O4-multiwalled carbon nanotubes, Analyst, 139(2014) 251-8.

[99] T. Mazzu-Nascimento, G.G. Morbioli, L.A. Milan, F.C. Donofrio, C.A. Mestriner, E. Carrilho, Development and statistical assessment of a paper-based immunoassay for detection of tumor markers, Anal. Chim. Acta., 950(2017) 156-61.

[100] T. Mazzu-Nascimento, P.A. Gomes Carneiro Leão, J.R. Catai, G.G. Morbioli, E. Carrilho, Towards low-cost bioanalytical tools for sarcosine assays for cancer diagnostics, Anal. Methods, 8(2016) 7312-8.

[101] M. Masumoto, S. Ohta, M. Nakagawa, Y. Hiruta, D. Citterio, Colorimetric paper-based sarcosine assay with improved sensitivity, Anal. Bioanal. Chem., 414(2022) 691-701.

[102] E. Aydindogan, A.E. Ceylan, S. Timur, Paper-based colorimetric spot test utilizing smartphone sensing for detection of biomarkers, Talanta, 208(2020) 120446.

[103] R. Yokchom, S. Laiwejpithaya, W. Maneeprakorn, S. Tapaneeyakorn, J. Rabablert, T. Dharakul, Paper-based immunosensor with signal amplification by enzyme-labeled anti-p16(INK4a) multifunctionalized gold nanoparticles for cervical cancer screening, Nanomed., 14(2018) 1051-8.

[104] O. Hosu, A. Ravalli, G.M. Lo Piccolo, C. Cristea, R. Sandulescu, G. Marrazza, Smartphone-based immunosensor for CA125 detection, Talanta, 166(2017) 234-40.

[105] K.S. Prasad, Y. Abugalyon, C. Li, F. Xu, X. Li, A new method to amplify colorimetric signals of paper-based nanobiosensors for simple and sensitive pancreatic cancer biomarker detection, Analyst, 145(2020) 5113-7.

[106] S.M. Shaban, J.Y. Lee, D.H. Kim, Dual-surfactant-capped ag nanoparticles as a highly selective and sensitive colorimetric sensor for citrate detection, ACS Omega, 5(2020) 10696-703.

[107] A.C. Fu, Y. Hu, Z.-H. Zhao, R. Su, Y. Song, D. Zhu, Functionalized paper microzone plate for colorimetry and up-conversion fluorescence dual-mode detection of telomerase based on elongation and capturing amplification, Sens. Actuators B Chem., 259(2018) 642-9.

[108] F. Ma, L. He, E. Lindner, D.-Y. Wu, Highly porous poly(l-lactic) acid nanofibers as a dual-signal paper-based bioassay platform for in vitro diagnostics, Appl Surf Sci, 542(2021).

[109] A.C. Mirica, D. Stan, I.C. Chelcea, C.M. Mihailescu, A. Ofiteru, L.A. Bocancia-Mateescu, Latest trends in lateral flow immunoassay (lfia) detection labels and conjugation process, Front. Bioeng. Biotechnol., 10(2022) 922772.

[110] W. Zheng, L. Yao, J. Teng, C. Yan, P. Qin, G. Liu, et al., Lateral flow test for visual detection of multiple microRNAs, Sens. Actuators B Chem., 264(2018) 320-6.

[111] S. Chen, T. Guan, Z. Qian, Q. Quan, J. Wang, X. Li, et al., A sensitive and quantitative immunochromatographic assay for simultaneous detection of three stimulant laxatives in slimming food, Food Chem., 398(2023) 133861.

[112] S. Ouyang, S. Yu, Y. Le, Current advances in immunoassays for the detection of beta2-agonists, Foods, 11(2022).

[113] B. Ince, M.K. Sezginturk, Lateral flow assays for viruses diagnosis: Up-to-date technology and future prospects, Trends Anal. Chem., 157(2022) 116725.

[114] L. Khelifa, Y. Hu, N. Jiang, A.K. Yetisen, Lateral flow assays for hormone detection, Lab Chip, 22(2022) 2451-75.

[115] D.D. Lou, L. Fan, T. Jiang, Y. Zhang, Advances in nanoparticle-based lateral flow immunoassay for point-of-care testing, View, 3(2022) 20200125.

[116] B. Dyan, P.P. Seele, A. Skepu, P.S. Mdluli, S. Mosebi, N.R.S. Sibuyi, A review of the nucleic acid-based lateral flow assay for detection of breast cancer from circulating biomarkers at a point-of-care in low income countries, Diagnostics, 12(2022) 1973.

[117] X. Gao, H. Xu, M. Baloda, A.S. Gurung, L.P. Xu, T. Wang, et al., Visual detection of microRNA with lateral flow nucleic acid biosensor, Biosens. Bioelectron., 54(2014) 578-84.

[118] Q. Jiang, T. Han, H. Ren, A.U.R. Aziz, N. Li, H. Zhang, et al., Bladder cancer hunting: A microfluidic paper-based analytical device, Electrophoresis, 41(2020) 1509-16.

[119] Y. Wang, H. Pei, Y. Jia, J. Liu, Z. Li, K. Ai, et al., Synergistic tailoring of electrostatic and hydrophobic interactions for rapid and specific recognition of lysophosphatidic acid, an early-stage ovarian cancer biomarker, J. Am. Chem. Soc., 139(2017) 11616-21.

[120] I.d.S. Sene, V. Costa, D.C. Bras, E.A.d.O. Farias, G.E. Nunes, I.H. Bechtold, et al., A point of care lateral flow assay for rapid and colorimetric detection of interleukin 6 and perspectives in bedside diagnostics, J. Clin. Med. Res., 2(2020) 1-16.

[121] V. Ranganathan, S. Srinivasan, A. Singh, M.C. DeRosa, An aptamer-based colorimetric lateral flow assay for the detection of human epidermal growth factor receptor 2 (HER2), Anal. Biochem., 588(2020) 113471.

[122] A.D. Warren, G.A. Kwong, D.K. Wood, K.Y. Lin, S.N. Bhatia, Point-of-care diagnostics for noncommunicable diseases using synthetic urinary biomarkers and paper microfluidics, Proc. Natl. Acad. Sci. U S A, 111(2014) 3671-6.

[123] W. Ren, S.I. Mohammed, S. Wereley, J. Irudayaraj, Magnetic focus lateral flow sensor for detection of cervical cancer biomarkers, Anal. Chem., 91(2019) 2876-84.

[124] Q. Yu, Q. Zhao, S. Wang, S. Zhao, S. Zhang, Y. Yin, et al., Development of a lateral flow aptamer assay strip for facile identification of theranostic exosomes isolated from human lung carcinoma cells, Anal. Biochem., 594(2020) 113591.

[125] X. Huang, Y. Zhou, L. Ding, G. Yu, Y. Leng, W. Lai, et al., Supramolecular recognition-mediated layer-by-layer self-assembled gold nanoparticles for customized sensitivity in paper-based strip nanobiosensors, Small, 15(2019) e1903861.

[126] K.M. Koczula, A. Gallotta, Lateral flow assays, Essays Biochem., 60(2016) 111-20.

[127] G.A. Posthuma-Trumpie, J. Korf, A. van Amerongen, Lateral flow (immuno)assay: its strengths, weaknesses, opportunities and threats. A literature survey, Anal. Bioanal. Chem., 393(2009) 569-82.

[128] T. Ozer, C. McMahon, C.S. Henry, Advances in paper-based analytical devices, Annu. Rev. Anal. Chem., 13(2020) 85-109.

[129] N. Colozza, V. Caratelli, D. Moscone, F. Arduini, Origami paper-based electrochemical (bio)sensors: state of the art and perspective, Biosensors, 11(2021) 328.

[130] Y. Chen, W. Chu, W. Liu, X. Guo, Distance-based carcinoembryonic antigen assay on microfluidic paper immunodevice, Sens. Actuators B Chem., 260(2018) 452-9.

[131] F. Mesgari, S.M. Beigi, N. Fakhri, M. Hosseini, M. Aghazadeh, M.R. Ganjali, Paper-based chemiluminescence and colorimetric detection of cytochrome c by cobalt hydroxide decorated mesoporous carbon, Microchem J, 157(2020) 104991.

[132] S. Abarghoei, N. Fakhri, Y.S. Borghei, M. Hosseini, M.R. Ganjali, A colorimetric paper sensor for citrate as biomarker for early stage detection of prostate cancer based on peroxidase-like activity of cysteine-capped gold nanoclusters, Spectrochim. Acta A Mol. Biomol. Spectrosc., 210(2019) 251-9.

[133] N. Fakhri, S. Abarghoei, M. Dadmehr, M. Hosseini, H. Sabahi, M.R. Ganjali, Paper based colorimetric detection of miRNA-21 using Ag/Pt nanoclusters, Spectrochim. Acta A Mol. Biomol. Spectrosc., 227(2020) 117529.

[134] J. Nie, Y. Zhang, L. Lin, C. Zhou, S. Li, L. Zhang, et al., Low-cost fabrication of paper-based microfluidic devices by one-step plotting, Anal. Chem., 84(2012) 6331-5.

[135] W. Liu, Y. Guo, M. Zhao, H. Li, Z. Zhang, Ring-oven washing technique integrated paper-based immunodevice for sensitive detection of cancer biomarker, Anal. Chem., 87(2015) 7951-7.

[136] L. Liang, S. Ge, L. Li, F. Liu, J. Yu, Microfluidic paper-based multiplex colorimetric immunodevice based on the catalytic effect of Pd/Fe(3)O(4)@C peroxidase mimetics on multiple chromogenic reactions, Anal. Chim. Acta., 862(2015) 70-6.

[137] K. Wang, J. Yang, H. Xu, B. Cao, Q. Qin, X. Liao, et al., Smartphone-imaged multilayered paper-based analytical device for colorimetric analysis of carcinoembryonic antigen, Anal. Bioanal. Chem., 412(2020) 2517-28.

[138] L.X. Wang, J.J. Fu, Y. Zhou, G. Chen, C. Fang, Z.S. Lu, et al., On-chip RT-LAMP and colorimetric detection of the prostate cancer 3 biomarker with an integrated thermal and imaging box, Talanta, 208(2020) 120407.

[139] G. Fu, X. Li, W. Wang, R. Hou, Multiplexed tri-mode visual outputs of immunoassay signals on a clip-magazine-assembled photothermal biosensing disk, Biosens. Bioelectron., 170(2020) 112646.

[140] M. Dou, S.T. Sanjay, M. Benhabib, F. Xu, X. Li, Low-cost bioanalysis on paper-based and its hybrid microfluidic platforms, Talanta, 145(2015) 43-54.

[141] W. Zhou, M. Dou, S.S. Timilsina, F. Xu, X. Li, Recent innovations in cost-effective polymer and paper hybrid microfluidic devices, Lab Chip, 21(2021) 2658-83.

[142] M.J. Lee, V. Soum, S.N. Lee, J.H. Choi, J.H. Shin, K. Shin, et al., Pumpless three-dimensional photo paper-based microfluidic analytical device for automatic detection of thioredoxin-1 using enzyme-linked immunosorbent assay, Anal. Bioanal. Chem., 414(2022) 3219-30.

[143] M.V. Romeo, E. Lopez-Martinez, J. Berganza-Granda, F. Goni-de-Cerio, A.L. Cortajarena, Biomarker sensing platforms based on fluorescent metal nanoclusters, Nanoscale Adv., 3(2021) 1331-41.

[144] Y. Wang, Y. Gao, Y. Yin, Y. Pan, Y. Wang, Y. Song, Nanomaterial-assisted microfluidics for multiplex assays, Microchim. Acta, 189(2022) 139.

[145] T. Ueno, T. Nagano, Fluorescent probes for sensing and imaging, Nat. Methods, 8(2011) 642-5.

[146] B. Gao, H. Liu, Z. Gu, Patterned photonic nitrocellulose for pseudo-paper microfluidics, Anal. Chem., 88(2016) 5424-9.

[147] A. Prasad, S.M.A. Hasan, S. Grouchy, M.R. Gartia, DNA microarray analysis using a smartphone to detect the BRCA-1 gene, Analyst, 144(2018) 197-205.

[148] H. Zhang, Z. Lei, R. Tian, Z. Wang, Polyamidoamine starburst dendrimer-activated chromatography paper-based assay for sensitive detection of telomerase activity, Talanta, 178(2018) 116-21.

[149] X. Cai, H. Zhang, X. Yu, W. Wang, A microfluidic paper-based laser-induced fluorescence sensor based on duplex-specific nuclease amplification for selective and sensitive detection of miRNAs in cancer cells, Talanta, 216(2020) 120996.

[150] Y.C. Jiao, C. Du, L.J. Zong, X.Y. Guo, Y.F. Han, X.P. Zhang, et al., 3D vertical-flow paper-based device for simultaneous detection of multiple cancer biomarkers by fluorescent immunoassay, Sens. Actuators B Chem., 306(2020).

[151] W. Wang, X. Cai, Q. Li, L. Zheng, X. Yu, H. Zhang, et al., Application of a microfluidic paper-based bioimmunosensor with laser-induced fluorescence detection in the determination of alpha-fetoprotein from serum of hepatopaths, Talanta, 221(2021) 121660.

[152] G. Jarockyte, V. Karabanovas, R. Rotomskis, A. Mobasheri, Multiplexed nanobiosensors: current trends in early diagnostics, Sensors, 20(2020) 6890.

[153] W. Wang, Z. Liu, X. Lan, Quantum dot-based simultaneous multicolor imaging, Mol. Imaging Biol., 22(2020) 820-31.

[154] A. Yemets, S. Plokhovska, N. Pushkarova, Y. Blume, Quantum dot-antibody conjugates for immunofluorescence studies of biomolecules and subcellular structures, J. Fluoresc., 32(2022) 1713-23.

[155] Q. Zhang, X. Zhang, F. Ma, C.-y. Zhang, Advances in quantum dot-based biosensors for DNA-modifying enzymes assay, Coord. Chem. Rev., 469(2022) 214674.

[156] M. Zhao, H.F. Li, W. Liu, W.R. Chu, Y. Chen, Paper-based laser induced fluorescence immunodevice combining with CdTe embedded silica nanoparticles signal enhancement strategy, Sens. Actuators B Chem., 242(2017) 87-94.

[157] L.L. Liang, M. Su, L. Li, F.F. Lan, G.X. Yang, S.G. Ge, et al., Aptamer-based fluorescent and visual biosensor for multiplexed monitoring of cancer cells in microfluidic paper-based analytical devices, Sens. Actuators B Chem., 229(2016) 347-54.

[158] P. Das, U.J. Krull, Detection of a cancer biomarker protein on modified cellulose paper by fluorescence using aptamer-linked quantum dots, Analyst, 142(2017) 3132-5.

[159] L. Liang, F. Lan, L. Li, M. Su, S. Ge, J. Yu, et al., Fluorescence "turn-on" determination of H_2O_2 using multilayer porous SiO_2/NGQDs and PdAu mimetics enzymatic/oxidative cleavage of single-stranded DNA, Biosens. Bioelectron., 82(2016) 204-11.

[160] T. Tian, L. Li, Y. Zhang, H.Y. Liu, L.N. Zhang, M. Yan, et al., Dual-mode fluorescence biosensor platform based on T-shaped duplex structure for detection of microRNA and folate receptor, Sens. Actuators B Chem., 261(2018) 44-50.

[161] L. Huang, J. Wang, Q. Wang, D. Tang, Y. Lin, Distance-dependent visual fluorescence immunoassay on CdTe quantum dot-impregnated paper through silver ion-exchange reaction, Microchim. Acta, 187(2020) 563.

[162] S. Lv, Y. Tang, K. Zhang, D. Tang, Wet NH3-Triggered NH2-MIL-125(Ti) structural switch for visible fluorescence immunoassay impregnated on paper, Anal. Chem., 90(2018) 14121-5.

[163] C. Baynes, J.Y. Yoon, muPAD fluorescence scattering immunoagglutination assay for cancer biomarkers from blood and serum, SLAS Technol., 23(2018) 30-43.

[164] A. Roda, M. Guardigli, Analytical chemiluminescence and bioluminescence: latest achievements and new horizons, Anal. Bioanal. Chem., 402(2012) 69-76.

[165] L.M. Fu, Y.N. Wang, Detection methods and applications of microfluidic paper-based analytical devices, Trends Anal. Chem., 107(2018) 196-211.

[166] C. Dodeigne, L. Thunus, R. Lejeune, Chemiluminescence as a diagnostic tool. A review, Talanta, 51(2000) 415-39.

[167] L.X. Zhao, L. Sun, X.G. Chu, Chemiluminescence immunoassay, Trends Anal. Chem., 28(2009) 404-15.

[168] J. Wang, W. Li, L. Ban, W. Du, X.J. Feng, B.F. Liu, A paper-based device with an adjustable time controller for the rapid determination of tumor biomarkers, Sens. Actuators B Chem., 254(2018) 855-62.

[169] X. Guo, Y. Guo, W. Liu, Y. Chen, W. Chu, Fabrication of paper-based microfluidic device by recycling foamed plastic and the application for multiplexed measurement of biomarkers, Spectrochim. Acta A Mol. Biomol. Spectrosc., 223(2019) 117341.

[170] S. Wang, L. Ge, X. Song, J. Yu, S. Ge, J. Huang, et al., Paper-based chemiluminescence ELISA: lab-on-paper based on chitosan modified paper device and wax-screen-printing, Biosens. Bioelectron., 31(2012) 212-8.

[171] L. Ge, S. Wang, X. Song, S. Ge, J. Yu, 3D origami-based multifunction-integrated immunodevice: low-cost and multiplexed sandwich chemiluminescence immunoassay on microfluidic paper-based analytical device, Lab Chip, 12(2012) 3150-8.

[172] S. Wang, L. Ge, X. Song, M. Yan, S. Ge, J. Yu, et al., Simple and covalent fabrication of a paper device and its application in sensitive chemiluminescence immunoassay, Analyst, 137(2012) 3821-7.

[173] W. Li, S. Ge, S. Wang, M. Yan, L. Ge, J. Yu, Highly sensitive chemiluminescence immunoassay on chitosan membrane modified paper platform using TiO2 nanoparticles/multiwalled carbon nanotubes as label, Luminescence, 28(2013) 496-502.

[174] B. Gao, Y. Yang, J. Liao, B. He, H. Liu, Bioinspired multistructured paper microfluidics for POCT, Lab Chip, 19(2019) 3602-8.

[175] W. Chu, Y. Chen, W. Liu, L. Zhang, X. Guo, Three-dimensional ring-oven washing technique for a paper-based immunodevice, Luminescence, 35(2020) 503-11.

[176] W. Dungchai, O. Chailapakul, C.S. Henry, Electrochemical detection for paper-based microfluidics, Anal. Chem., 81(2009) 5821-6.

[177] M. Hasanzadeh, N. Shadjou, Electrochemical and photoelectrochemical nano-immunesensing using origami paper based method, Mater. Sci. Eng. C Mater. Biol. Appl., 61(2016) 979-1001.

[178] J. Adkins, K. Boehle, C. Henry, Electrochemical paper-based microfluidic devices, Electrophoresis, 36(2015) 1811-24.

[179] E. Noviana, C.P. McCord, K.M. Clark, I. Jang, C.S. Henry, Electrochemical paper-based devices: sensing approaches and progress toward practical applications, Lab Chip, 20(2020) 9-34.

[180] Y. Wang, J. Luo, J. Liu, S. Sun, Y. Xiong, Y. Ma, et al., Label-free microfluidic paper-based electrochemical aptasensor for ultrasensitive and simultaneous multiplexed detection of cancer biomarkers, Biosens. Bioelectron., 136(2019) 84-90.

[181] K. Sudhakara Prasad, X. Cao, N. Gao, Q. Jin, S.T. Sanjay, G. Henao-Pabon, et al., A Low-cost nanomaterial-based electrochemical immunosensor on paper for high-sensitivity early detection of pancreatic cancer, Sens. Actuators B Chem., 305(2020).

[182] H. Torul, E. Yarali, E. Eksin, A. Ganguly, J. Benson, U. Tamer, et al., Paper-based electrochemical biosensors for voltammetric detection of mirna biomarkers using reduced graphene oxide or MoS2 nanosheets decorated with gold nanoparticle electrodes, Biosensors 11(2021) 236.

[183] F. Bahavarnia, A. Saadati, S. Hassanpour, M. Hasanzadeh, N. Shadjou, A. Hassanzadeh, Paper based immunosensing of ovarian cancer tumor protein CA 125 using novel nano-ink: A new platform for efficient diagnosis of cancer and biomedical analysis using microfluidic paper-based analytical devices (muPAD), Int. J. Biol. Macromol., 138(2019) 744-54.

[184] S. Ji, M. Lee, D. Kim, Detection of early stage prostate cancer by using a simple carbon nanotube@paper biosensor, Biosens. Bioelectron., 102(2018) 345-50.

[185] M.S. Draz, M. Moazeni, M. Venkataramani, H. Lakshminarayanan, E. Saygili, N.K. Lakshminaraasimulu, et al., Hybrid paper-plastic microchip for flexible and high-performance point-of-care diagnostics, Adv. Funct. Mater., 28(2018).

[186] J. Qi, B. Li, N. Zhou, X. Wang, D. Deng, L. Luo, et al., The strategy of antibody-free biomarker analysis by in-situ synthesized molecularly imprinted polymers on movable valve paper-based device, Biosens. Bioelectron., 142(2019) 111533.

[187] P. Wang, L. Ge, M. Yan, X. Song, S. Ge, J. Yu, Paper-based three-dimensional electrochemical immunodevice based on multi-walled carbon nanotubes functionalized paper for sensitive point-of-care testing, Biosens. Bioelectron., 32(2012) 238-43.

[188] W. Li, L. Li, M. Li, J. Yu, S. Ge, M. Yan, et al., Development of a 3D origami multiplex electrochemical immunodevice using a nanoporous silver-paper electrode and metal ion functionalized nanoporous gold-chitosan, Chem. Commun., 49(2013) 9540-2.

[189] Y.F. Wu, P. Xue, K.M. Hui, Y.J. Kang, Electrochemical- and fluorescent-mediated signal amplifications for rapid detection of low-abundance circulating tumor cells on a paper-based microfluidic immunodevice, Chemelectrochem., 1(2014) 722-7.

[190] G. Sun, L. Zhang, Y. Zhang, H. Yang, C. Ma, S. Ge, et al., Multiplexed enzyme-free electrochemical immunosensor based on ZnO nanorods modified reduced graphene oxide-paper electrode and silver deposition-induced signal amplification strategy, Biosens. Bioelectron., 71(2015) 30-6.

[191] Y. Wang, H. Xu, J. Luo, J. Liu, L. Wang, Y. Fan, et al., A novel label-free microfluidic paper-based immunosensor for highly sensitive electrochemical detection of carcinoembryonic antigen, Biosens. Bioelectron., 83(2016) 319-26.

[192] L. Cao, C. Fang, R. Zeng, X. Zhao, Y. Jiang, Z. Chen, Paper-based microfluidic devices for electrochemical immunofiltration analysis of human chorionic gonadotropin, Biosens. Bioelectron., 92(2017) 87-94.

[193] D. Zang, L. Ge, M. Yan, X. Song, J. Yu, Electrochemical immunoassay on a 3D microfluidic paper-based device, Chem. Commun., 48(2012) 4683-5.

[194] B. Wei, K. Mao, N. Liu, M. Zhang, Z. Yang, Graphene nanocomposites modified electrochemical aptamer sensor for rapid and highly sensitive detection of prostate specific antigen, Biosens. Bioelectron., 121(2018) 41-6.

[195] L. Li, W.P. Li, H.M. Yang, C. Ma, J.H. Yu, M. Yan, et al., Sensitive origami dual-analyte electrochemical immunodevice based on polyaniline/Au-paper electrode and multi-labeled 3D graphene sheets, Electrochimica Acta, 120(2014) 102-9.

[196] L. Li, J. Xu, X. Zheng, C. Ma, X. Song, S. Ge, et al., Growth of gold-manganese oxide nanostructures on a 3D origami device for glucose-oxidase label based electrochemical immunosensor, Biosens. Bioelectron., 61(2014) 76-82.

[197] W. Li, L. Li, S. Ge, X. Song, L. Ge, M. Yan, et al., Multiplex electrochemical origami immunodevice based on cuboid silver-paper electrode and metal ions tagged nanoporous silver-chitosan, Biosens. Bioelectron., 56(2014) 167-73.

[198] J.M. Petroni, B.G. Lucca, L.C. da Silva Júnior, D.C. Barbosa Alves, V. Souza Ferreira, Paper-based electrochemical devices coupled to external graphene-cu nanoparticles modified solid electrode through meniscus configuration and their use in biological analysis, Electroanal., 29(2017) 2628-37.

[199] A. Sánchez-Calvo, M.T. Fernández-Abedul, M.C. Blanco-López, A. Costa-García, Paper-based electrochemical transducer modified with nanomaterials for mercury determination in environmental waters, Sens. Actuators B Chem., 290(2019) 87-92.

[200] G.Q. Sun, Y.N. Ding, C. Ma, Y. Zhang, S.G. Ge, J.H. Yu, et al., Paper-based electrochemical immunosensor for carcinoembryonic antigen based on three dimensional flower-like gold electrode and gold-silver bimetallic nanoparticles, Electrochimica Acta, 147(2014) 650-6.

[201] S. Ge, L. Zhang, Y. Zhang, H. Liu, J. Huang, M. Yan, et al., Electrochemical K-562 cells sensor based on origami paper device for point-of-care testing, Talanta, 145(2015) 12-9.

[202] S.G. Ge, Y. Zhang, L. Zhang, L.L. Liang, H.Y. Liu, M. Yan, et al., Ultrasensitive electrochemical cancer cells sensor based on trimetallic dendritic Au@PtPd nanoparticles for signal amplification on lab-on-paper device, Sens. Actuators B Chem., 220(2015) 665-72.

[203] Y. Fan, S. Shi, J. Ma, Y. Guo, A paper-based electrochemical immunosensor with reduced graphene oxide/thionine/gold nanoparticles nanocomposites modification for the detection of cancer antigen 125, Biosens. Bioelectron., 135(2019) 1-7.

[204] M. Su, L. Ge, S. Ge, N. Li, J. Yu, M. Yan, et al., Paper-based electrochemical cyto-device for sensitive detection of cancer cells and in situ anticancer drug screening, Anal. Chim. Acta., 847(2014) 1-9.

[205] Y. Wu, P. Xue, K.M. Hui, Y. Kang, A paper-based microfluidic electrochemical immunodevice integrated with amplification-by-polymerization for the ultrasensitive multiplexed detection of cancer biomarkers, Biosens. Bioelectron., 52(2014) 180-7.

[206] C. Ma, W. Li, Q. Kong, H. Yang, Z. Bian, X. Song, et al., 3D origami electrochemical immunodevice for sensitive point-of-care testing based on dual-signal amplification strategy, Biosens. Bioelectron., 63(2015) 7-13.

[207] J. Adhikari, M. Rizwan, N.A. Keasberry, M.U. Ahmed, Current progresses and trends in carbon nanomaterials-based electrochemical and electrochemiluminescence biosensors, J Chin Chem Soc-Taip, 67(2020) 937-60.

[208] I. Rahmawati, Y. Einaga, T.A. Ivandini, A. Fiorani, Enzymatic biosensors with electrochemiluminescence transduction, Chemelectrochem., 9(2022).

[209] T. Sun, J. Du, Z. Li, F. Zhao, Recent Advancement in the development of hybridization chain reaction-based electrochemiluminescence biosensors, Int. J. Electrochem. Sci., 17(2022) 220650.

[210] Q. Zhang, X. Zhang, Q. Ma, Recent advances in visual electrochemiluminescence analysis, J. Anal. Test., 4(2020) 92-106.

[211] I. Rahmawati, I. Irkham, R. Wibowo, J. Gunlazuardi, Y. Einaga, T.A. Ivandini, Electrogenerated chemiluminescence for immunoassay applications, Indones. J. Chem., 21(2021).

[212] M.M. Richter, Electrochemiluminescence (ECL), Chem. Rev., 104(2004) 3003-36.

[213] L. Ge, J. Yan, X. Song, M. Yan, S. Ge, J. Yu, Three-dimensional paper-based electrochemiluminescence immunodevice for multiplexed measurement of biomarkers and point-of-care testing, Biomater., 33(2012) 1024-31.

[214] X. Sun, B. Li, C. Tian, F. Yu, N. Zhou, Y. Zhan, et al., Rotational paper-based electrochemiluminescence immunodevices for sensitive and multiplexed detection of cancer biomarkers, Anal. Chim. Acta., 1007(2018) 33-9.

[215] L. Ge, J. Yu, S. Ge, M. Yan, Lab-on-paper-based devices using chemiluminescence and electrogenerated chemiluminescence detection, Anal. Bioanal. Chem., 406(2014) 5613-30.

[216] S. Wang, L. Ge, Y. Zhang, X. Song, N. Li, S. Ge, et al., Battery-triggered microfluidic paper-based multiplex electrochemiluminescence immunodevice based on potential-resolution strategy, Lab Chip, 12(2012) 4489-98.

[217] S. Wang, L. Ge, M. Yan, J.H. Yu, X.R. Song, S.G. Ge, et al., 3D microfluidic origami electrochemiluminescence immunodevice for sensitive point-of-care testing of carcinoma antigen 125, Sens. Actuators B Chem., 176(2013) 1-8.

[218] H. Yang, Q. Kong, S. Wang, J. Xu, Z. Bian, X. Zheng, et al., Hand-drawn&written pen-on-paper electrochemiluminescence immunodevice powered by rechargeable battery for low-cost point-of-care testing, Biosens. Bioelectron., 61(2014) 21-7.

[219] F. Liu, S. Ge, M. Su, X. Song, M. Yan, J. Yu, Electrochemiluminescence device for in-situ and accurate determination of CA153 at the MCF-7 cell surface based on graphene quantum dots loaded surface villous Au nanocage, Biosens. Bioelectron., 71(2015) 286-93.

[220] C. Gao, M. Su, Y. Wang, S. Ge, J. Yu, A disposable paper-based electrochemiluminescence device for ultrasensitive monitoring of CEA based on $Ru(bpy)_3^{2+}$@Au nanocages, RSC Adv., 5(2015) 28324-31.

[221] W. Li, M. Li, S. Ge, M. Yan, J. Huang, J. Yu, Battery-triggered ultrasensitive electrochemiluminescence detection on microfluidic paper-based immunodevice based on dual-signal amplification strategy, Anal. Chim. Acta., 767(2013) 66-74.

[222] C. Ma, H.Y. Liu, L.N. Zhang, L. Li, M. Yan, J.H. Yu, et al., Microfluidic paper-based analytical device for sensitive detection of peptides based on specific recognition of aptamer and amplification strategy of hybridization chain reaction, ChemElectroChem., 4(2017) 1744-9.

[223] W. Li, L. Li, S. Ge, X. Song, L. Ge, M. Yan, et al., A 3D origami multiple electrochemiluminescence immunodevice based on a porous silver-paper electrode and multi-labeled nanoporous gold-carbon spheres, Chem. Commun., 49(2013) 7687-9.

[224] Y. Zhang, L. Li, H. Yang, Y.-n. Ding, M. Su, J. Zhu, et al., Gold–silver nanocomposite-functionalized graphene sensing platform for an electrochemiluminescent immunoassay of a tumor marker, RSC Adv., 3(2013) 14701-14709.

[225] L. Wu, C. Ma, L. Ge, Q. Kong, M. Yan, S. Ge, et al., Paper-based electrochemiluminescence origami cyto-device for multiple cancer cells detection using porous AuPd alloy as catalytically promoted nanolabels, Biosens. Bioelectron., 63(2015) 450-7.

[226] J. Yan, L. Ge, X. Song, M. Yan, S. Ge, J. Yu, Paper-based electrochemiluminescent 3D immunodevice for lab-on-paper, specific, and sensitive point-of-care testing, Chem. Eur. J., 18(2012) 4938-45.

[227] W. Li, L. Li, S. Li, X. Wang, M. Li, S. Wang, et al., 3D origami electrochemiluminescence immunodevice based on porous silver-paper electrode and nanoporous silver double-assisted signal amplification, Sens. Actuators B Chem., 188(2013) 417-24.

[228] J. Yan, M. Yan, L. Ge, S. Ge, J. Yu, An origami electrochemiluminescence immunosensor based on gold/graphene for specific, sensitive point-of-care testing of carcinoembryonic antigen, Sens. Actuators B Chem., 193(2014) 247-54.

[229] S. Wang, W. Dai, L. Ge, M. Yan, J. Yu, X. Song, et al., Rechargeable battery-triggered electrochemiluminescence detection on microfluidic origami immunodevice based on two electrodes, Chem. Commun., 48(2012) 9971-3.

CHAPTER 2 Straightforward high-temperature antibody immobilization for rapid and simple microfluidic paper-based ELISA for detection of β'-component (Onc k 5) protein, a major IgE-binding protein in salmon roe

2.1 Introduction

Food allergies affect various organs and cause symptoms ranging from mild, such as simple skin rash, to severe, such as shock and death. They are commonly caused by certain allergenic proteins in food that trigger immunoglobulin E (IgE) mediated immune reactions within 2 hours from exposure to the food allergy proteins [1, 2]. Currently, there are no effective treatments for food allergies, only for the developed symptoms. Therefore, preventing exposure to food allergens is the only effective strategy. Globally, the establishment of an accurate food allergy labeling system for processed food is mandatory for maintaining the health of persons with food allergies [3, 4]. In the Japanese food allergy labeling system, there are seven specific allergenic ingredients (Milk, Wheat, Buckwheat, Egg, Shrimp, Crab, and Peanut and walnut) and twenty-one sub-specific allergenic ingredients (for example, Salmon, Salmon roe, Mackerel) [1, 5]. In Japan, seafood is considered the main source of animal protein intake, and it is one of the major allergenic foods, especially in children. Among the food allergy cases in preschool-age children, more than 9% were caused by fish roe [1]. Among the major yolk proteins, β'-component (β'-c) protein is the major allergen in salmon roe with strong IgE cross-reactivity, as reported by Shimizu et al. [6]. In 2012, under the name Onc K 5, β'-c was registered as the major allergenic protein in chum salmon roe by the World Health Organization and International Union of Immunological Societies (WHO/IUIS) Allergen Nomenclature Sub-Committee (https://www.allergen.org/). While salmon roe can be recognized by eyesight, the contamination of processed food by the roe yolk protein increases the risk for persons with salmon roe allergy. Developing an accurate detection method for β'-c allergen protein in food is important for the establishment of a good allergy labeling system and risk assessment of seafood. One report has been published on the detection of β'-c [7]; it uses a conventional sandwich enzyme-linked immunosorbent assay (ELISA) to determine β'-c in salmon roe yolk.

Sandwich ELISA is a common analytical technique used for the detection of antibodies and proteins or antigens in biological samples. Typically, sandwich ELISA is performed using a 96-microwell plate, where a capture antibody (cAb) specific for the required antigen is immobilized on the surface of the wells. When the sample is added to the wells, the antigen attached to the immobilized cAb. Then, after a suitable washing process, another enzyme-labeled detection antibody (dAb) is added to attach to the antigen. This is followed by a second washing, and a substrate is added, which reacts with the enzyme and produces a signal that is related to the antigen concentration. Conventional sandwich ELISA is a specific and sensitive technique; however, it is time-consuming because overnight incubation is needed to immobilize cAb, and it has other disadvantages that large sample and reagent volumes are required, the microwell plate reader used for signal readout is expensive, and a highly trained analyst must carry out the work. Microfluidic paper-based analytical devices (μPADs) are a very attractive approach for overcoming all these disadvantages.

Since the introduction of μPADs by Whitesides' group in 2007 [8], μPADs have attracted huge interest from researchers as ways to simplify complex analytical techniques in different applications [9-13]. Several analytical techniques have been integrated into μPADs, like colorimetry [14], fluorescence spectrometry [15], chemiluminescence spectrometry [16], and electrochemistry [17, 18]. Colorimetry methods implemented on the μPADs are the most common. These μPADs are the easiest to fabricate, and the signal readout can be done using a simple camera or smartphone. They require smaller amounts (or volumes) of reagents and samples and also shorter analysis times, thereby cutting analysis costs. These μPADs are mainly fabricated by patterning a hydrophobic barrier on a hydrophilic substrate for which several techniques are available, including wax printing, inkjet printing, stamping, screen printing, hand drawing, and laser cutting [19-22]. Wax printing is the most common because it is fast, easy, and suitable for mass production.

ELISA-based μPADs are widely used for several applications [14, 21, 23], in which the immobilization of cAb is the most important step for a successful ELISA assay. Typically, the paper substrate is chemically modified using chitosan and glutaraldehyde to get covalent immobilization of cAb. Chemical modification takes multiple steps and several hours [24-27]. In contrast, Zhao et al. [28] introduced another immobilization approach done through adding the antibody solution into the reaction zone and incubating it at 4 ^{o}C for 30 min. However, their process needs a long time. In addition, Whitesides's group introduced indirect paper-based ELISA that immobilized target proteins, including an IgG antibody, by drying the protein-loaded paper at ambient conditions for 10 min, although this ELISA uses no immobilized cAb [29].

A low temperature below room temperature for immobilization can reduce antibody denaturation caused by the unfolding of protein chains. However, prolonged hydration of antibodies can also promote denaturing. Several studies were reported on the effect of temperature on the binding activity of antibodies. In aqueous solutions, IgG antibodies begin to denature significantly at temperatures above 65 ^{o}C and lose almost all activity after being heated at 90 ^{o}C for several minutes [30]. In contrast, antibodies immobilized on the paper surface can retain more than 80% of their activity when heated at 40–60 ^{o}C for over 23 h. Additionally, they remain stable despite increasing humidity and can have a half-life of over 10 days [31]. These findings indicate that the immobilization of antibodies enhances their stability against denaturation by quickly restricting their movement on the solid surface, thereby slowing the unfolding process. Therefore, it is expected that immobilizing antibodies on cellulose paper at a temperature higher than room temperature can significantly reduce immobilization time and preserve antibody activity through the complete evaporation of the water medium. In this study, instead of covalent immobilization and physical adsorption at 4

°C or room temperature, the antibodies were immobilized on cellulose paper in just 5 min by drying at 50 °C.

In this study, a rapid, simple, and low-cost sandwich ELISA-based μPAD is presented for the determination of β'-component protein. For antibody immobilization, a straightforward technique based on physical adsorption has been also developed instead of covalent immobilization of antibodies. After the antibody solution was loaded on the paper substrate, the antibody immobilization was accomplished by drying the substrate in an oven at 50 °C for 5 min without any modification. This technique greatly reduced the number of steps, the total time for the assay, and the cost of antibody immobilization. In addition, the assay parameters, such as immobilization conditions, antibody concentrations, incubation time and temperature, and reaction time, were optimized to achieve the best performance. Compared to the conventional ELISA method, the proposed μPAD cut the total assay time to 15 min and lowered the amounts of reagents used.

2.2 Experimental

2.2.1 Materials

Phosphate buffer saline (PBS, pH 7.4) and bovine serum albumin (BSA) were purchased from FUJIFILM Wako Pure Chemical Corporation (Japan). 3,3',5,5'-tetramethylbenzidine (TMB) substrate solution and Tween 20 was purchased from Sigma-Aldrich (USA). Cyanine5 (Cy5)-labeled goat anti-Rabbit IgG HL was purchased from Abcam (UK). All reagents were of analytical grade and used without further purification. Ultrapure Milli-Q water (18.2 MΩ cm, Millipore, Germany) was used for the preparation of all the aqueous solutions. PBS (10 mM) containing 0.05 % v/v Tween 20 (0.05 % PBST) was used as a dilution and washing buffer for the β'-c protein and antibodies.

2.2.2 β'-c protein and antibodies

Purified β'-c protein and anti-β'-c antibodies were prepared as described by Shimizu et al. [6, 7]. β'-c protein was extracted from chum salmon roes using dilution precipitation and gel-permeation chromatography. The purified β'-c protein was dissolved in 0.5 M NaCl and 20 mM Tris-HCl (pH 8.0) and stored at -20 ºC. The capture anti- β'-c antibody was prepared by immunizing three-month-old male New Zealand White rabbits with the purified β'-c protein. The extracted and purified antibody was dissolved in 0.15 M NaCl and 20 mM phosphate buffer (pH 7.5), and 0.1% ProClin (Sigma-Aldrich) was added as a preservative. This was stored at -20 ºC. The detection anti- β'-c antibody was prepared like the capture antibody. The Fab' fragment of the antibody conjugated with horseradish peroxidase (HRP) was dissolved in D-PBS and 0.05% ProClin as a preservative and stored at -20 ºC. The conjugation process was performed by Hokudo Co., Ltd. (Japan). The thawed protein and antibodies were micropipetted into suitably sized containers and stored at 4 ºC until use. All animal experiments in this study were approved by the Hokkaido University Animal Care and Use Committee (Permit number: 10-0025), and the experiments were performed according to the Guidelines Concerning Animal Experiments at Hokkaido University.

2.2.3 Design and fabrication of ELISA μPAD

As explained in Fig. 2-1A, the fabrication process started with designing the device using Inkscape software ver. 1.2 (https://inkscape.org/). After that, the design was printed on Whatman #1 chromatography paper using a wax printer (ColorQube 8570, Xerox, USA). The printed design was heated in an oven at 120 ºC for 120 s to get wax penetration through the paper, forming the hydrophobic barriers. The device consisted of two layers; the upper layer contained the reaction zone, which was used to immobilize the capture antibodies and perform the ELISA assay as shown in Fig. 2-1B, while the lower layer contained an absorption pad

which removed the excess reagents and washing solutions. The two layers were stacked together by applying a commercial glue stick on the hydrophobic parts.

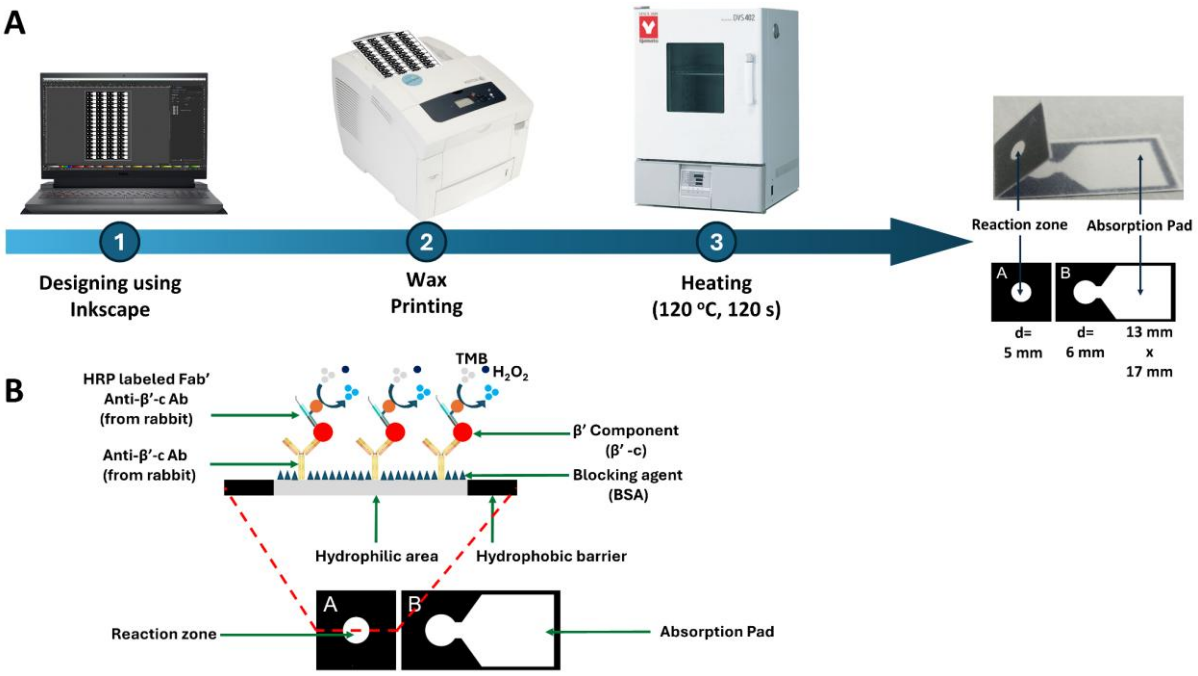

Fig. 2- 1 µPAD ELISA fabrication process starts with designing using Inkscape, then wax printing and heating to form hydrophobic barriers, and finally stacking two layers. (B) Illustration of sandwich ELISA for β'-c on the reaction zone.

2.2.4 Sandwich ELISA for β'-c protein detection

A sandwich ELISA for β'-c protein determination was performed using the fabricated μPAD as shown in Fig. 2-2. Briefly, a 3 μL aliquot of anti- β'-c cAb (10 μg/mL) was spotted into the reaction zone and dried at 50 ºC for 5 min. The excess non-immobilized cAb was washed twice by adding 15 μL of 0.05 % PBST. Then, 3 μL of 0.05 % PBST containing 2% w/v BSA was added and dried at 50 ºC for 5 min to block non-specific binding sites in the reaction zone. A solution (3 μL) containing β'-c was added to the reaction zone, followed by incubation at room temperature (~25 ºC) for 0.5 min. Then 3 μL HRP-labeled anti- β'-c dAb (0.5 μg/mL) was added, and a second incubation was done at room temperature for 2 min. The unreacted dAb was washed out twice using 15 μL of 0.05 % PBST. Finally, 3 μL of TMB substrate solution was added. After 2 min, an image for the developed blue color was taken using a digital camera (Canon EOS Kiss X10i).

2.2.5 Image capturing and data analyses

To capture images, the camera was fixed using a photography copy stand at a distance of 15 cm between the lens and a paper-based device. Grid mode was employed to adjust the XY position of the device to the center of the screen. All images were captured under ceiling lighting. The device received uniformly distributed light as a result of the considerable distance between the light source and the device. Additionally, to maintain consistent lighting conditions, both the sample and blank were captured in a single image, ensuring they were exposed to identical imaging conditions.

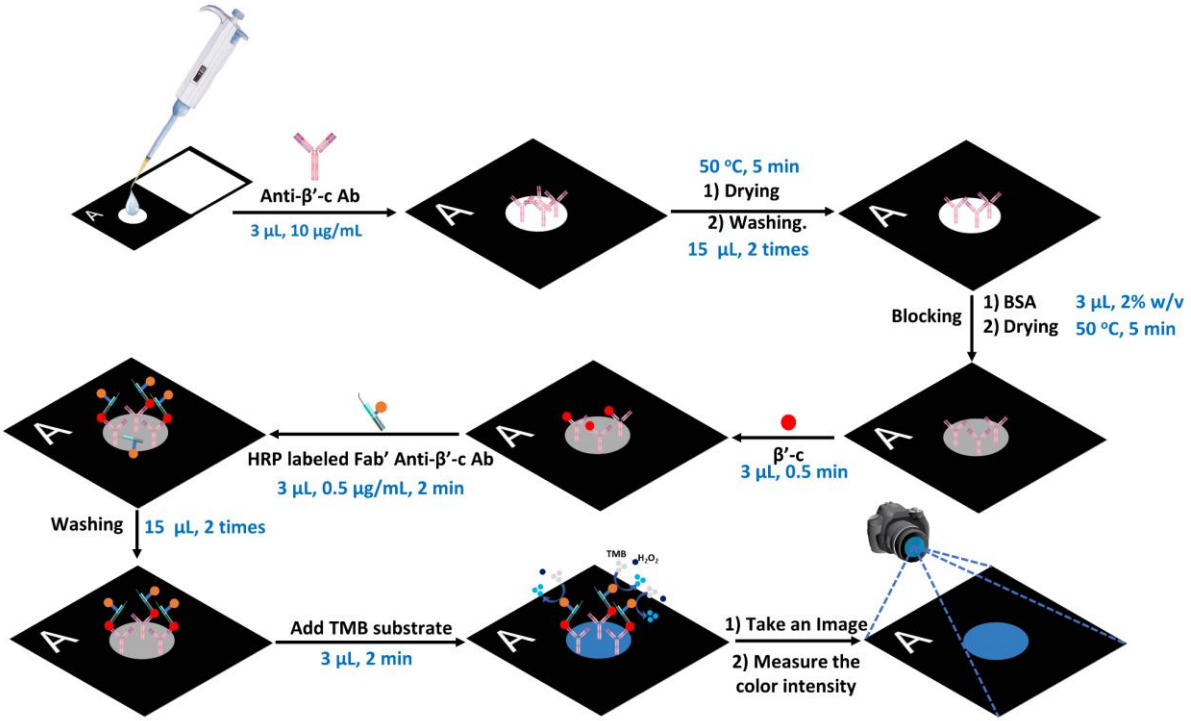

Fig. 2- 2 Schematic illustration of the steps with the sandwich ELISA for β'-component protein under optimized conditions, starting from immobilization of cAb, then blocking of non-specific binding sites, adding antigen, adding dAb, adding TMB substrate, and finally taking an image.

Images taken using the digital camera were transferred to a computer for further processing and analysis using the ImageJ software ver. 1.53 (https://imagej.net/ij/). The images were imported to ImageJ and converted from RGB to CMYK using the software plugin. The oval selection tool was used to select a circular area covering the whole reaction zone, and the cyan channel intensity was obtained. The difference between cyan intensities obtained with β'-c and a blank was used as the signal (ΔCyan). A relationship between the signal and the concentration of β'-c was plotted and analyzed using OriginPro 10.1 (https://www.originlab.com/) and Minitab software (https://www.minitab.com/en-us/).

2.3 Results and discussion

2.3.1 Optimization of sandwich ELISA parameters

2.3.1.1 Immobilization of antibody

In this study, cAb was immobilized by a simple and rapid technique, which only dries the antibody solution loaded on bare cellulose fibers (the reaction zone) in an oven, as described in Section 2.2.4. This immobilization is thought to be based on the physical adsorption of antibodies onto cellulose fibers. Here, the drying temperature and time for the immobilization of cAb were examined (Fig. 2-3). Drying the antibody at 50 ^{o}C provided a higher signal than at room temperature (~25 ^{o}C). In addition, a higher signal was obtained for a drying time of 5 min with a smaller variance than that of 3 min at a drying temperature of 50 ^{o}C. Furthermore, the cAb (rabbit IgG) immobilized at both room temperature and 50 ^{o}C were visualized through binding with a Cy5-labeled anti-rabbit IgG antibody under a fluorescence microscope (Fig. 2-4). Higher fluorescence was observed with drying at 50 ^{o}C for 5 min compared to those obtained after drying at room temperature for 5 and 15 min. These results indicate that drying the antibody at 50 ^{o}C for 5 min ensures immobilization of the antibody with a higher binding capability onto the paper substrate. Therefore, drying at 50 ^{o}C for 5 min was chosen for antibody immobilization for further experiments.

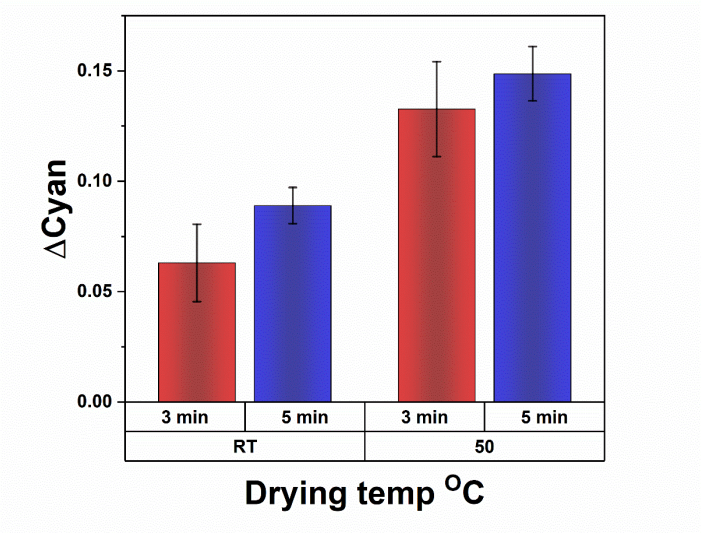

Fig. 2- 4 Effects of drying time and temperature on the immobilization of cAb. cAb (10 µg mL^{-1}) and dAb (0.5 µg mL^{-1}) were used. Washing was performed twice using 15 µL of 0.05% PBST. As a blocking buffer, 3 µL of 2% w/v BSA was used.

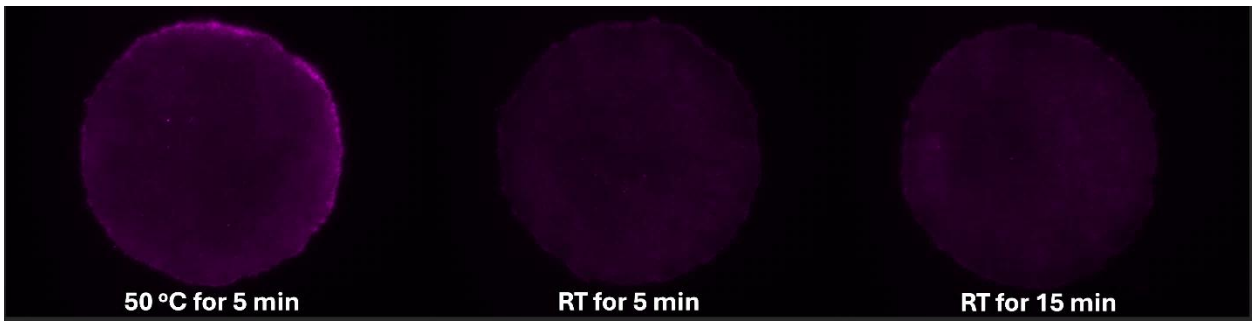

Fig. 2- 3 Fluorescence images for capture antibody immobilized at 50 °C for 5 min, and room temperature at 5 and 15 min. The procedure was done as follow, first 3 µL of 10 µg/mL anti β'-c Ab (from rabbit) was added to the detection zone and dried at 50 °C or room temperature. Next the unreacted antibody was washed twice using 15 µL of 0.05% PBST, the paper was blocked using 3 µL of 2% BSA. Then 3 µL of 10 µg/mL Cy5-labeled anti-rabbit antibody was added and incubated 2.5 min at room temperature to attach to the immobilized antibody. Finally, the unreacted cy5 labeled antibody washed twice using 15 µL of 0.05% PBST.

Next, this immobilization was validated by testing the stability of the immobilized antibody in washing processes because the antibody undergoes several washings to remove excess unreacted antibodies and the antigen. Washing was performed using 0.05% PBST at various volumes and washing times after adding the cAb and after adding the dAb. As shown in Fig. 2-5A-B, the cyan intensities obtained with β'-c (50 ng/mL) were almost constant for different washing times and volumes, while the cyan intensity of the blank decreased with increasing washing times and washing buffer volumes. Thus, increasing the washing times and washing volumes enhanced the signal (ΔCyan) (Fig. 2-5C). In addition, there was no notable difference between using 30 μL and 40 μL of the washing solution. Also, there was no significant difference between washing three times with 10 μL and washing two times with 15 μL. These results indicate that washing did not affect the cyan intensity of the sample, although it lowered the blank intensity, and the high stability of the immobilized cAb against washing was demonstrated. This result also proves that the present technique, which dries the antibody solution at 50 ºC for 5 min, is excellent for immobilizing cAb. For further experiments, two washes of 15 μL each were done. Furthermore, to confirm the strong adsorption of the antibodies, fluorescence images for Cy5-labeled antibody immobilized on the paper device at 50 ºC for 5 min, and fluorescence images were captured after several times of washing (Fig. 2-6). The fluorescence significantly decreased after the first washing, attributed to the removal of the non-immobilized Cy5-labeled antibodies. However, from the second washing onward, there was no significant change in the fluorescence, confirming the stability of the immobilized antibodies against washing.

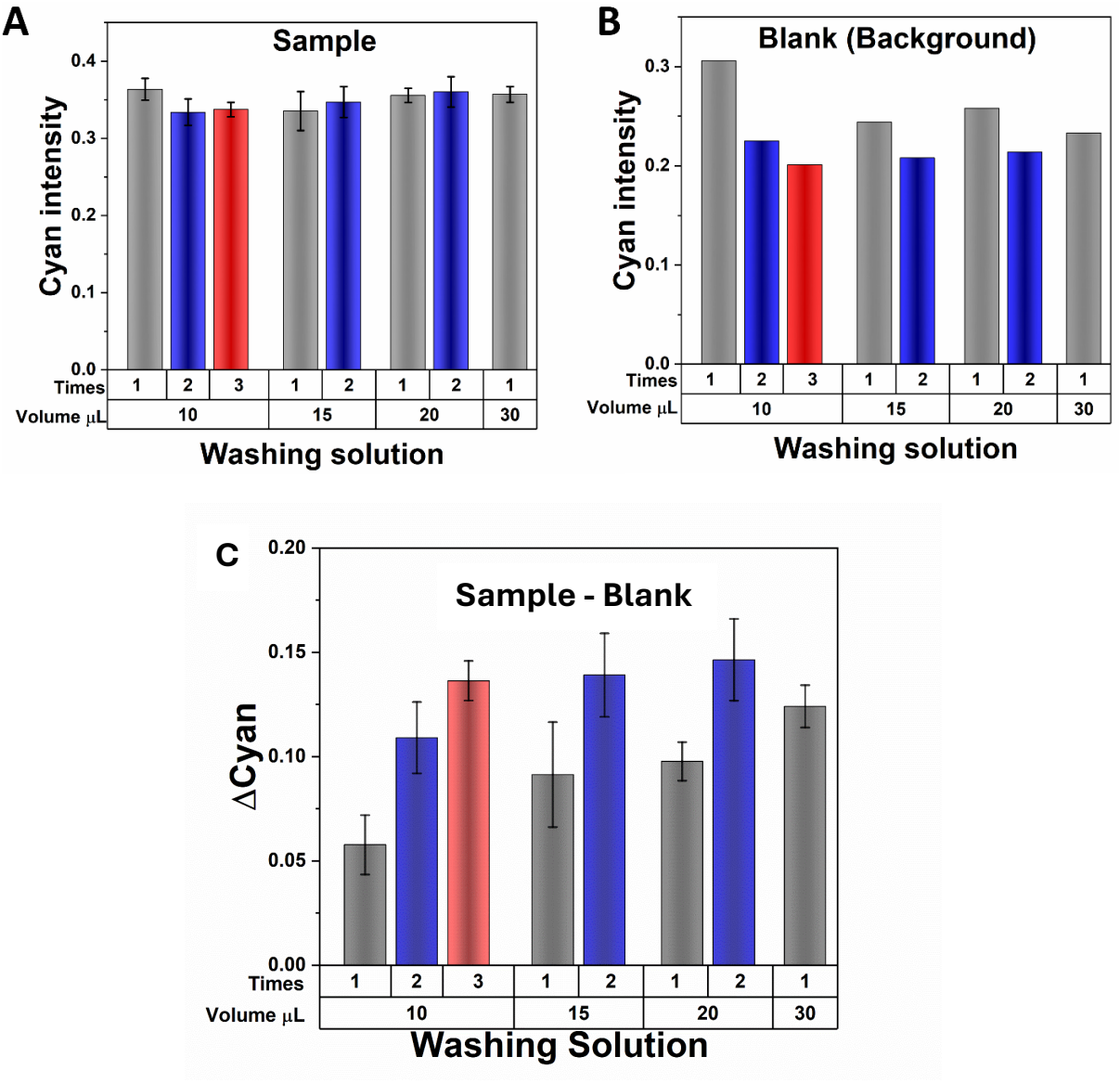

Fig. 2- 5 Effect of washing solution volume and times of washing on the signals of (A) sample, (B) background, and (C) Difference. Drying at 50 ºC for 5 min was performed. cAb (10 µg mL^{-1}) and dAb (0.5 µg mL^{-1}) were used. As a blocking buffer, 3 µL of 2% w/v BSA was used.

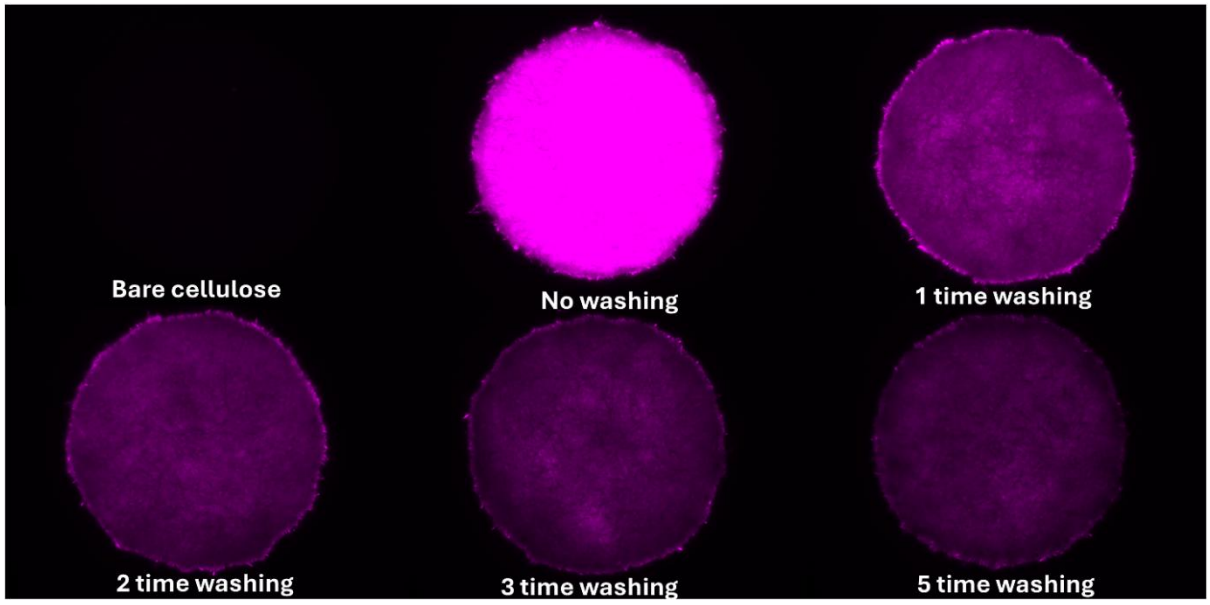

Fig. 2- 6 Fluorescence images of paper devices with immobilized Cy5-labeled antibody after various times of washing. A portion (3 µL) of 10 µg/mL Cy5-labeled antibody was added to each paper device and dried at 50 ºC for 5 min, then washed using 15 µL of 0.05% PBST.

2.3.1.2 Capture and detection antibodies

To choose the best concentration for cAb and dAb, two combinations of cAb: dAb ratios (20:1 and 40:1) with concentrations ranging from 5 to 40 µg mL^{-1} for cAb and from 0.25 to 2.00 µg mL^{-1} for dAb were tested as demonstrated in Fig. 2-7A. At high concentrations of cAb, higher dAb concentrations lower ΔCyan, which is attributed to increases in the blank (background) value due to incomplete washing to remove the excess dAb. This behavior could be due to the high viscosity of the ProClin preservative contained in the original stock solutions of the antibodies. As the concentration of antibodies in the working solutions increases, the amount of ProClin left in the reaction zone also increases, which forms a viscous layer on the paper. This layer makes washing more difficult and increases the drying time. Best results were obtained at cAb:dAb ratios of 10:0.5, 20:0.5, and 40:1.0 µg mL^{-1}. The lowest concentrations (10 µg mL^{-1} for cAb and 0.5 µg mL^{-1} for dAb) were chosen to reduce the assay cost.

Besides the normal order mentioned above, the order of addition of β'-c and dAb was investigated. First, after the immobilization of cAb, dAb was dried on the reaction zone, then β'-c was added, followed by the addition of TMB after 2 min. Second, the mixture of β'-c and the dAb was added to the immobilized cAb, and after 2 min, the TMB was added. As shown in Fig. 2-7B, the signal largely decreased when the dAb was dried on the reaction zone before adding the antigen, and this is because when ProClin in solutions of the antibodies was dried on the reaction zone, it affected the reaction between β'-c and cAb in the next step. Also, the addition of a mixture of β'-c and dAb to the reaction zone slightly decreased the signal; thus, the normal sequence of addition was chosen for the subsequent experiments.

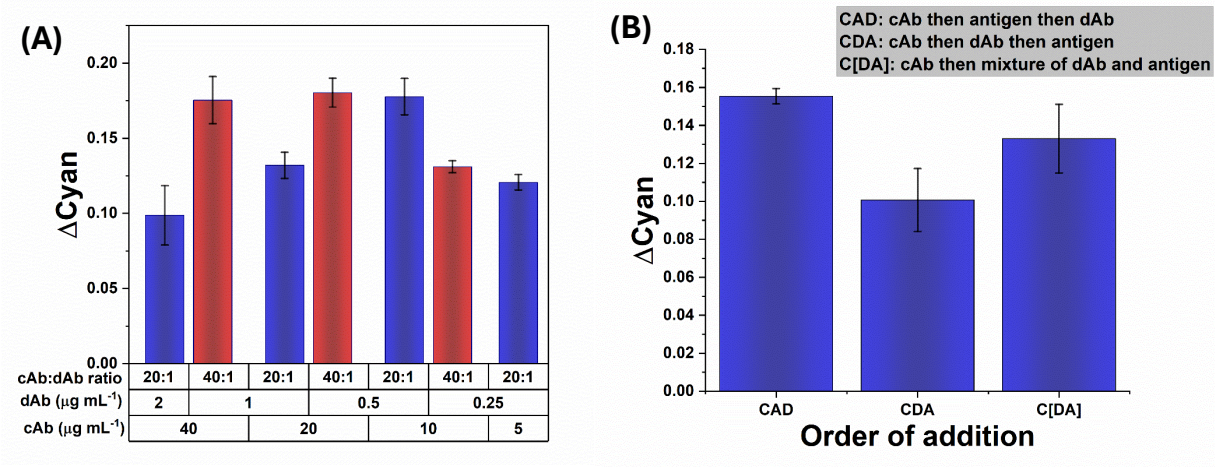

Fig. 2- 7 (A) Effects of capture and detection antibody concentration. (B)Order of addition of capture antibody, antigen, and detection antibody. Drying at 50 ºC for 5 min was performed. As a blocking buffer, 3 µL of 2% w/v BSA was used. Washing was performed twice using 15 µL of 0.05% PBST.

2.3.1.3 Blocking buffers

Various volumes of 0.05% PBST supplemented with BSA (2, 4, 6, and 10%) were used to block the non-specific binding sites on the reaction zone after the immobilization of cAb. Increasing the BSA concentration in the blocking buffer decreased the signal (Fig. 2-8A**)**, which is due to a negative effect on the interaction between cAb and β'-c in the next step. It is known that the viscosity of BSA aqueous solutions increases with increasing concentration [32]; therefore in the conventional ELISA, after blocking the well plate, unreacted BSA is removed by discarding the excess BSA solution and washing each well three times using PBST (typically, 200 µL of 0.05% PBST is employed). On the other hand in the µPAD-ELISA, the BSA solution on the paper surface was completely dried up. This process left behind any excess BSA that did not react. The amount of remaining BSA increases as the concentration of BSA in the blocking buffer increases. However, during the next step when the sample is added, this dried BSA needs to be redissolved. Redissolving becomes more difficult with higher amounts of BSA, which can then affect the reaction between β'-c and cAb. A low volume of blocking buffer leads to incomplete blocking of the non-specific binding sites, lowering the signal. While a large volume of blocking buffer contains a high amount of BSA, it causes only a slight decrease in the signal because the excess volume is drained through the absorption pad (Fig. 2-8B**)**. For the subsequent experiments, 3 µL and 2% BSA were chosen as the optimum volume and concentration.

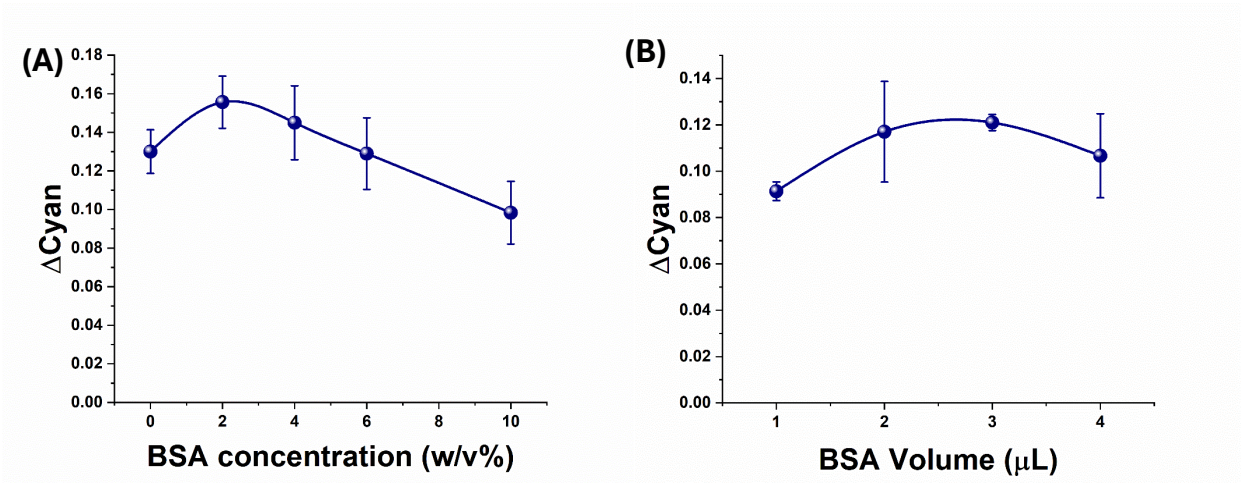

Fig. 2- 8 . Effects of BSA blocking buffer: (E) concentration and (F) volume. Drying at 50 ºC for 5 min was performed. cAb (10 µg mL^{-1}) and dAb (0.5 µg mL^{-1}) were used. Washing was performed twice using 15 µL of 0.05% PBST. 10% w/v BSA was used in panel B.

2.3.1.4 Incubation time for the reaction of β'-c with cAb and dAb

After blocking the non-specific binding sites using BSA, the device was ready for the introduction of the sample and the start of the assay. The incubation time for the reaction between β'-c and cAb was examined. The signal increased for 30 s, and then became nearly stable for the next 150 s, as shown in Fig. 2-9A. Next, the incubation time for the reaction between β'-c captured by cAb and dAb was studied by adding dAb 30 s after introducing the sample. The signal reached the maximum value at 2 min and then decreased after 3 min, as shown in Fig. 2-9B. This decrease can be explained by the increased excess unreacted dAb in the reaction zone with increasing incubation time. This decreases the washing efficiency, leading to the increased background signal.

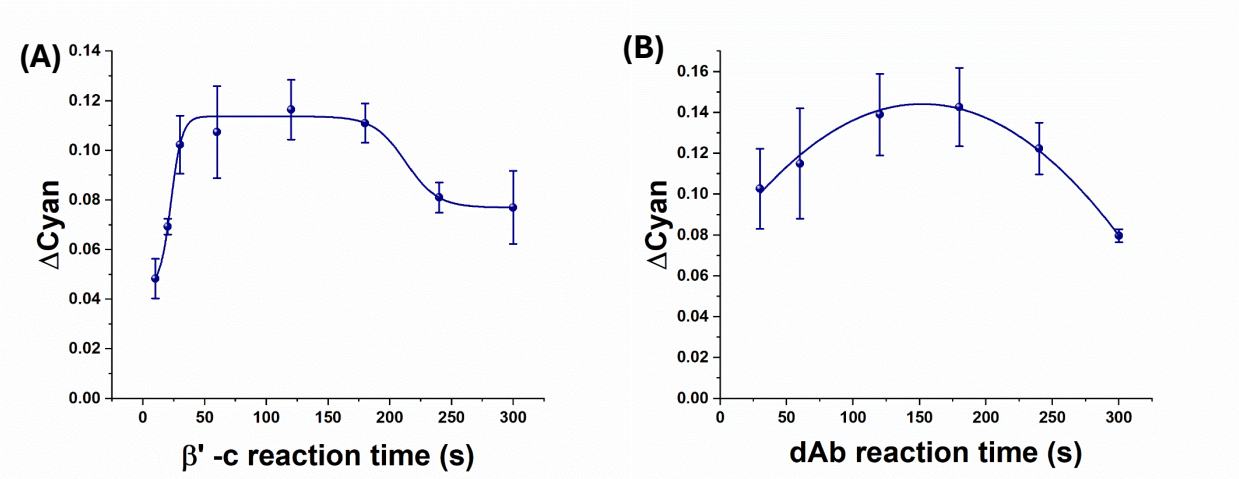

Fig. 2- 9 Effects of reaction time of: (A) β'-component and (B) detection antibody.

2.3.1.5 TMB substrate volume and reaction time

The final step in the assay is adding the TMB substrate to obtain color formation, which results from the oxidation of TMB catalyzed by the enzyme (HRP) conjugated with the dAb. First, the reaction time of TMB was investigated in a range from 10 to 600 s (Fig. 2-10A). The signal (ΔCyan) reached a maximum value at 120 to 150 s, after which it dropped. This behavior arises from the difference in the TMB oxidation rate between the sample and the blank because they contain different HRP concentrations (Fig. 2-10B). Samples contain higher HRP concentrations, which allow rapid TMB oxidation, compared to the blank, which contains a low concentration of HRP due to non-specific binding. Thus, while all TMB in the sample is completely oxidized and reaches a steady state after about 2 min, the TMB in the blank continues to oxidize and stabilizes around 5 min. Next, various volumes of TMB solution were tested, as shown in Fig. 2-10C. Although no significant difference in the signal was observed, 3 µL was selected because it filled the reaction zone, which provided better color uniformity and a slightly improved signal. In contrast, 1 µL and 2 µL did not fill the entire zone, and 4 µL overfilled the reaction zone and flowed into the lower layer containing washed dAb.

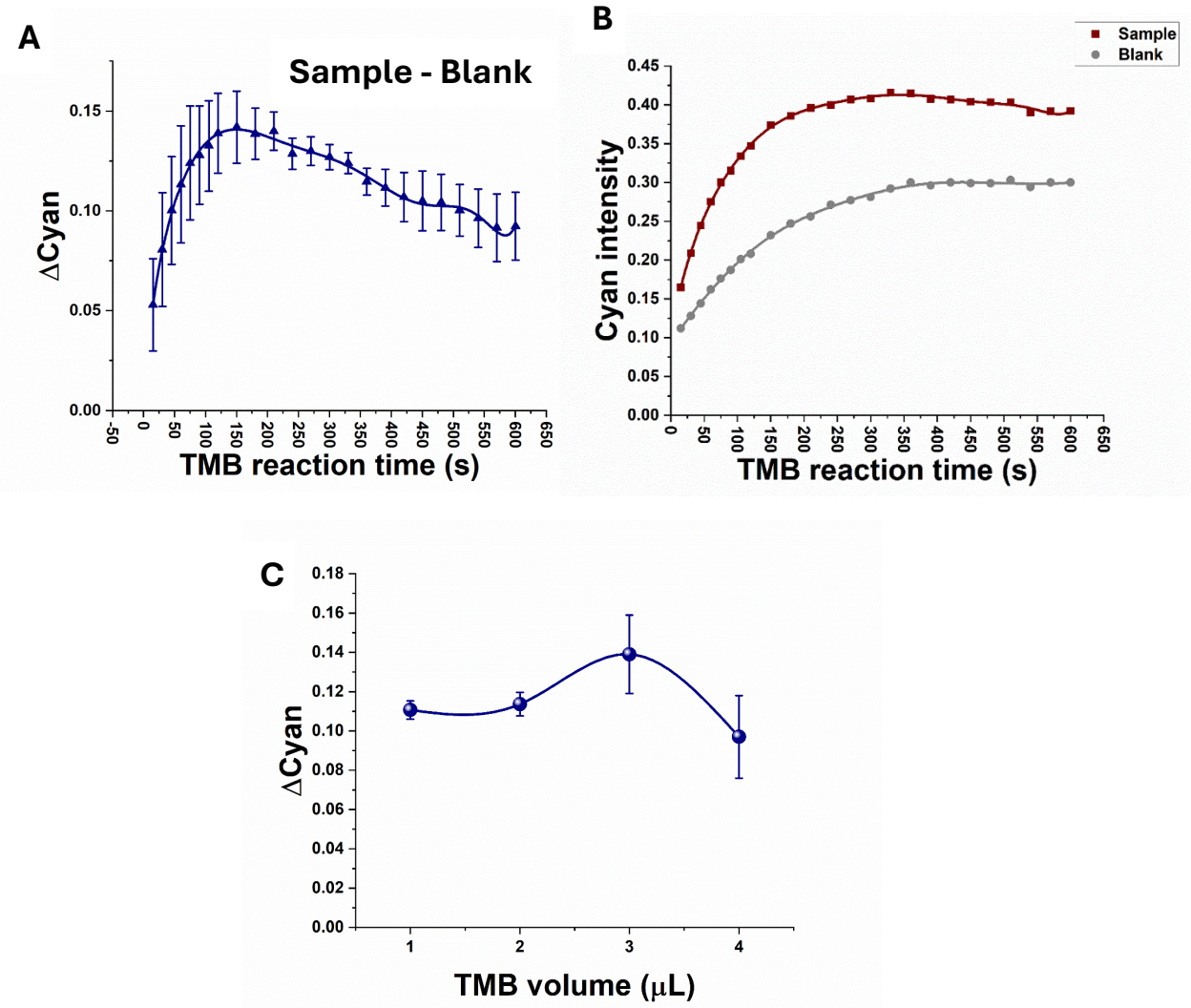

Fig. 2- 10 Effects of: (A-B) TMB reaction time and (C) TMB volume.

2.3.2 µPAD ELISA vs. conventional ELISA for β'-c detection

The µPAD-ELISA was evaluated over a wide range of β'-c protein concentrations under the optimized assay conditions (Fig. 2-11). The µPAD-ELISA had consistent performance over the range 0.01–800 ng mL^{-1}, as shown in Fig. 2-12. All assays were run using triplicate µPADs at each concentration. The average coefficient of variation (CV) of 4.1% was obtained, indicating good inter-device repeatability. A linear relationship was obtained across the range 0.10–60.00 ng mL^{-1}, as indicated in the inset of Fig. 2-12. The developed µPAD-ELISA provided a limit of detection of 1.59 ng mL^{-1}, which is comparable to the conventional ELISA [7]. Moreover, Table 1 summarizes the comparison between µPAD-ELISA and conventional ELISA for β'-c detection which clearly indicates that the µPAD-ELISA has a shorter assay time and requires smaller volumes of reagents to reduce analysis costs.

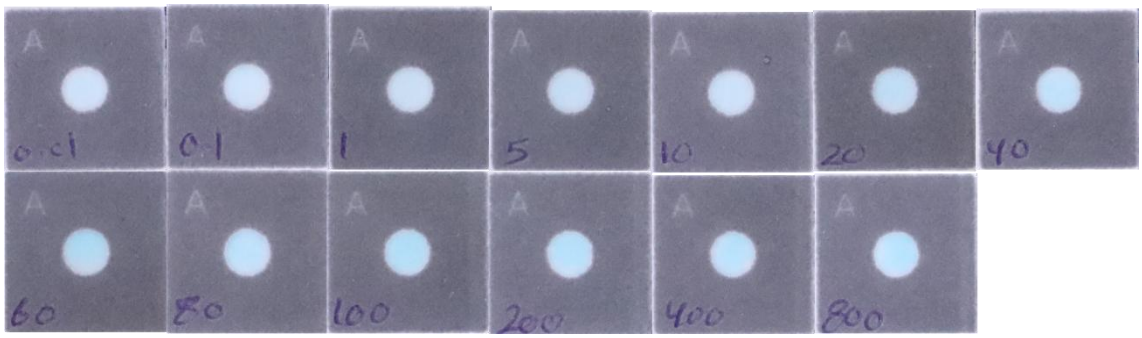

Fig. 2- 11 Real images of the µPAD-ELISA after analysis of various concentrations (0.01–800 ng mL^{-1}) of β'-component protein.

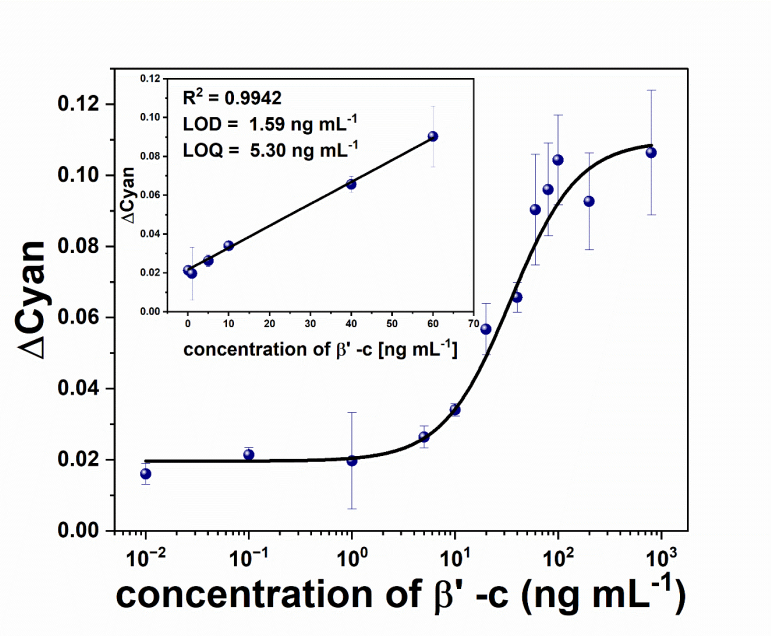

Fig. 2- 12 Standard curve for β'-component protein obtained with the optimized μPAD-ELISA in the range from 0.01 to 800 ng mL^{-1}. All assays were run using triplicate μPADs at each concentration, yielding an average CV of 4.1%. The solid line represents the 4-parameter logistic fit. The inset curve shows the linear standard curve over the range from 0.10 to 60 ng mL^{-1}. The solid line is the linear fitting.

Table 2- 1 Comparison between the developed μPAD-ELISA and the conventional ELISA for detection of β'-component protein

	μPAD-ELISA (This study)	Conventional ELISA [7]
Capture antibody	30 ng (3 μL, 10 μg mL^{-1})	500 ng (100 μL, 5 μg mL^{-1})
Detection Fab' antibody	1.5 ng (3 μL, 0.5 μg mL^{-1})	100 ng (100 μL, 1.0 μg mL^{-1})
Sample volume (β'-component protein)	3 μL	100 μL
TMB substrate	3 μL	100 μL
Immobilization time	5 min	15 h
Assay time	10 min	3 h 50 min
LOD*	1.59 ng mL^{-1}	1.95 ng mL^{-1}
LOQ*	5.30 ng mL^{-1}	6.51 ng mL^{-1}
Cost	Low	High

*For μPAD-ELISA: LOD was calculated as 3 S_b/m and LOQ as 10 S_b/m, where S_b is the standard deviation of the intercept and m is the slope of the calibration curve [33]. Regression equation: $y = 0.00113x + 0.02175$, $S_b = 0.00060$.

2.4 Conclusion

The μPAD-ELISA, which was easy to fabricate and use, cost-effective, and sensitive, was presented for detecting the allergenic β'-component protein in salmon roe. This μPAD employed a simple and rapid method to immobilize the capture antibody. The immobilization was done by drying the capture antibody at 50 °C for just 5 min. The assay parameters were optimized to achieve the optimal sensitivity with a minimal assay time. Under the optimal conditions, the μPAD-ELISA assay took 15 min and it provided consistent performance over a wide range of β'-component concentrations: there was a good linear relationship over a range of 0.10–60.0 ng mL^{-1} and a limit of detection of 1.59 ng mL^{-1}. Compared to the conventional ELISA assay, the developed μPAD-ELISA requires minimal reagent volumes and shorter assay times. These advantages are expected to contribute to the rapid and sensitive detection of food allergens in processed food as well as the establishment of a good food allergy labeling

system. Moreover, the developed immobilization protocol is a general protocol for the immobilization of antibodies on cellulose paper so that it can be used for developing paper-based ELISA assays for other targets.

In the future, it would be valuable to study stability of the device over extended periods and under various storage conditions, as well as to validate possible applications by analyzing β-component allergens in processed foods.

2.5 References

[1] M. Ebisawa, K. Ito, T. Fujisawa, Committee for Japanese Pediatric Guideline for Food Allergy, The Japanese Society of Pediatric Allergy and Clinical Immunity; Japanese Society of Allergology, Japanese guidelines for food allergy 2020, Allergol. Int., 69 (2020) 370-386.

[2] V. Sampath, E.M. Abrams, B. Adlou, C. Akdis, M. Akdis, H.A. Brough, et al., Food allergy across the globe, J. Allergy Clin. Immunol., 148 (2021) 1347-1364.

[3] D. Seth, P. Poowutikul, M. Pansare, D. Kamat, Food Allergy: A Review, Pediatr. Ann., 49 (2020) e50-e8.

[4] F. Chang, L. Eng, C. Chang, Food allergy labeling laws: international guidelines for residents and travelers, Clin. Rev. Allergy. Immunol., 65 (2023) 148-165.

[5] H. Akiyama, R. Adachi, Japanese food allergy-labeling system and comparison with the international experience; detection and thresholds, Food Saf. (Tokyo), 9 (2021) 101-116.

[6] Y. Shimizu, A. Nakamura, H. Kishimura, A. Hara, K. Watanabe, H. Saeki, Major allergen and its IgE cross-reactivity among salmonid fish roe allergy, J. Agric. Food. Chem., 57 (2009) 2314-2319.

[7] Y. Shimizu, H. Oda, K. Seiki, H. Saeki, Development of an enzyme-linked immunosorbent assay system for detecting beta'-component (Onk k 5), a major IgE-binding protein in salmon roe, Food Chem., 181 (2015) 310-317.

[8] A.W. Martinez, S.T. Phillips, M.J. Butte, G.M. Whitesides, Patterned paper as a platform for inexpensive, low-volume, portable bioassays, Angew. Chem. Int. Ed., 46 (2007) 1318-1320.

[9] M.L. Wang, J.R. Cui, Y. Wang, L. Yang, Z.Z. Jia, C.J. Gao, et al., Microfluidic paper-based analytical devices for the determination of food contaminants: developments and applications, J. Agric. Food Chem., 70 (2022) 8188-8206.

[10] S. Soni, B.J. Toley, Paper-based nucleic acid sample preparation for point-of-care diagnostics, Sens. Actuators B Chem., 355 (2022) 131272.

[11] Y. Hou, C.C. Lv, Y.L. Guo, X.H. Ma, W. Liu, Y. Jin, et al., Recent advances and applications in paper-based devices for point-of-care testing, J. Anal. Test., 6 (2022) 247-273.

[12] A.A. Shalaby, C.-W. Tsao, A. Ishida, M. Maeki, M. Tokeshi, Microfluidic paper-based analytical devices for cancer diagnosis, Sens. Actuators B Chem., 379 (2023) 133243.

[13] S. Das, Gagandeep, R. Bhatia, Paper-based microfluidic devices: fabrication, detection, and significant applications in various fields, Rev. Anal. Chem., 41 (2022) 112-136.

[14] M. Carneiro, L.R. Rodrigues, F.T.C. Moreira, M.G.F. Sales, Colorimetric paper-based sensors against cancer biomarkers, Sensors, 22 (2022) 3221.

[15] W. Wang, X. Cai, Q. Li, L. Zheng, X. Yu, H. Zhang, et al., Application of a microfluidic paper-based bioimmunosensor with laser-induced fluorescence detection in the determination of alpha-fetoprotein from serum of hepatopaths, Talanta, 221 (2021) 121660.

[16] F. Mesgari, S.M. Beigi, N. Fakhri, M. Hosseini, M. Aghazadeh, M.R. Ganjali, Paper-based chemiluminescence and colorimetric detection of cytochrome c by cobalt hydroxide decorated mesoporous carbon, Microchem. J., 157 (2020) 104991.

[17] N. Colozza, V. Caratelli, D. Moscone, F. Arduini, Origami paper-based electrochemical (bio)sensors: state of the art and perspective, Biosensors, 11 (2021) 328.

[18] E. Noviana, C.P. McCord, K.M. Clark, I. Jang, C.S. Henry, Electrochemical paper-based devices: sensing approaches and progress toward practical applications, Lab Chip, 20 (2020) 9-34.

[19] K.T.L. Trinh, W.R. Chae, N.Y. Lee, Recent advances in the fabrication strategies of paper-based microfluidic devices for rapid detection of bacteria and viruses, Microchem. J., 180 (2022) 107548.

[20] T. Ozer, C. McMahon, C.S. Henry, Advances in paper-based analytical devices, Annu. Rev. Anal. Chem., 13 (2020) 85-109.

[21] E. Noviana, T. Ozer, C.S. Carrell, J.S. Link, C. McMahon, I. Jang, et al., Microfluidic paper-based analytical devices: from design to applications, Chem. Rev., 121 (2021) 11835-11885.

[22] S. Nishat, A.T. Jafry, A.W. Martinez, F.R. Awan, Paper-based microfluidics: simplified fabrication and assay methods, Sens. Actuators B Chem., 336 (2021) 129681.

[23] W. Li, X. Ma, Y.C. Yong, G. Liu, Z. Yang, Review of paper-based microfluidic analytical devices for in-field testing of pathogens, Anal. Chim. Acta, 1278 (2023) 341614.

[24] S. Wang, L. Ge, X. Song, J. Yu, S. Ge, J. Huang, et al., Paper-based chemiluminescence ELISA: lab-on-paper based on chitosan modified paper device and wax-screen-printing, Biosens. Bioelectron., 31 (2012) 212-218.

[25] L. Ma, A. Nilghaz, J.R. Choi, X. Liu, X. Lu, Rapid detection of clenbuterol in milk using microfluidic paper-based ELISA, Food Chem., 246 (2018) 437-441.

[26] S. Feng, M.Z. Hua, M.S. Roopesh, X. Lu, Rapid detection of three mycotoxins in animal feed materials using competitive ELISA-based origami microfluidic paper analytical device (muPAD), Anal. Bioanal. Chem., 415 (2023) 1943-1951.

[27] T. Komatsu, Y. Sato, M. Maeki, A. Ishida, H. Tani, M. Tokeshi, Rapid, sensitive universal paper-based device enhances competitive immunoassays of small molecules, Anal. Chim. Acta., 1144 (2021) 85-95.

[28] Y. Zhao, D. Zeng, C. Yan, W. Chen, J. Ren, Y. Jiang, et al., Rapid and accurate detection of Escherichia coli O157:H7 in beef using microfluidic wax-printed paper-based ELISA, Analyst, 145 (2020) 3106-3115.

[29] C.M. Cheng, A.W. Martinez, J. Gong, C.R. Mace, S.T. Phillips, E. Carrilho, et al., Paper-based ELISA, Angew. Chem. Int. Ed., 49 (2010) 4771-4774.

[30] Y. Akazawa-Ogawa, H. Nagai, Y. Hagihara, Heat denaturation of the antibody, a multi-domain protein, Biophys. Rev., 10 (2018) 255-258.

[31] J. Wang, B. Yiu, J. Obermeyer, C.D. Filipe, J.D. Brennan, R. Pelton, Effects of temperature and relative humidity on the stability of paper-immobilized antibodies, Biomacromolecules, 13 (2012) 559-564.

[32] M.A. Masuelli, Study of bovine serum albumin solubility in aqueous solutions by intrinsic viscosity measurements, Adv. Phys. Chem., 2013 (2013) 360239.

[33] J. Miller, J.C. Miller, Statistics and Chemometrics for Analytical Chemistry, Seventh ed.: Harlow, England: Pearson Education Limited; 2018.

CHAPTER 3 Paper in 3D printed microplate hybrid microfluidic device for low-cost, rapid, and ultrasensitive paper-based bioluminescence detection of human epidermal growth factor receptor2 (HER2) breast cancer biomarker

3.1 Introduction

Cancer is the second leading cause of death worldwide after cardiovascular diseases. In 2020, globally, newly diagnosed cases exceeded 19 million cases with about 10 million cancer deaths [1]. In 2024, approximately 2,001,140 new cancer cases were diagnosed in the United States which is equivalent to about 5480 new cases being diagnosed every day[2]. There are more than 40 types of cancer, and breast cancer is the most common type in women with 310,270 new cases and 42,250 deaths reported annually in the US. Moreover, among all other cancer types, breast cancer has the highest probability of developing into invasive cancer. During the last 10 years, the breast cancer incidence rate has continued to increase by 1% annually in th US [3]. The high mortality rate of breast cancer is mainly due to late diagnosis which leads to delayed receipt of the proper treatment. Currently, breast cancer is diagnosed using various imaging techniques such as mammography, positron emission tomography (PET), computed tomography (CT), and magnetic resonance imaging (MRI) [4]. The techniques are not suitable for early diagnosis, and they suffer from low sensitivity and specificity. Additionally, their instrumentation systems are expensive and bulky, and need highly trained operators. Histopathology can determine the malignancy of a tumor discovered through imaging by analyzing a tissue biopsy, but it is unsuitable for early detection or follow-up.

The development of rapid and sensitive tests to detect cancer in its earliest stages, when symptoms are absent, is a significant global research challenge. Detection of cancer biomarker proteins in liquid biopsy samples is a highly interesting approach for cancer diagnosis because these proteins are sensitive, specific, can be measured quickly, and are suitable for follow-up. Various methods have been used to detect cancer biomarker proteins including colorimetry [5, 6], fluorescence spectroscopy [7, 8], electrochemical methods [9, 10], chemiluminescence

(CL) [11], electrochemiluminescence (ECL) [12, 13], surface plasmon resonance (SPR) [14], surface-enhanced Raman spectroscopy (SERS) [15, 16], polymerase chain reaction (PCR) [17], and enzyme-linked immunosorbent assay (ELISA) [18]. However, these methods are time-consuming, require complex protocols, and consume large amounts of reagents. Furthermore, the early stages of tumors typically express very low concentrations of cancer biomarkers. Hence, the development of rapid, low-cost, and ultrasensitive detection of cancer biomarkers is important for early diagnosis.

Microfluidic paper-based analytical devices (μPADs) are a promising way to develop rapid and sensitive assays that consume minimum sample and reagent volumes. Several μPADs have been developed for detecting breast cancer biomarkers using different techniques like colorimetry, fluorimetry, chemiluminescence, and electrochemical methods [19, 20]. Several proteins in human serum were used as biomarkers for breast cancer including human epidermal growth factor receptor (HER2), carcinoembryonic antigen (CEA), and cancer antigen 15-3 (CA15-3). More than approximately 13 % of all breast cancer cases are classified as HER2 positive subtypes which are commonly more aggressive and have a worse prognosis, but they will respond to treatment if they are diagnosed early [3, 21]. Several electrochemical immunoassays for the detection of HER2 have been introduced, but these methods require multiple steps for modification of the electrode surface which takes several hours and complicates the fabrication [22, 23]. A lateral flow immunoassay was reported for the detection of HER2 based on an adsorption-desorption colorimetric approach using HER2 binding aptamers adsorbed on the surface of gold nanoparticles; it is simple in operation but it has low sensitivity [24].

Here, I propose a hybrid device using of paper in a 3D printed microplate for simple, rapid, and ultrasensitive detection of HER2 breast cancer biomarker using bioluminescence sandwich ELISA. Whatman Grade 1 chromatographic paper served as a substrate for

immobilization of anti-HER2 capture antibody (cAb) and performing the ELISA assay. Using the paper as substrate allows a rapid assay in about 20 min with minimum volumes of sample and reagents. The paper was cut into circular discs and placed inside the wells of a custom 3D printed microplate. The 3D printed microplate was designed with microvalves in the bottom of each well; these microvalves allow incubation of the sample and reagents for a desired time and they allow the vertical drainage of the washing solution which ensures removal of the excess unreacted antibodies. Bioluminescence was chosen due to its high sensitivity compared to the other detection techniques. The detection antibody (dAb) was labeled with NanoLuc (Nluc) luciferase to achieve the best assay sensitivity; Nluc produces a luminescence signal about 100 times higher than Firefly and Renilla luciferases do.

Using this setup, I can detect HER2 at picogram levels. Moreover, after finishing the measurements, the used paper discs can be removed, and the 3D printed microplate can be washed and restocked with new discs for another use.

This study introduces a novel custom microplate design featuring microvalves that regulate reagent and washing solution flow, improving both incubation and washing processes. Additionally, it presents the first paper-based device for the ultrasensitive detection of HER2 and demonstrates, for the first time, the use of bioluminescence ELISA for detecting cancer biomarkers with paper-based microfluidic devices. The proposed assay and microplate offer a versatile platform that can be adapted to various targets by selecting the appropriate capture and detection antibody pair.

3.2 Experimental

3.2.1 Materials and instruments

Sandwich ELISA assay: Phosphate buffer saline (PBS, pH 7.4) and bovine serum albumin (BSA) were purchased from FUJIFILM Wako Pure Chemical Corporation (Japan). Tween 20 was purchased from Sigma-Aldrich (USA). A NanoLuc labeling kit and Lumit detection reagent A (Furimazine) were purchased from Promega (USA). The labeling kit contains, IGEPAL CA-630 (catalog number: VB141A), HaloTag ligand (catalog number: VB125A), and NanoLuc-HaloTag (catalog number: VB131A). Human HER2/ErbB2 protein (His Tag) (catalog number: 10004-H08H), HER2/ErbB2 antibody - rabbit Mab (catalog number: 10004-R205) as a detection antibody, and HER2/ErbB2/CD340 antibody - rabbit Mab (catalog number: 10004-R511) as capture antibody were purchased from Sino Biological (USA). Pooled human serum (catalog number: 12181450C) was purchased from COSMO Bio (Japan). Human ErbB2/Her2 DuoSet ELISA (catalog number: DY1129B) was purchased from bio-techne R&D Systems (USA). All reagents were of analytical grade and used without further purification. Ultrapure Milli-Q water (18.2 MΩ cm, Millipore, Germany) was used for the preparation of all the aqueous solutions. The 0.5 mL Zeba spin desalting columns (catalog number: 89882) were purchased from ThermoFisher (USA). Magne HaloTag magnetic beads (catalog number: G7281) were purchased from Promega. A Promega Explorer plate reader (Promega) was used for measuring the bioluminescence signal.

3D printing of the device microplate: Poly(ethylene glycol) diacrylate average Mn 250 (PEGDA-250), pentaerythritol tetraacrylate (PETTA), and diphenyl(2,4,6-trimethylbenzoyl)phosphine oxide (TPO) were purchased from Sigma-Aldrich (USA) and 2-isopropylthioxanthone (ITX) was purchased from TCI (Japan). Isopropanol (IPA) was purchased from FUJIFILM Wako Pure Chemical Corporation (Japan). White pigment was

purchased from Formlabs (USA). An Elegoo Saturn 3 Ultra LCD 3D printer (Elegoo, China) was used for printing the custom microplate.

3.2.2 Labeling the detection antibody with Nluc

A 250 µL aliquot of detection antibody (1.0 mg/mL) was labeled with Nluc according to the instructions in the Promega labeling kit. First, the antibody solution was divided into two parts (125 µL each) and the antibody buffer was exchanged with 10 mM sodium bicarbonate buffer (pH 8.5) using a desalting column. Next, 0.85 µL HaloTag ligand was added to each 125 µL aliquot of antibody and this was gently mixed for 90 min at 22 to 25 ºC. Then the antibody buffer was exchanged with 10 mM PBS (pH 7.4) using two desalting columns, in series, to ensure complete removal of free HaloTag ligand. Next, 1.5 µL 10% IGEPAL CA-630 and 170 µL NanoLuc-HaloTag were added to each 125 µL aliquot of antibody and this was incubated for 20 h at 4 ºC while gently mixing. Then the free Nluc was removed using the Magne HaloTag magnetic beads. Finally, the labeled antibodies were stored in 50% glycerol at -20 ºC until use. The appearance of multiple higher molecular weight bands in the reducing SDS-PAGE gel confirmed the successful labeling as shown in Fig. 3-1.

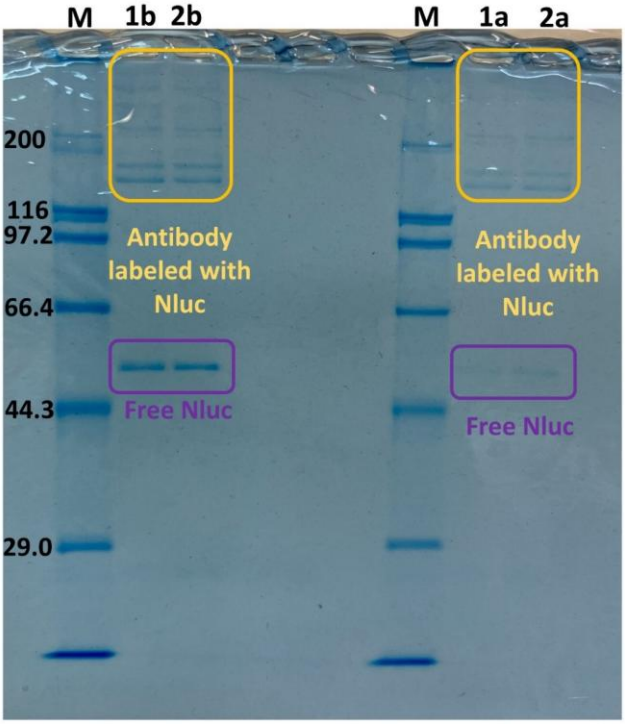

Fig. 3- 1 Reducing SDS-PAGE for antibodies labeled with Nluc before (1b and 2b) and after (1a and 2a) removing the free Nluc using the Magne HaloTag magnetic beads. M is the protein marker, 1 is the first 125 µL part of antibody, and 2 is the second 125 µL part of the antibody. The multiple higher molecular weight bands represent the successful labeling, and the large decrease in the free Nluc bands in 1a and 2a lanes confirm the good removing of the free Nluc after labeling.

3.2.3 Removing unreacted NanoLuc-HaloTag protein

Firstly, a 76 µL of Magne Halotag beads was transferred to 1.5 mL microcentrifuge tube. The tube was placed on magnetic stand for 30 seconds to capture the magnetic beads, and the supernatant was removed and discarded. Then the tube was removed and 500 µL 0.05% IGEPAL CA-630 was added and mixed thoroughly for 2 minutes. The tube was placed on the magnetic stand for 30 seconds and the supernatant was discarded. This washing process was repeated more two times. Next, 295 µL NanoLuc labeled antibody was added to the magnetic

beads and incubated for 1 hour at room temperature (22-25 ºC) with constant mixing. Finally, the tube was placed on a magnetic stand for 30 seconds and the supernatant was collected which contains the purified NanoLuc-labeled antibody.

3.2.4 3D printing ink formulation

The ink was formulated based on Shafique *et al*., who used PEGDA-250 as monomer supplemented with 0.5% w/w TPO as photoinitiator, 1.5% w/w ITX as photoabsorber, and 2% w/w PETTA as crosslinker. The reagents were mixed in a 500 mL amber glass bottle, then stirred for at least 2 h using magnetic stirrer and stored at room temperature until use [25]. To dye the ink, 10 mL white dye was added to each 100 g ink, followed by stirring for about 10 min and storing at room temperature. The ink should be mixed well before use every time due to the dye sedimentation.

3.2.5 Design and fabrication of the paper-3D printed microplate hybrid device

The fabrication process is shown in Fig. 3-2. The microplate was designed using Autodesk Fusion 360, exported as an "STL" file, and sliced in CHITUBOX software; the slices were uploaded to the Saturn 3 Ultra masked stereolithography LCD 3D printer with LED wavelength of 405 nm. The microplate was printed using the preformulated ink with the following printing parameters: exposure time per layer, 1.7 s (except 17 s for the 5 bottom layers); transition layers, 5 layers; layer thickness, 20 μm; rest time, 5 s; lifting speed, 80 mm min^{-1}; and retracting speed, 80 mm min^{-1}. The printed microplate was washed using IPA to remove the uncured resin and dried with pressurized nitrogen or air, followed by UV curing for 1 min (Mercury XS Cure Machine, Elegoo). The cured microplate was ready for use after the UV curing. An A4 sheet of chromatographic paper was cut into circular discs with diameters

of 6.96 mm using a 30W CO_2 laser cutter (Etcher Laser Pro, SMART DIYs, Japan), then the cut paper discs were inserted into the wells of the cured microplate.

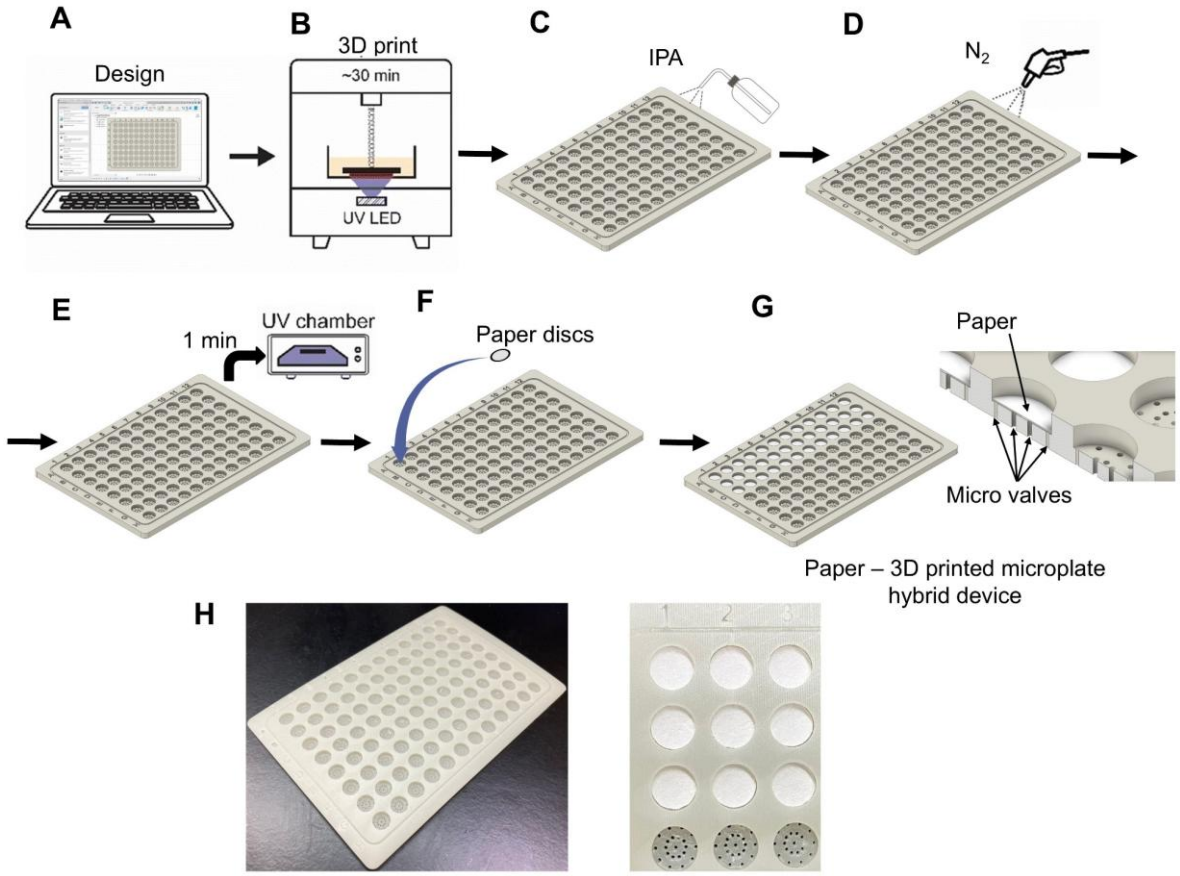

Fig. 3- 2 Fabrication procedure of the paper-3D printed microplate hybrid device. The fabrication includes: (A) microplate design using computer aided design software; (B) 3D printing using the LCD 3D printer; (C) washing with IPA to remove the uncured resin; (D) drying under a stream of pressurized nitrogen gas (N_2) or air; (E) UV curing for 1 min in a UV chamber; and (F) inserting the paper discs into the microwells. (G) is an illustration of the final device and a cross-sectional view inside the microwells. (H) shows photos for the 3D printed microplate after drying (left) and after inserting the paper discs (right).

3.2.6 Optimization of capture antibody and detection antibody concentrations

The immunoassay was performed with different concentrations of capture and detection antibodies: cAb with concentrations of 0.5, 2.0, and 10.0 µg/mL and dAb with concentrations of 0.1 and 0.5 µg/mL which gave six different combinations. First, 5 µL of cAb was added to each well and incubated at 50 ºC for 5 min. Then the excess cAb was washed out two times by adding 20 µL PBST (10 mM PBS containing 0.05% v/v Tween 20) to each well, and an adsorption pad was put under the microplate to adsorb the washing solution. After that, the device was blocked by adding 5 µL BSA 10% to each well and incubating it at 50 ºC for 5 min. Next 5 µL HER2 (100 pg/mL) was added to the sample wells, and 10 mM PBS was added to the blank wells, followed by incubation for 5 min at room temperature. Then 5 µL dAb was added to each well and incubated for 5 min at room temperature. Afterward, the device was washed twice using 20 µL PBST. Finally, 5 µL 50X diluted furimazine substrate was added to each well and the bioluminescence signal was measured using a plate reader.

3.2.7 Optimization of blocking buffer concentration

I optimized the blocking buffer concentration using the optimized concentration of cAb and dAb. First, 5 µL of cAb was added to each well and incubated at 50 ºC for 5 min, followed by washing two times using 20 µL PBST. Then the device was blocked by adding 5 µL BSA (2%, 4%, 6%, 8%, and 10% w/w) and incubating at 50 ºC for 5 min. Next, 5 µL HER2 (100 p/mL) was added to the sample wells, PBS was added to the blank wells, and the device and its contents were incubated for 5 min at room temperature. Then 5 µL dAb was added and incubated for 5 min at room temperature followed by washing two times using 20 µL PBST. Finally, 5 µL 50X diluted furimazine substrate was added and the bioluminescence signal was measured.

3.2.8 Optimization of antigen reaction time

After optimizing the cAb and dAb concentrations, I optimized the HER2 reaction time. First, 5 µL cAb was added to each well with incubation for 5 min at 50 ºC, followed by washing two times using 20 µL PBST. Then the device was blocked by adding 5 µL BSA to each well and incubating for 5 min at 50 ºC. Next, 5 µL HER2 (100 pg/mL) was added to the sample wells, and PBS was added to the blank wells, followed by incubation at room temperature for 30, 60, 120, 300, and 600 s. After that, 5 µL dAb was added and incubated for 5 min, followed by washing two times using 20 µL PBST before adding 5 µL 50X diluted furimazine substrate and measuring the bioluminescence signal.

3.2.9 Optimization of detection antibody reaction time

Finally, I optimized the detection antibody reaction time. First, 5 µL cAb was added to each well and incubated for 5 min at 50 ºC, followed by washing twice using 20 µL PBST and then blocking using 5 µL BSA for 5 min at 50 ºC. Then 5 µL HER2 (100 pg/mL) was added to the sample wells and PBS was added to the blank wells before incubation at room temperature. Next, 5 µL dAb was added to each well and incubated at room temperature for 30, 60, 120, 300, and 600 s followed by washing two times using PBST. Finally, 5 µL 50X diluted furimazine substrate was added and the bioluminescence signal was measured.

3.2.10 Sandwich ELISA for HER2 detection

The chromatographic paper I have proposed for use in the 3D printed microplate hybrid device can be used with a wide range of immunoassay types for the detection of biomolecules. Here, I detected HER2 using bioluminescence sandwich ELISA and all the optimized conditions. As shown in Fig. 3-3, 5 µL cAb was added and incubated for 5 min at 50 ºC

followed by washing two times using 20 µL PBST to remove the excess cAb. Then 5 µL BSA blocking solution was added and incubated for another 5 min at 50 °C. Next, 5 µL HER2 with different concentrations (0.01 pg/mL, 0.1 pg/mL, 1 pg/mL, 10 pg/mL, 100 pg/mL, and 1000 pg/mL) was added and incubated at room temperature. Then 5 µL dAb was added and incubated at room temperature, followed by washing two times using 20 µL PBST. Finally, 5 µL 50X diluted furimazine substrate was added and the bioluminescence signal was measured. The bioluminescence signal was plotted against the logarithm of the HER2 concentrations, and

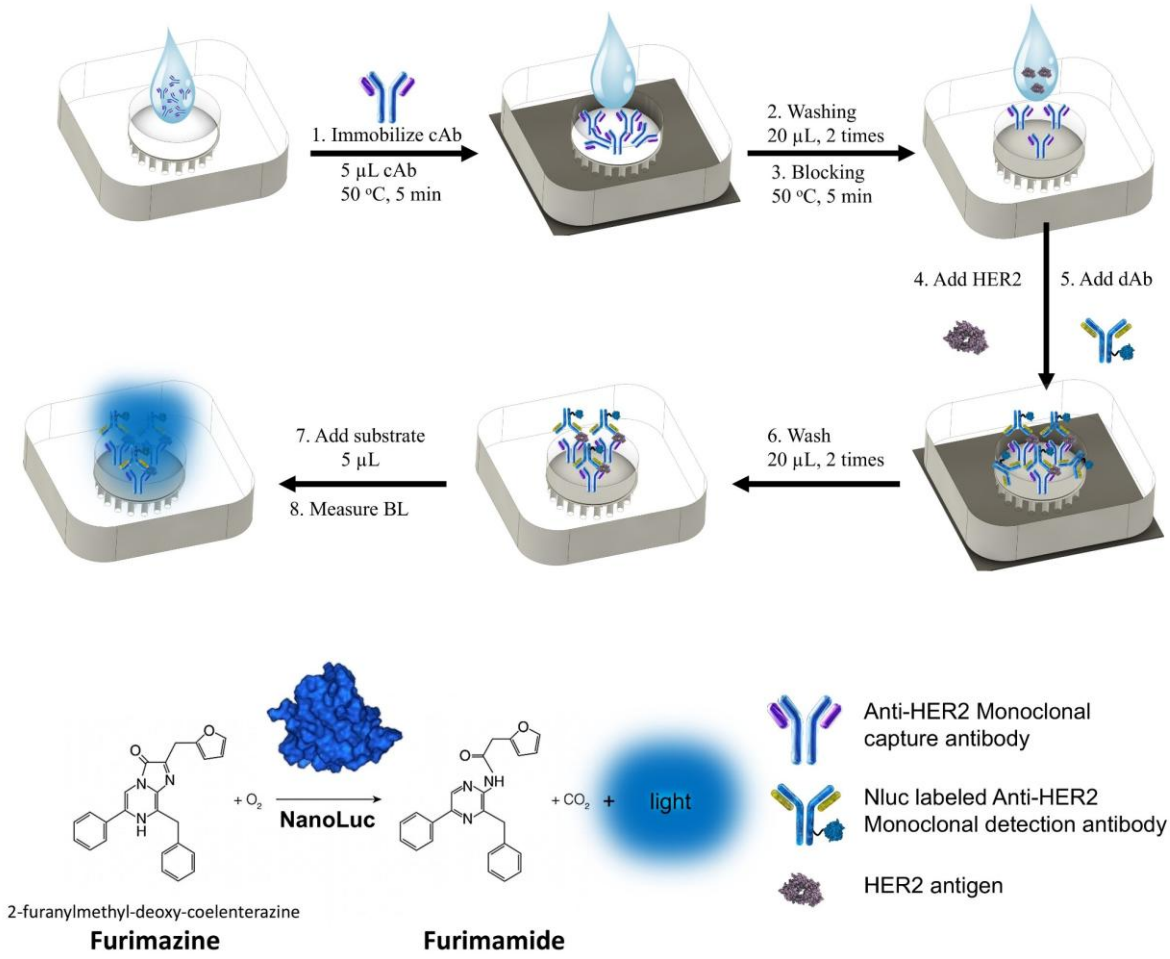

Fig. 3- 3 Schematic illustration of bioluminescence immunoassay for the detection of HER2 using paper in 3D printed microplate hybrid device. (1) immobilization of cAb on the paper substrate, (2) washing, (3) blocking the nonspecific binding sites, (4) addition of HER2, (5) addition of dAb, (6) washing, (7) addition of substrate, and (8) measure produced bioluminescence.

linear fitting was applied. The limit of detection (LOD) was calculated as 3-fold SD above the blank value. OriginPro was used for plotting graphs.

3.2.11 Detection of HER2 in human serum

To validate the developed hybrid device and assay, and to evaluate their feasibility for analyzing real human samples, HER2 was spiked into normal human serum. Different volumes of 1 ng/mL HER2 were mixed with 5 μL of 10-fold prediluted human serum, and the mixture was then diluted to 1 mL with 10 mM PBS to achieve the final concentrations of 5 pg/mL, 10 pg/mL, 100 pg/mL, 500 pg/mL, and 800 pg/mL in 2000-fold diluted human serum. After thorough mixing, the spiked samples were analyzed using both the developed hybrid device and commercial HER2 detection kits, and the spike recoveries were calculated.

3.2.12 Storage condition of reagents and plate

cAb and dAb were aliquoted and stored at -20 oC, while the HER2 protein was aliquoted and stored at -70 oC until use. The furimazine substrate was stored at -20 oC, and the plate and the paper discs were stored at room temperature until use.

3.3 Results and discussion

3.3.1 Paper disc use in the 3D printed microplate hybrid device

The proposed microplate hybrid device consists of two parts, paper discs as substrate for the immobilization of cAb and performing the immunoassay reaction, and a 3D printed microplate with the same dimensions as commercially available microplates to allow its use with conventional microplate readers, Fig. 3-4. The 3D printed microplate contains microvalves in the bottom of the wells that stop the reagents for incubation from flowing out and allow the washing solution to flow in the washing steps. To achieve this feature the

selection of the microplate material is important, and I chose PEGDA-based ink because its cured printed parts have a contact angle with water of about 65 – 70^{o} which is considered moderately hydrophilic [25]. Such an angle prevents the antibodies and antigen solutions which are diluted using 10 mM PBS from draining through the microvalves. Therefore, the solutions can be adsorbed by the paper discs for reaction, Fig. 3-5 (A). Fig. 3-6 shows how 5 µL of blue dye in 10 mM PBS was adsorbed well by the paper disc but it did not flow through the microvalves. When adding a surfactant, 0.05% Tween 20, the contact angle decreases to 46^{o} which allows the washing solution to fill the microvalves, and when the bottom of the microplate is placed on an adsorption pad, the washing solution will flow out and remove the unreacted reagents, Fig. 3-5 (B). Fig. 3-7 shows the drainage of 20 µL 0.05% PBST solution through the microvalves. The microplate was designed to contain the largest number of microvalves with the smallest possible diameter that can be accurately printed using a low-cost LCD 3D printer. After several iterations of design, printing, optimization, and reprinting, the final design features 21 microvalves, each with a diameter of 500 µm, uniformly distributed in two concentric circles, with one microvalve at the center of each well. The small diameter of the microvalves prevents the aqueous reagents from flowing due to capillary action and gravity, thanks to the high contact angle. By reducing the contact angle with the addition of a surfactant, capillary flow and drainage of the washing solution are enabled. Essentially, the more microvalves there are, the faster the washing solution drains. The device demonstrates the efficiency of the microvalves in preventing the flow of increasing volumes of PBS solution (up to 50 µL), while draining 10 µL of a 0.05% Tween-20 solution. The volume of reagent used in the assay is small (5 µL), so it is primarily adsorbed by the paper disc. In contrast, the washing solution has a relatively larger volume (20 µL) compared to the paper disc size. Therefore, it flows through the paper disc, reaching the microvalves for drainage, even in the presence of a small void between the paper disc and the well. An expected operational limitation is that if a

reagent contains surfactants or organic solvents, it may affect the water contact angle, potentially causing leakage through the microvalves when used in large volumes. The microplate was dyed white to reflect the produced luminescence and improve the sensitivity of the assay. Moreover, PEGDA-250 has low protein adsorption which allows the reuse of the microplate by removing the old paper discs, washing and drying the microplate, and loading new paper discs for the new assay.

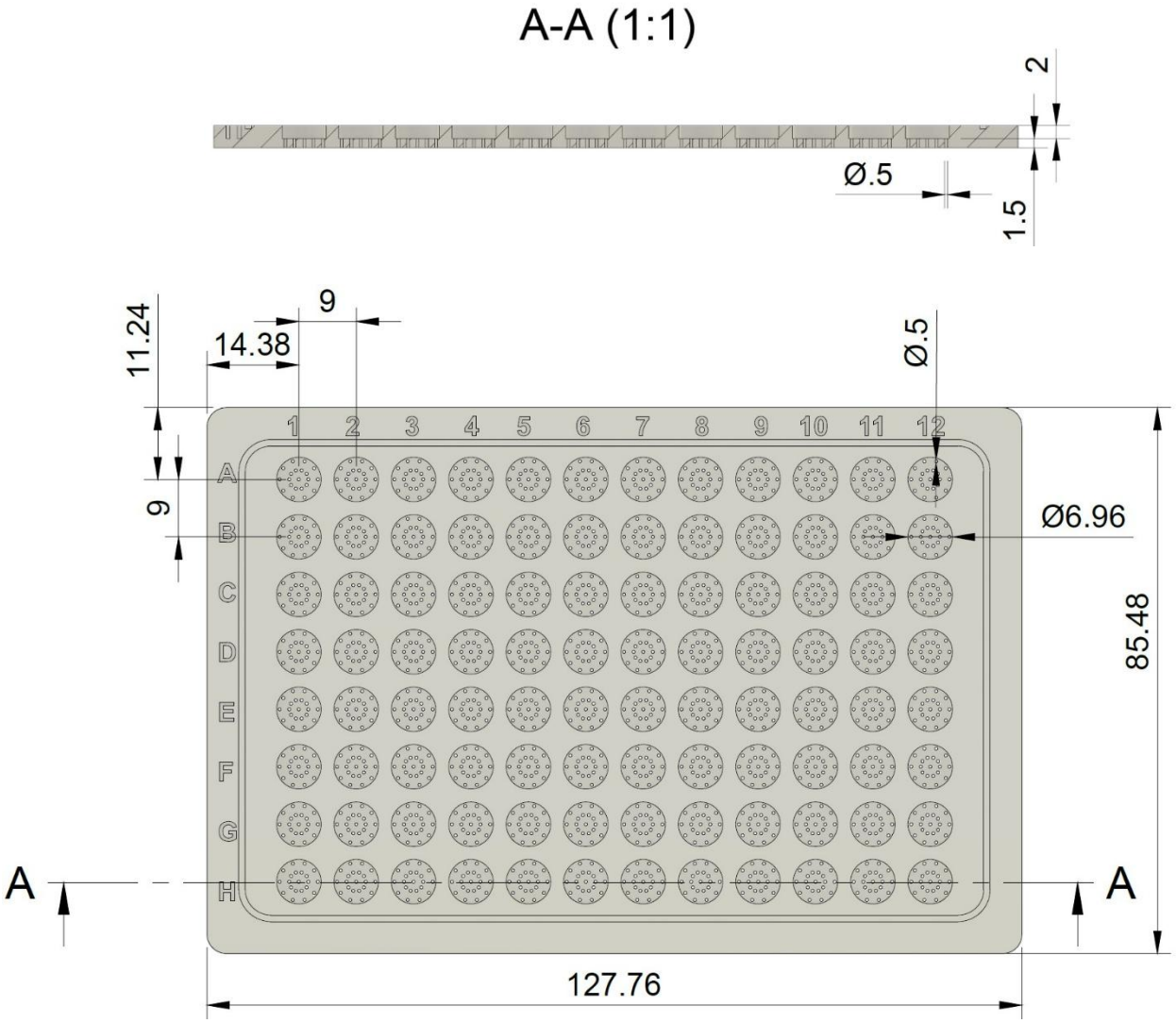

Fig. 3- 4 3D design of the custom microplate with dimensions, all dimensions in mm

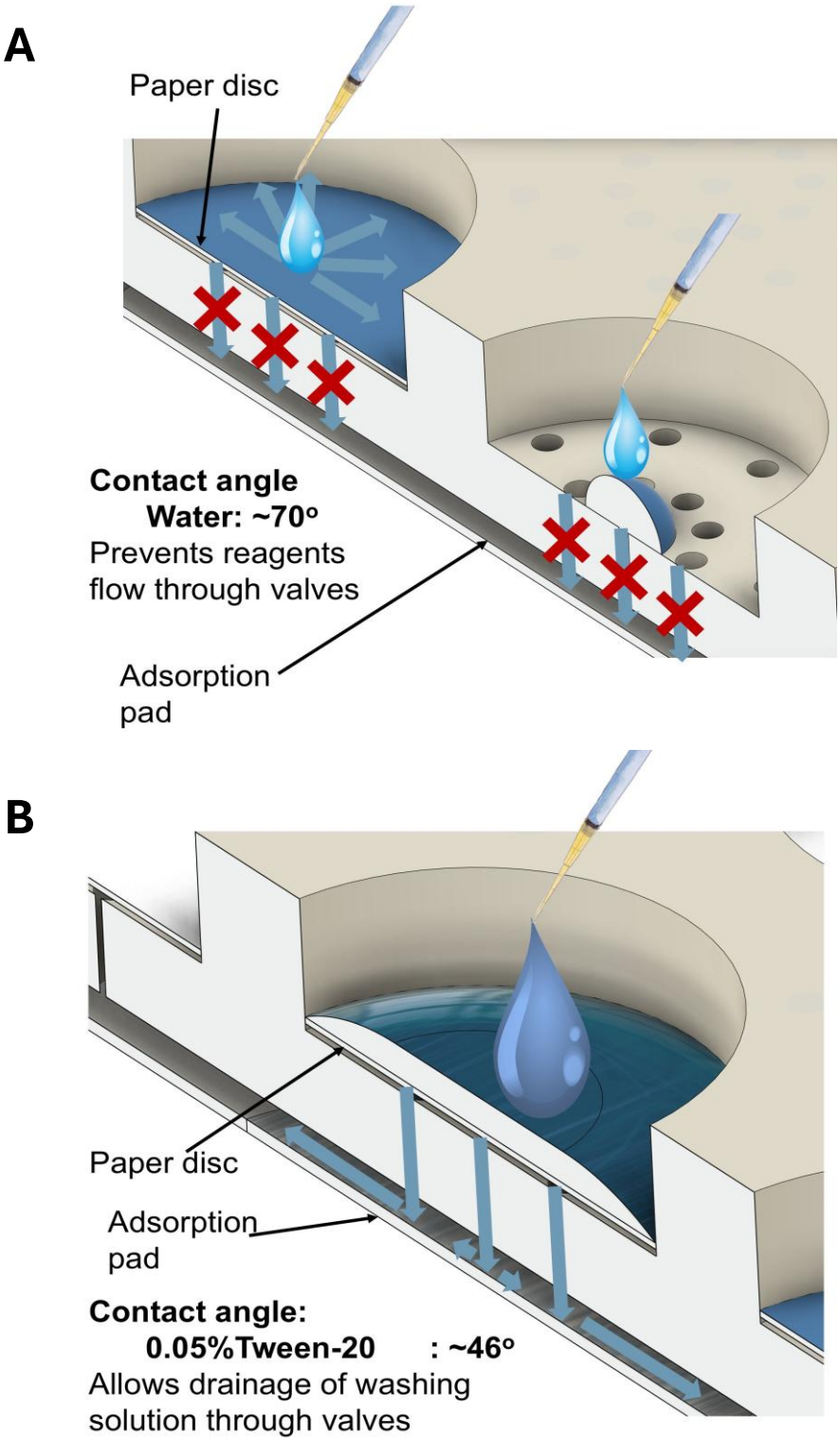

Fig. 3- 5 Illustration about the working principle of the microvalves, the water contact angle is about 70° which prevent the reagents flow so that the reagents completely adsorbed by the paper (A), while by using 0.05% tween-20 the contact angle decrease to about 46o which allow the drainage of the washing solution (B)

Fig. 3- 6 A 5 µL of blue dyes in 10 mM PBS adsorbed well through the paper disc while it did not flow through the microvalves

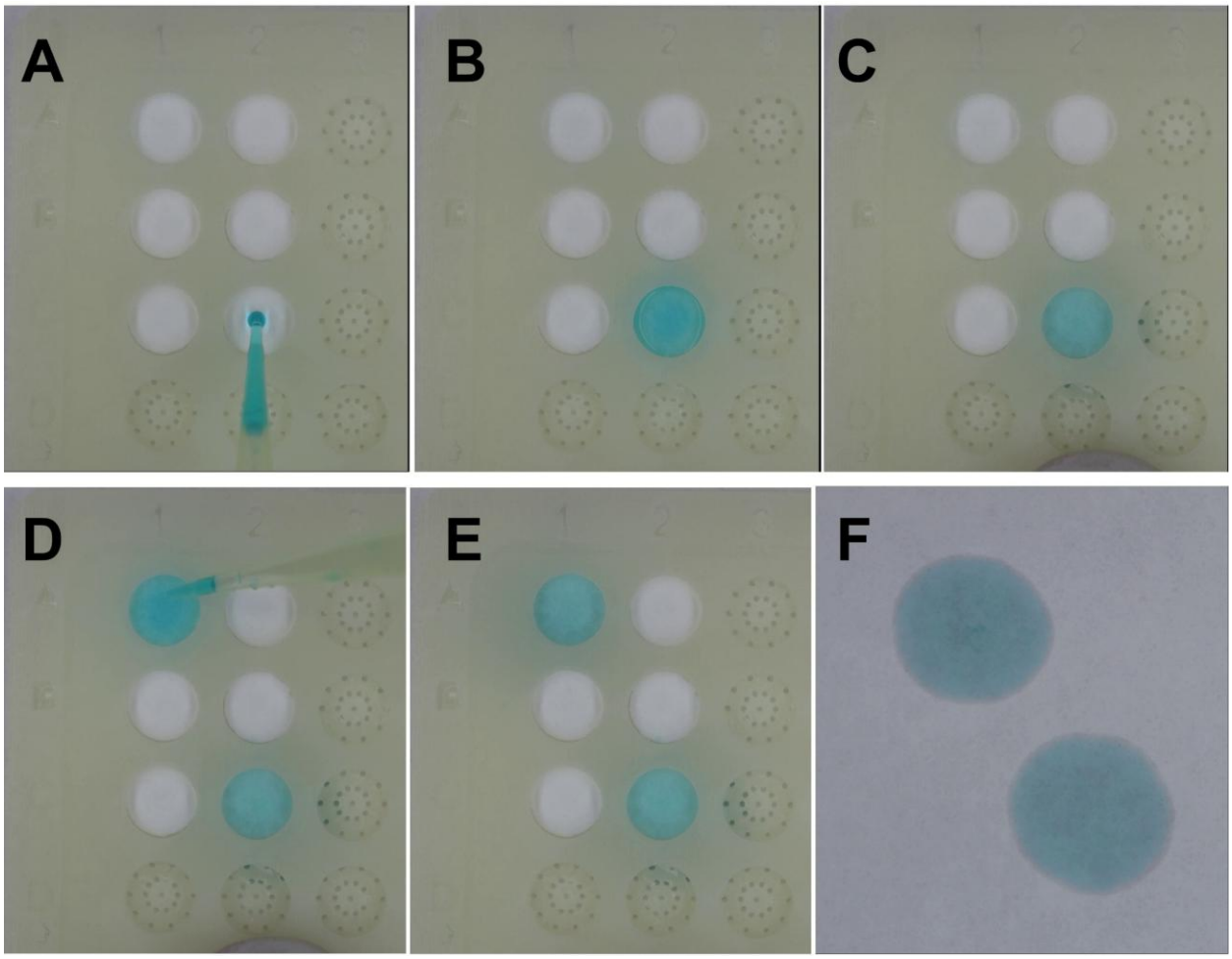

Fig. 3- 7 The drainage of 20 µL 0.05% PBST solution through the microvalves.

3.3.2 Immobilization of capture antibody

The immobilization of the capture antibody was carried out by physical adsorption at a high temperature (50 °C) as I reported previously [26]. Compared to immobilization at room temperature or 4°C, this method achieves better immobilization in a shorter time (5 minutes). Moreover, the high temperature enhances molecular motion, facilitating greater surface coverage with antibodies in a short time. Additionally, the high hydrophilicity of cellulose paper promotes antibody immobilization through hydrophilic and electrostatic interactions, which reduces antibody denaturation and preserves its activity. As a result, the immobilized cAb interacts more rapidly with the sample and the dAb, leading to a faster assay with improved sensitivity.

3.3.3 Optimization of capture antibody and detection antibody concentrations

The optimization of cAb and dAb concentrations was carried out by performing the immunoassay of HER2 while varying concentrations of cAb (1.0, 2.0, and 10.0 µg/mL) and dAb (0.1 and 0.5 µg/mL). The concentrations were chosen based on our experience and the concentrations used in some commercial kits for the detection of HER2. As seen from Fig. 3-8, dAb concentration of 0.5 µg/mL provides a better signal than 0.1 µg/mL does. Moreover, there are only slight differences in the signal between cAb concentrations of 10 µg/mL and 2 µg/mL. So, the higher cAb concentration is preferred to ensure better antibody immobilization. Therefore 10 µg/mL cAb and 0.5 µg/mL dAb were chosen for the subsequent experiments.

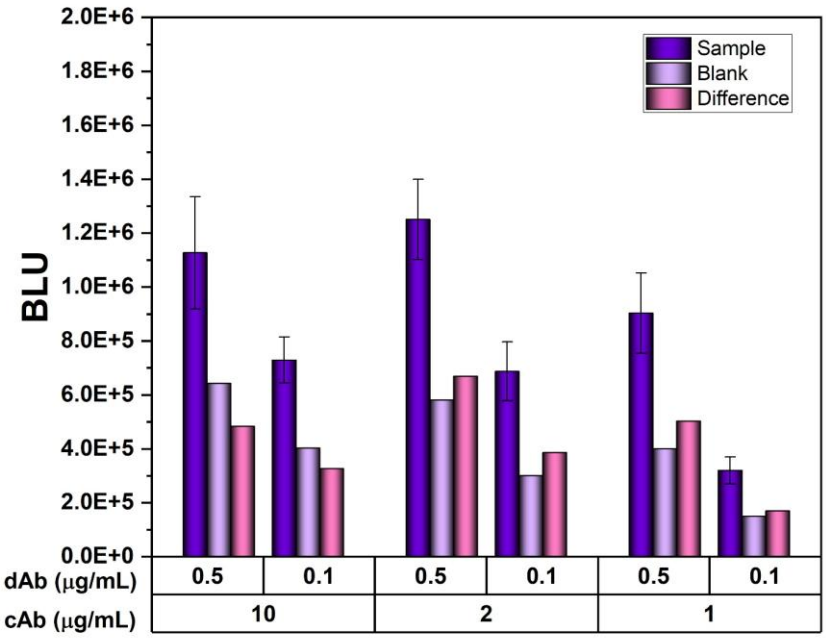

Fig. 3- 8 Optimization of the concentration of capture antibody and detection antibody, 10% BSA was used as blocking buffer, 5 min was used as a reaction time for HER2 and detection antibody.

3.3.4 Optimization of blocking buffer concentration

BSA was used for blocking the nonspecific binding sites after immobilization of the cAb. To choose the best concentration for blocking buffer, I tested various concentrations from 2 to 10 %w/v. As seen from Fig. 3-9, the signal of the sample (100 pg/mL) is nearly constant for the 4-8% BSA concentration range, while it is low at 2% and 10 % BSA. In addition, the signal increases when BSA is increased from 2% to 4% then it slightly decreases with further increase of the BSA concentration. Also, as shown from the difference, the best signal is achieved at 6% BSA as a blocking buffer. Moreover, using a higher concentration of BSA causes the BSA to recrystallize inside the microvalves and around the paper fibers, Fig. 3-10,

which affects the flow of the reagents and washing buffer in the next steps. Therefore, 6% BSA was used as the optimum blocking buffer concentration for the subsequent experiments.

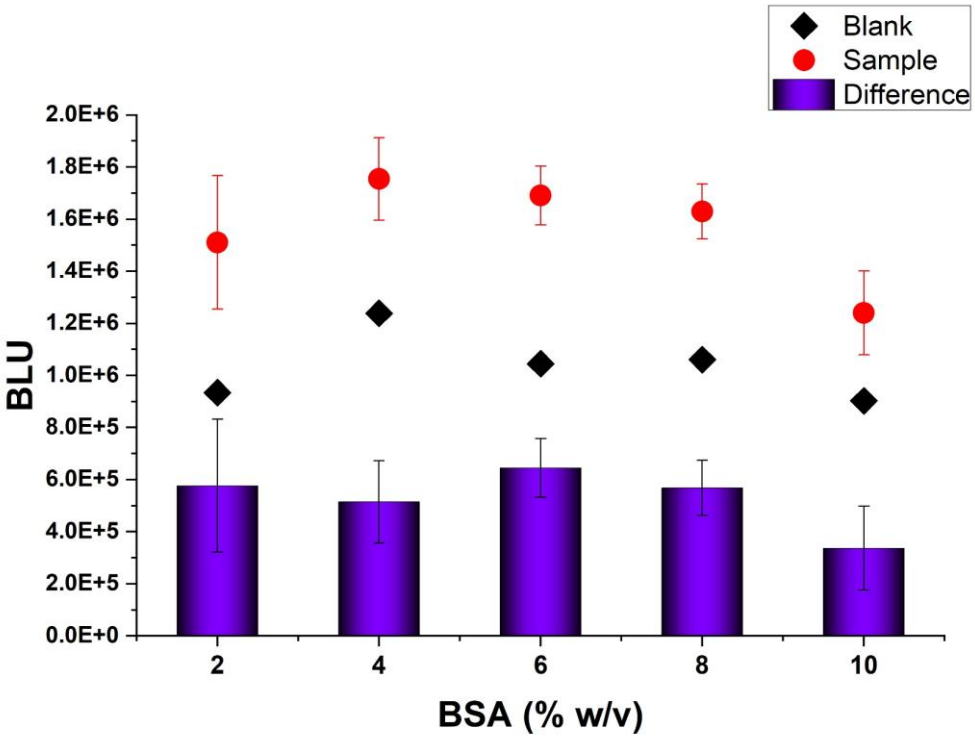

Fig. 3- 9 Optimization of BSA concentration as blocking buffer, 10 µg/mL capture antibody and 0.5 µg/mL detection antibody were used. 5 min was used as a reaction time for HER2 and detection antibody.

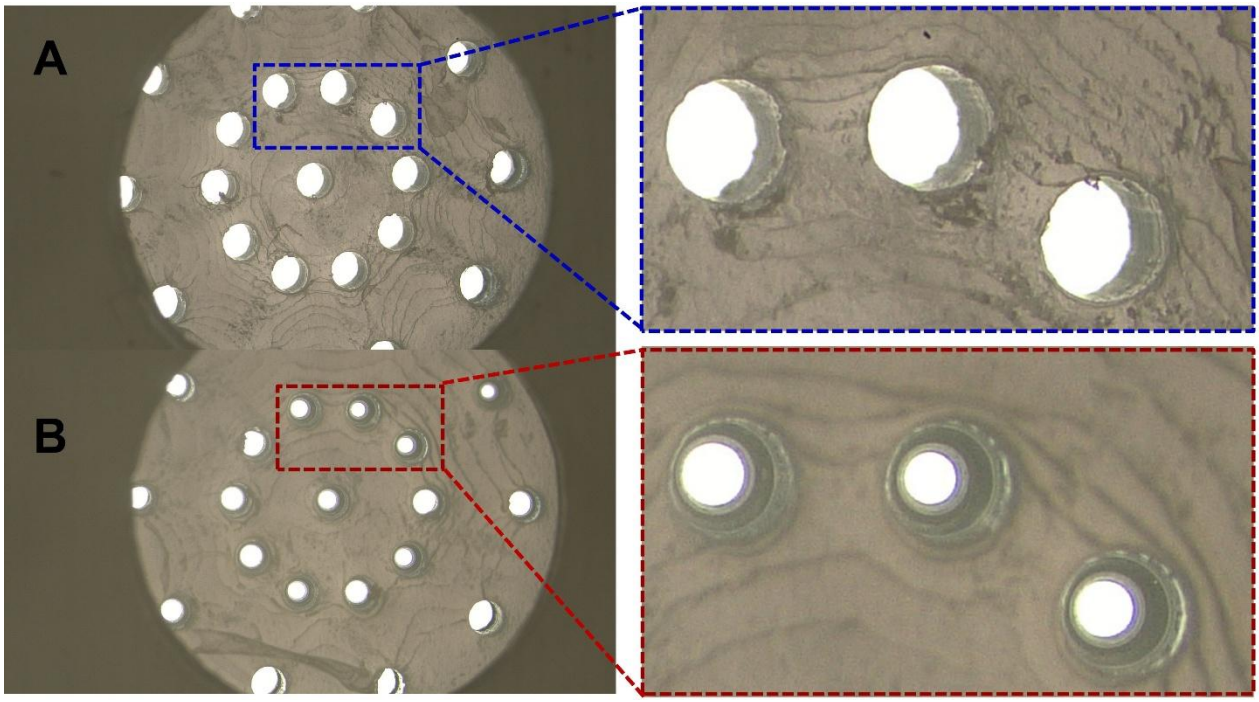

Fig. 3- 10 image for the microvalves before using BSA (A) and after using 10% BSA and incubation for 5 min at 50 °C (B). The high concentration of BSA causes to recrystallize of the BSA inside the microvalves which affects the flow of the reagents and washing buffer.

3.3.5 Optimization of antigen reaction time

Next, the reaction time of the HER2 antigen was optimized. After immobilizing the cAb and blocking the nonspecific binding sites, the HER2 antigen was added and incubated at room temperature for 30 to 600 s. As shown in Fig. 3-11, the signal of the sample (100 pg/mL) increases with increasing reaction time from 30 s to 60 s, then the signal is nearly constant until 300 s, and finally the signal decreases with increasing reaction time until 600 s. Moreover, the signal of the blank changes in the same manner as the sample. Therefore, the difference between the signals of the sample and the blank is approximately constant with increasing reaction time. Conservatively, to ensure a complete reaction between antigen and cAb, a 300 s reaction time for HER2 antigen was chosen for the subsequent experiments.

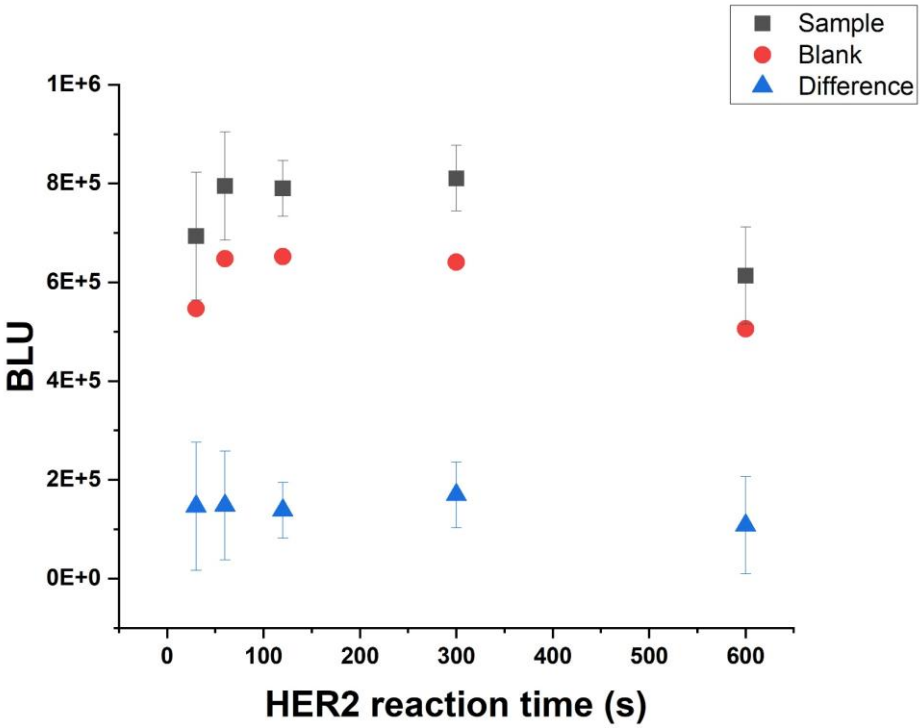

Fig. 3- 11 Optimization of HER2 reaction time, 10 µg/mL capture antibody and 0.5 µg/mL detection antibody were used. 6% BSA was used as blocking buffer, and 5 min was used as detection antibody reaction time.

3.3.6 Optimization of detection antibody reaction time

The detection antibody reaction time was optimized after optimizing the HER2 antigen reaction time. After immobilizing cAb and blocking the nonspecific binding sites, HER2 was added and incubated at room temperature for 5 min. Then 5 µL dAb was added and incubated at room temperature from 30 – 600 s before washing out the non-reacted dAb with PBST. As observed from Fig. 3-12, the signal of both the HER2 sample (100 pg/mL) and the blank sharply increase with the increase in the reaction time from 30 s to 60 s. Then the signal of the sample continues to increase slightly with increasing time, while the signal of the blank starts to slightly increase again after 120 s. The difference between the sample and blank signals is the best between 120 – 600 s; therefore 300 s was chosen as the optimum reaction time for dAb.

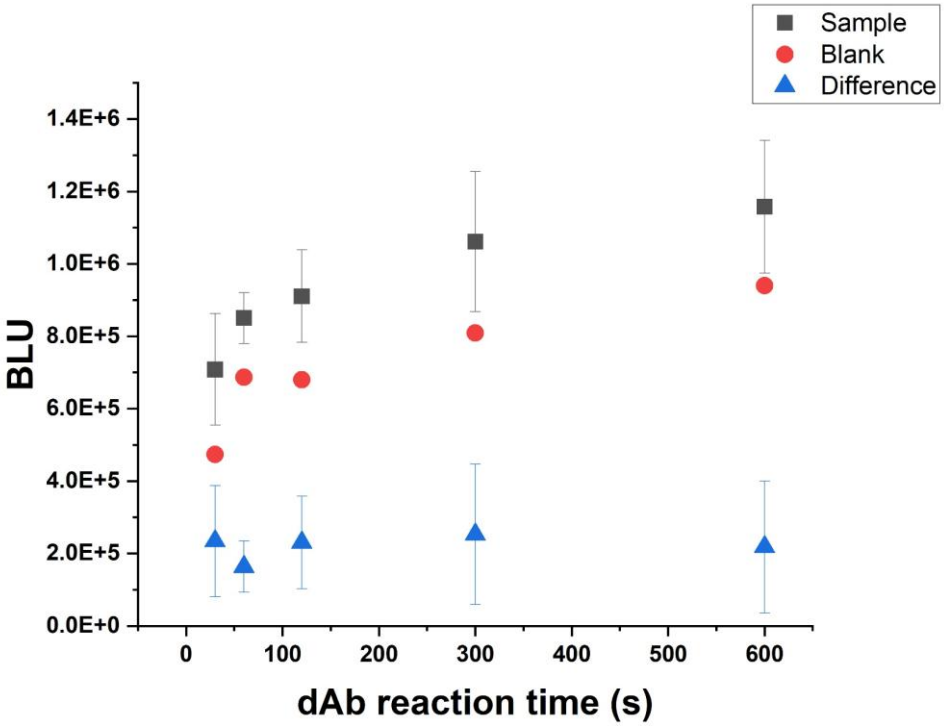

Fig. 3- 12 Optimization of detection antibody rection time. 10 µg/mL capture antibody and 0.5 µg/mL detection antibody were used. 6% BSA was used as blocking buffer, and 5 min was used as HER2 reaction time. In all graphs, 100 pg/mL HER2 was used as sample, and 10 mM PBS was used as blank.

3.3.7 Bioluminescence sandwich ELISA for detection of HER2

The proposed assay utilizes paper as a substrate for immobilizing the cAb instead of the conventional microplate. Immobilization is performed at a high temperature (50°C), allowing for rapid immobilization in just 5 minutes, compared to the overnight process typically used in conventional ELISA [26]. Moreover, the proposed assay requires much smaller reagent volumes (5 µL) than conventional ELISA, which typically uses around 100 µL.

The paper substrate has high hydrophilicity and a large surface area-to-volume ratio, facilitating rapid interaction between the immobilized cAb, sample, and detection antibody (dAb). The proposed 3D-printed microplate with microvalves enables vertical drainage of the washing solution, simplifying and accelerating the washing process compared to conventional ELISA, where each well is filled with washing solution and aspirated three times. Thus, compared to conventional ELISA, the proposed assay is simpler, faster, requires smaller reagent volumes, and offers enhanced sensitivity.

After optimization, use of the paper disc in the 3D printed microplate hybrid device was evaluated over a wide range of HER2 protein concentrations. First 5 µL cAb (10 µg/mL) was added to each well and incubated for 5 min at 50 ºC followed by washing twice using 20 µL 0.05% PBST. Then 5 µL BSA 6% was added to each well and incubated for 5 min at 50 ºC to block the nonspecific binding sites. Next 5 µL HER2 protein with a concentration of 0.01 – 1000 pg/mL was added and incubated for 5 min at room temperature. After that, 5 µL dAb (0.5 µg/mL) was added to each well and incubated for 5 min at room temperature followed by washing twice using 20 µL 0.05% PBST. Finally, 5 µL furimazine substrate (50X diluted) was added, and the bioluminescence signal was measured. The device had consistent performance over the range of 0.01 – 1000 pg/mL; all samples were measured in triplicate and an average coefficient of variation (CV) of 9.5 % was obtained, indicating good repeatability. A calibration curve was plotted between the logarithm of HER2 concentration and the bioluminescence signal of the samples, and it is shown in Fig. 3-13. A good linear relationship was obtained over the range from 0.1 to 1000 pg/mL with a linear regression equation of BLU = 3.03 (± 0.14) × 10^4 log (HER2) + 4.85 (±0.02) × 10^5 (R^2 = 0.994). Based on this equation, the LOD for HER2 is 1.3 fg/mL demonstrating the ultra-sensitivity of the hybrid device. Table 3-1 allows a comparison to be made between the proposed device and other reported biosensors. Our proposed device using the bioluminescence method achieved a LOD at least 10^6-fold lower

the colorimetric and surface plasmon resonance (SPR) techniques. Although electrochemical techniques are considered highly sensitive, our device achieves better sensitivity and more than 10^3-fold better detection limit with a simpler and faster assay paper-based sandwich ELISA. In addition, I compared our assay performance with some commercial ELISA kits for the detection of HER2. As shown in Table 3-2, our proposed device has a better detection limit with a very short assay time (15 min) compared to commercial kits (average 5 h). Moreover, the amounts of sample and reagent used are significantly decreased which hugely reduces the analysis cost.

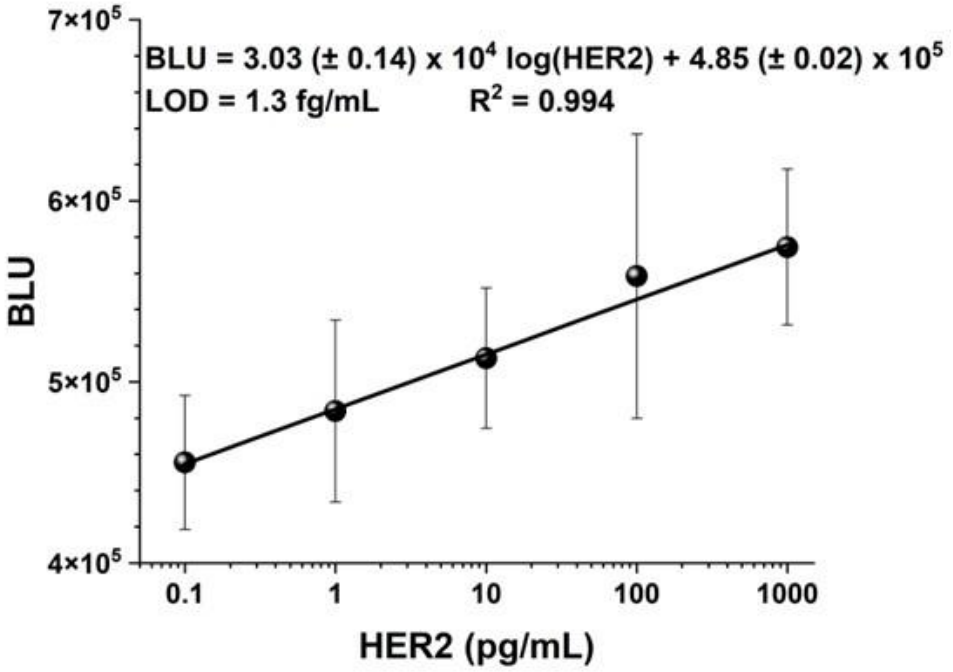

Fig. 3- 13 Calibration curve for detection of HER2 protein obtained with the optimized paper in 3D printed microplate hybrid device. A linear relationship obtained between bioluminescence signal and log(HER2) across the range of 0.1 to 1000 pg/mL.

Table 3- 1 Comparison of the paper disc use in 3D printed microplate hybrid device for bioluminescence detection of HER2 to other reported biosensors

Technique	Testing probes	Linear range	LOD	Reference
SPR	Au/UiO-66-NH_2	1-30 ng/mL	457 pg/mL	[27]
SPR	Optical fiber assay	0.1-10 μg/mL	660 ng/mL	[28]
Electrochemical (DPV)	BSA/HER2 Antibody/N-CQDs/GS modified electrode	0.1-1 ng/mL	4.8 pg/mL	[29]
Electrochemical (DPV)	Screen-printed carbon electrode-modified carbon nanotube/gold nanoparticles	0.001-25 ng/mL	4.4 pg/mL	[30]
Colorimetric	Coassembled peptide and dye molecule	3-24 ng/mL	3 ng/mL	[31]
Colorimetric	AuNP based Lateral flow immunoassay	1.7-400 n/mL	1.7 ng/mL	[32]
Bioluminescence (Paper-based)	Paper-based Sandwich ELISA	0.1-1000 pg/mL	1.3 fg/mL	This work

Table 3- 2 Paper disc use in the 3D printed microplate hybrid device for bioluminescence ELISA in comparison with two commercial microplate ELISA kits for HER2 detection

	Bio-techne Human ErbB2/Her2 DuoSet ELISA	Sino Biological Human Her2/ERBB2 Matched ELISA Antibody Pair Set [a]	Paper in 3D printed microplate hybrid device
Detection technique	Colorimetric	Colorimetric	Bioluminescence
Amount of capture antibody per well	200 ng	100 ng	50 ng
Amount of detection antibody per well	10 ng	50 ng	2.5 ng
Volume of sample	100 µL	100 µL	5 µL
Volume of substrate[b]	100 µL	200 µL	5 µL
Immobilization time	Overnight	Overnight	5 min
Assay time	5 h 40 min	4 h 20 min	15 min
Assay range pg/mL	54.7-3500	24-1500	0.1-1000
LOD pg/mL	54.7	24	0.0013

[a] Sino Biological kit uses the same antibodies and HER2 protein used in this study.

[b] both kits use TMB colorimetric substrate, while our hybrid device uses furimazine substrate

3.3.8 Detection of HER2 in human serum

To validate the analytical accuracy of the hybrid device for detecting HER2 in real human samples, normal human serum was spiked with various concentrations of HER2. The cutoff value for HER2 levels in normal human serum is approximately 15 ng/mL [33,34]. To reduce background signal and bring the concentration within the assay's detection range (in the pg/mL level), the serum was diluted 2000-fold. Five different concentrations (5 pg/mL, 10 pg/mL, 100 pg/mL, 500 pg/mL, and 800 pg/mL), which are within the linear range and above the LOD, were tested, and the recovery

percentages were calculated. As shown in Table 3, the recovery percentages ranged from 86% to 108%, falling within the acceptable criteria for bioanalytical method validation [35]. Furthermore, a strong correlation was observed with the values obtained using the commercial ELISA kit.

Table 1-3 Detection of HER2 spiked into human serum samples by the hybrid device and commercial ELISA kit

Sample	Spiked HER2 concentration (pg/mL)	Paper disc in 3D printed microplate hybrid device		Bio-techne Human ErbB2/Her2 DuoSet ELISA kit	
		Measured values (pg/mL)	Recovery (%)	Measured values (pg/mL)	Recovery (%)
1	800	688	86.0	674	84.2
2	500	441	88.2	445	89.0
3	100	93.0	93.0	74.0	74.0
4	10	9.79	97.9	ND	NA
5	5	5.41	108	ND	NA

ND: not detected, the detection limit of the commercial ELISA kit is 54.7 pg/mL.

NA: not applicable

3.4 Conclusion

I have developed a simple, rapid, and ultrasensitive hybrid device using chromatographic paper discs in a 3D printed microplate for bioluminescence detection of HER2 breast cancer biomarker with a very low LOD. The hybrid device provides the advantages of cellulose paper which ensures good immobilization of antibodies and proteins within a few minutes through physical adsorption without any surface modification so that the entire assay needs only 20 min. The 3D printed microplate has two features, the first one is the

microvalves, and the second one is the changing of the water contact angle with the addition of surfactant. With these two features, the 3D printed microplate is able to stop the sample and reagent solutions from draining so they have ample time for reaction, and then allow the washing solution to drain out and be adsorbed through the adsorption pad for efficient washing. The 3D printed microplate has the same dimensions as commercial microplates so it can be used with any common plate reader. The 3D printed microplate can be reused by removing the paper discs, washing and drying the plate, and inserting new paper discs. After optimization of the different assay conditions, a simple and rapid bioluminescence sandwich ELISA for detection of HER2 biomarker was performed using the 3D printed hybrid microplate device. A LOD of 1.3 fg/mL was achieved which is more than 10^4-fold better than that of the commercial colorimetric kits. The average CV was 9.5% which I considered to be good because the assay is ultrasensitive. Also, very small reagent volumes (5 μL) are used throughout the assay which makes the assay very sensitive to changes in the volumes. Therefore, the CV can be improved by using a more precise pipetting system. The diagnostic accuracy of the device in practical clinical settings will need to be further confirmed with clinical samples in the future. But considering these notable features, this affordable 3D printed microplate hybrid microfluidic device using replaceable paper discs holds potential for broad applications in rapid, highly sensitive, and quantitative detection of various disease biomarkers, including those for cancers and infectious diseases, and for other biomolecules.

3.5 References

[1] H. Sung, J. Ferlay, R.L. Siegel, M. Laversanne, I. Soerjomataram, A. Jemal, et al., Global cancer statistics 2020: GLOBOCAN estimates of incidence and mortality worldwide for 36 cancers in 185 countries, CA Cancer J. Clin., 71(2021) 209-49.

[2] R.L. Siegel, A.N. Giaquinto, A. Jemal, Cancer statistics, 2024, CA Cancer J. Clin., 74(2024) 12-49.

[3] A.N. Giaquinto, H. Sung, L.A. Newman, R.A. Freedman, R.A. Smith, J. Star, et al., Breast cancer statistics 2024, CA Cancer J. Clin., 74(2024) 477-95.

[4] P.R. Karmakar, Epidemiology of Cancer: Asian Perspective Revised, in: S.K. Basu, C.K. Panda, S. Goswami (Eds.), Cancer Diagnostics and Therapeutics, Springer, Singapore, 2022, pp. 489-508.

[5] S. Suan Ng, H. Ling Lee, P. Bothi Raja, R.A. Doong, Recent advances in nanomaterial-based optical biosensors as potential point-of-care testing (PoCT) probes in carcinoembryonic antigen detection, Chem. Asian J., 17(2022) e202200287.

[6] M. Carneiro, L.R. Rodrigues, F.T.C. Moreira, M.G.F. Sales, Colorimetric paper-based sensors against cancer biomarkers, Sensors (Basel), 22(2022) 3221.

[7] K. Djebbi, J. Xing, T. Weng, M. Bahri, M.A. Elaguech, C. Du, et al., Highly sensitive fluorescence multiplexed miRNAs biosensors for accurate clinically diagnosis lung cancer disease using LNA-modified DNA probe and DSN enzyme, Anal. Chim. Acta., 1208(2022) 339778.

[8] X. Zhao, X. Dai, S. Zhao, X. Cui, T. Gong, Z. Song, et al., Aptamer-based fluorescent sensors for the detection of cancer biomarkers, Spectrochim. Acta. A Mol. Biomol. Spectrosc., 247(2021) 119038.

[9] L. Jing, C. Xie, Q. Li, M. Yang, S. Li, H. Li, et al., Electrochemical biosensors for the analysis of breast cancer biomarkers: from design to application, Anal. Chem., 94(2022) 269-96.

[10] I.M. Mostafa, Y. Tian, S. Anjum, S. Hanif, M. Hosseini, B.H. Lou, et al., Comprehensive review on the electrochemical biosensors of different breast cancer biomarkers, Sens. Actuatators B Chem., 365(2022) 131944.

[11] Q.L. Shu, Y.F. Zhu, Y.P. Xiao, K.S. Chen, X. Mai, X.J. Zheng, et al., A novel chemiluminescence biosensor based on dual aptamers bound nanoparticles with multi-site signal amplification for sensitive detection of carcinoembryonic antigen, Microchem J, 179(2022).

[12] X. Fan, S. Wang, H. Liu, Z. Li, Q. Sun, Y. Wang, et al., A sensitive electrochemiluminescence biosensor for assay of cancer biomarker (MMP-2) based on NGQDs-Ru@SiO2 luminophore, Talanta, 236(2022) 122830.

[13] Y.G. Feng, J.H. Zhu, X.Y. Wang, A.J. Wang, L.P. Mei, P.X. Yuan, et al., New advances in accurate monitoring of breast cancer biomarkers by electrochemistry, electrochemiluminescence, and photoelectrochemistry, J. Electroanal. Chem., 882(2021) 115010.

[14] A. Gade, A. Sharma, N. Srivastava, S.J.S. Flora, Surface plasmon resonance: A promising approach for label-free early cancer diagnosis, Clin. Chim. Acta., 527(2022) 79-88.

[15] A. Pollap, P. Swit, Recent Advances in Sandwich SERS Immunosensors for Cancer Detection, Int. J. Mol. Sci., 23(2022) 4740.

[16] M. Haroon, M. Tahir, H. Nawaz, M.I. Majeed, A.A. Al-Saadi, Surface-enhanced Raman scattering (SERS) spectroscopy for prostate cancer diagnosis: A review, Photodiagn. Photodyn. Ther., 37(2022) 102690.

[17] X. Chen, H. Ruan, Z. Ma, J. Hu, W. Xu, L. Yin, et al., Polymerase chain reaction in the detection of mir-455-5p and sphingosine-1 phosphate proteins in cervical carcinoma with the help of gold nanoparticles-based, J. Biomed. Nanotechnol., 17(2021) 1535-44.

[18] J. Shen, B. Situ, X. Du, Z. Wang, R. Hu, B. Li, et al., Aggregation-induced emission luminogen-based dual-mode enzyme-linked immunosorbent assay for ultrasensitive detection of cancer biomarkers in a broad concentration range, ACS Sens., 7(2022) 766-74.

[19] Z. Liu, Y. Zhou, J. Lu, T. Gong, E. Ibanez, A. Cifuentes, et al., Microfluidic biosensors for biomarker detection in body fluids: a key approach for early cancer diagnosis, Biomark. Res., 12(2024) 153.

[20] A.A. Shalaby, C.-W. Tsao, A. Ishida, M. Maeki, M. Tokeshi, Microfluidic paper-based analytical devices for cancer diagnosis, Sens. Actuators B Chem., 379(2023) 133243.

[21] Y. Wu, L. Li, D. Zhang, F. Ma, Prognostic value of the serum her2 extracellular domain level in breast cancer: A systematic review and meta-analysis, Cancers (Basel), 14(2022) 4551.

[22] L. Chun, S.E. Kim, M. Cho, W.S. Choe, J. Nam, D.W. Lee, et al., Electrochemical detection of HER2 using single stranded DNA aptamer modified gold nanoparticles electrode, Sens. Actuators B Chem., 186(2013) 446-50.

[23] I. Diaconu, C. Cristea, V. Harceaga, G. Marrazza, I. Berindan-Neagoe, R. Sandulescu, Electrochemical immunosensors in breast and ovarian cancer, Clin. Chim. Acta, 425(2013) 128-38.

[24] V. Ranganathan, S. Srinivasan, A. Singh, M.C. DeRosa, An aptamer-based colorimetric lateral flow assay for the detection of human epidermal growth factor receptor 2 (HER2), Anal. Biochem., 588(2020) 113471.

[25] H. Shafique, V. Karamzadeh, G. Kim, M.L. Shen, Y. Morocz, A. Sohrabi-Kashani, et al., High-resolution low-cost LCD 3D printing for microfluidics and organ-on-a-chip devices, Lab Chip, 24(2024) 2774-90.

[26] A.A. Shalaby, R. Maeda, A. Ishida, Y. Shimizu, H. Saeki, M. Maeki, et al., Straightforward high-temperature antibody immobilization for rapid and simple microfluidic paper-based ELISA for detection of β'-component (Onc k 5) protein, a major IgE-binding protein in salmon roe, Sens. Actuators. B Chem., 422(2025) 136536.

[27] L. Rahmidar, G. Gumilar, N.L.W. Septiani, C. Wulandari, M. Iqbal, Nugraha, et al., Label-free and early detection of HER2 breast cancer biomarker based on UiO-66-NH modified gold chip (Au/UiO-66-NH) using surface plasmon resonance technique, Microchem J, 199(2024).

[28] M. Loyez, M. Lobry, E.M. Hassan, M.C. DeRosa, C. Caucheteur, R. Wattiez, HER2 breast cancer biomarker detection using a sandwich optical fiber assay, Talanta, 221(2021) 121452.

[29] H. Amir, V. Subramanian, S. Sornambikai, N. Ponpandian, C. Viswanathan, Nitrogen-enhanced carbon quantum dots mediated immunosensor for electrochemical detection of HER2 breast cancer biomarker, Bioelectrochem., 155(2024) 108589.

[30] Y. Makableh, T. Athamneh, M. Ajlouni, S. Hijazi, A. Alnaimi, Enhanced response and selective gold nanoparticles/carbon nanotubes biosensor for the early detection of HER2 biomarker, Sens. Actuator Rep., 5(2023) 100158.

[31] Q.Z. Liang, Q.X. Zhou, J.H. Yang, Y.W. Han, Y.Y. Pan, S. Zhu, et al., Assembly of peptide with dye molecules for the fabrication of colorimetric biosensor with application to diagnose her2-positive breast cancer, ACS Mater. Lett., 6(2024) 2136-43.

[32] L.Y. Ye, X.X. Xu, A.H. Qu, L.Q. Liu, C.L. Xu, H. Kuang, Quantitative assessment of the breast cancer marker HER2 using a gold nanoparticle-based lateral flow immunoassay, Nano Res., 17(2024) 5452-60.

[33] Lee, M.H., Jung, S.Y., Kang, S.H., Song, E.J., Park, I.H., Kong, S.Y., Kwon, Y.M., Lee, K.S., Kang, H.S., Lee, E.S., 2016. The significance of serum her2 levels at diagnosis on intrinsic subtype-specific outcome of operable breast cancer patients. PLoS One 11(10), e0163370.

[34] Lee, S.B., Lee, J.W., Yu, J.H., Ko, B.S., Kim, H.J., Son, B.H., Gong, G., Lee, H.J., Kim, S.B., Jung, K.H., Ahn, J.H., Lee, W., Sung, J., Ahn, S.H., 2014. Preoperative serum HER2 extracellular domain levels in primary invasive breast cancer. BMC Cancer 14, 929.

[35] International Council for Harmonisation (ICH), M10 bioanalytical method validation and study sample analysis: guidance for industry, U.S. Food and Drug Administration (FDA), 2022.

CHAPTER 4 Conclusion and Future Prospectives

4.1 Conclusion

There is a global interest in developing analytical tools for point-of-need (PON) applications, especially for medical diagnostics and food safety. Sensitive detection of proteins in biological samples attracts a huge interest, where specific proteins can be detected in body fluids for early diagnosis of diseases such as cancers which leads to receiving proper treatment and decreases the mortality rate, and also allergenic proteins can be detected in food sample which lead to decrease the deaths due to allergenic shocks. Sandwich enzyme-linked immunosorbent assay (ELISA) is a common technique for detection of proteins in biological samples due to its specificity and sensitivity. Commonly, Sandwich ELISA uses capture antibody immobilized on microwell plate surface to capture the antigen, next an enzyme labeled detection antibody is added to attach the antigen, and finally a substrate is added to react with the enzyme and produce analytical signal. Sandwich ELISA is a very sensitive and specific technique, but it suffers from the very long assay time, uses very large volume of reagents, and should be performed by highly experienced person. Microfluidic paper-based analytical devices (μPADs) are a very promising approach for developing low-cost, rapid, and sensitive analytical devices for sandwich ELISA assays. μPADs based ELISA can be performed in less than one hour and provide ultra-sensitive detection levels with using the minimum amounts of reagents. The current prospectives of μPADs-based detection of cancer biomarkers protein was discussed in Chapter 1.

In Chapter 2, a sandwich ELISA on μPAD was developed for detection of β'-c allergenic protein. The μPAD-ELISA was designed as a cost-effective solution, easy-to-fabricate, and sensitive method for detecting the allergenic β'-component protein. A simple and rapid antibody immobilization process was employed by drying the capture antibody at 50°C for 5 minutes. The assay parameters were optimized to achieve high sensitivity within minimal

assay time, completing the analysis in 15 minutes. Under optimal conditions, the μPAD-ELISA demonstrated a good linear response across β'-component concentrations of 0.10–60.0 ng mL^{-1}, with a detection limit of 1.59 ng mL^{-1}. Compared to conventional ELISA, the μPAD-ELISA requires significantly reduced reagent volumes and assay times. These features make it well-suited for the rapid and sensitive detection of food allergens in processed foods and for improving food allergy labeling systems.

In Chapter 3, I have developed a simple, rapid, and ultra-sensitive hybrid device combining paper and a 3D-printed microplate for bioluminescence detection of the HER2 breast cancer biomarker with an exceptionally low detection limit. The device leverages microporous cellulose paper, enabling effective antibody and protein immobilization within minutes through physical adsorption, eliminating the need for surface modifications and allowing the entire assay to be completed in just 20 minutes. The 3D-printed microplate incorporates two key features: microvalves and adjustable water contact angles achieved by adding surfactants. These features facilitate controlled stopping of sample and reagent solutions for reactions while enabling efficient washing via solution drainage into an adsorption pad. The microplate matches the dimensions of commercial microplates, making it compatible with standard plate readers, and it can be reused by replacing the paper discs after washing and drying. Following assay optimization, a bioluminescence-based sandwich ELISA achieved a limit of detection (LOD) of 1.3 fg/mL, which is at least 10^4 times more sensitive than conventional colorimetric kits. The assay demonstrated good reproducibility with an average coefficient of variation (CV) of 9.5%, though precision could be further improved using advanced pipetting systems due to the small reagent volume (5 μL) required. While further validation using clinical samples is necessary, the affordability, speed, and ultra-sensitivity of this hybrid microfluidic device make it promising for rapid, quantitative detection of disease biomarkers, including those for cancers, infectious diseases, and other biomolecules.

4.2 Future Prospectives

The developed μPAD-ELISA and hybrid paper/3D-printed microplate platforms show significant potential for enabling rapid, low-cost diagnostics across diverse fields. Future work should focus on clinical validation—particularly for the HER2 detection device—to confirm its suitability for early cancer diagnosis. With their high sensitivity and short assay times, these platforms are ideal for rapid ELISA applications in cancer diagnostics, infectious disease screening, and biomarker monitoring in resource-limited settings. Further improvements could include automation of fluid handling, enhanced precision via integration with pipetting systems, and multiplexing to detect multiple biomarkers simultaneously. Incorporating portable or smartphone-based readers would also support point-of-care use in clinical and remote environments. In the food industry, μPAD-ELISA can be adapted for on-site allergen detection to enhance food safety and labeling compliance. These platforms also hold promise for environmental monitoring, such as detecting toxins or pathogens in water.

The technologies developed in this work lay the foundation for a new generation of rapid, affordable, and ultra-sensitive diagnostic platforms. With continued innovation and interdisciplinary collaboration, these systems could transform various sectors by enabling:

- **Rapid ELISA platforms** for high-throughput screening and personalized medicine.
- **Early cancer diagnostics** based on ultra-low biomarker detection.
- **Point-of-care detection** of infectious and chronic diseases.
- **On-site food allergen testing** for consumer safety and regulation.
- **Environmental monitoring** of pollutants and pathogens in water and soil.

Overall, the combination of microfluidics, paper-based materials, and 3D printing paves the way for scalable, ultra-sensitive, and accessible diagnostic tools for medical, food, and environmental applications

Acknowledgement

"وَقُلْ رَبِّ زِدْنِي عِلْمًا" [سورة طه - الآية: 114]

"And say, 'My Lord, increase me in knowledge.'" **(Surah Taha, 20:114)**

All praise and thanks are due to Allah, the Most Gracious, the Most Merciful, for granting me the strength, patience, and guidance to complete this Ph.D. journey. Without His blessings, none of this would have been possible.

I would like to express my deepest respect and heartfelt gratitude to my supervisor, Professor Manabu Tokeshi of the Division of Applied Chemistry, Faculty of Engineering, Hokkaido University. His invaluable guidance, wisdom, and unwavering support have been instrumental throughout my Ph.D. journey. Professor Tokeshi's meaningful advice and encouragement have helped me navigate the challenges of research and have provided me with insights not only into science but also into life itself. While words may never fully capture the extent of my appreciation, I will always remain eternally grateful to him.

I am deeply grateful and proud that I am part of the Microsystems Chemistry Laboratory (Tokeshi Lab). I am especially grateful to Associate Professor Masatoshi Maeki and Assistant Professor Akihiko Ishida for all the assistance, advice, support, and valuable discussions.

I am also immensely grateful to my beloved wife for her unwavering support, patience, and understanding throughout this journey. Her love and encouragement have been my constant source of strength, especially during the most challenging times. Without her sacrifices and belief in me, this achievement would not have been possible.

Finally, I extend my deepest appreciation to my parents, whose love, sacrifices, and prayers have been the foundation of my life. To my late father, who passed away during my Ph.D. journey, I dedicate this achievement to your memory. Your wisdom, support, and the values you instilled in me continue to guide my steps every day. Although you are no longer with me, your presence remains in my heart, inspiring me to persevere and make you proud. To my mother, your boundless love, patience, and prayers have been my strength, and I am forever indebted to you for your unwavering support.